Title
Surface-Based Assays for Enzyme Adsorption and Activity on Model Cellulose Films

Author
Maurer, Samuel Andrew

Publication Date
2012

Peer reviewed|Thesis/dissertation

Surface-Based Assays for Enzyme Adsorption and Activity on Model Cellulose Films

by
Samuel Andrew Maurer

A dissertation submitted in partial satisfaction of the
requirements for the degree of
Doctor of Philosophy

in
Chemical Engineering

in the
Graduate Division

of the
University of California, Berkeley

Committee in charge:

Prof. Clayton J. Radke, Chair
Prof. Jhih-Wei Chu
Prof. Susan J. Muller
Prof. Carolyn R. Bertozzi

Fall 2012

Abstract

Surface-Based Assays for Enzyme Adsorption and Activity on Model Cellulose Films

Sam Maurer

Doctor of Philosophy in Chemical Engineering
University of California, Berkeley
Professor Clayton J. Radke, Chair

Transportation fuels produced by harvesting and breaking down sturdy, fast-growing prairie grasses offer a renewable alternative to diminishing fossil-fuel supplies. The rate-limiting step in the production of renewable fuels from these lignocellulosic feedstocks is the enzymatic deconstruction of solid cellulose into glucose oligomers that are subsequently processed to form transportation fuels and fuel additives. Despite continuing research interest and significant subsidy of biofuel production, the mechanisms and kinetics governing this fundamental interaction remain largely unknown.

Cellulose, the world's most abundant biopolymer, is comprised of long glucose chains organized in an extensive hydrogen-bonding network that makes cellulose insoluble in water and recalcitrant to enzymatic degradation. Complete deconstruction of cellulose into soluble glucose oligomers requires the concerted action of several enzymes, collectively known as cellulases, that adsorb to the cellulose surface from aqueous solution and complex with cellulose chains. Current assays of cellulase activity are performed in the bulk, and thus fail to characterize this important surface interaction. Recently, thin model films of solid cellulose adhered to metal supports have become available. These model films offer well-defined substrates of known surface area on which cellulase activity can be characterized.

This work describes the development and application of surface-based assays for elucidating cellulase kinetics on model films of cellulose. The developed surface-based assays allow continuous, non-invasive, inhibition-free measurement of both enzyme adsorption and activity, and are, therefore, preferable to bulk assays. Ellipsometry, an optical technique that uses changes in the polarization of light to detect film thickness, is applied to prove the efficacy of surface-based assays for measuring the activity of a cellulase mixture on model cellulose films. Degradation rates measured by ellipsometry are identical to those measured by a traditional bulk glycan assay on Avicel, a laboratory-standard cellulose. Quartz crystal microgravimetry (QCM), an acoustic technique that uses changes in the resonance of a quartz crystal to detect adsorbed mass, is then used to measure the competitive adsorption and cooperative activity of two individual cellulases and their binary mixtures. Results obtained from both the optical and acoustic assays are commensurate.

Using data from these assays, cellulase adsorption and activity are described according to a two-enzyme surface kinetic model incorporating both Langmuir adsorption to the cellulose surface and Michaelis-Menten activity of adsorbed enzyme. The model additionally quantifies observed irreversible binding of cellulases and the cooperative activity of two cellulases in

creating and degrading cellulose chain ends. Cel7A, a processive cellobiohydrolase that complexes with cellulose chain ends and digests cellulose chains into glucose oligomers, is shown to have 14 times higher adsorption affinity for the cellulose surface than does Cel7B, a non-processive endoglucanase that disrupts the hydrogen-bonding structure of the cellulose surface and creates chain ends. Both enzymes rapidly bind irreversibly to the cellulose surface, with 75 – 85% irreversibly bound after 1 h contact between aqueous enzyme and solid cellulose. Nevertheless, irreversibly bound enzymes remain catalytically active. The cellulytic activity of Cel7A is maximized by increasing cellulose surface chain-end concentration without leaving a large quantity of Cel7B irreversibly bound. These findings underscore the importance of considering surface concentration, rather than bulk concentration, in the design of optimal cellulase mixtures for biofuel production.

The kinetic constants governing adsorption and activity of Cel7A and Cel7B on the cellulose surface are obtained from single-enzyme experiments and used subsequently to predict the transient behavior of binary enzyme mixtures. In all cases, good agreement is shown between kinetic model and experiment, validating the surface-based assays. The ellipsometry and QCM techniques described in this thesis can be used further to measure the adsorption and complexation constants of other cellulases, to inform the design of cellulase cocktails, to quantify cellulase inhibition by aqueous glycans, to explore the role of substrate structure in cellulase activity, and to characterize loss of cellulase activity due to surface and thermal denaturation. Surface-based assays, therefore, represent an important new tool for addressing many outstanding problems in cellulose deconstruction.

Table of Contents

List of Figures

List of Tables

Acknowledgments

Honestly, nobody is more surprised to be reading this dissertation than I am. Here are some people who made possible what has for many years seemed to me an impossible proposition.

Professional

Well, first of all, there's Professor Clayton J. Radke. I still can't figure out how he does it, but he does it. Summarizing Clay would itself fill a dissertation, so suffice to say that I cannot imagine having a better experience completing my thesis work with any other advisor. Many thanks to Clay.

I've been tremendously fortunate to work with a number of talented undergraduates at Berkeley. If it were possible to include coauthors on a dissertation, I would without hesitation include Claire Bedbrook, whose brilliant analysis and tireless work ethic inspired me to greater heights. Thanks also to Yang Shirley Song and Crystal Lee for obtaining ellipsometry-adsorption and sulfuric-acid-assay data presented in Chapter 2; and to Neil Fajardo and Nick Brady for obtaining the QCM activity data presented in Chapters 3 and 4.

It has been a pleasure to interface with many capable colleagues in the Radke Lab over the years. Special thanks to Dr. Elisa Porcel and Dr. Ladan Foose for introducing me to the wonders of ellipsometry, and to soon-to-be-Dr. Colin Cerretani for always making me look like the normal one.

Material thanks to: Justin Virgili and Segalman Lab for helping obtain the AFM pictured in Chapter 2; Blandine Jerome and LBNL for helping characterize cellulose films; Eric Granlund for machine shop work; Dr. Tatyana Svitova for advice and mentorship; and many within the Energy Biosciences Institute for inspiring new directions in this work.

I am perpetually in awe of the Chemical Engineering department administration—Christine Balolong, Aileen Harris, Rocio Sanchez, and Fred Deakin, among many others. I can scarcely imagine the courage necessary to stare down campus bureaucracy on a daily basis. Thanks to the efforts of this wonderful staff, I never had to worry about where my next paycheck was coming from.

Which brings me around to say—This work was funded by the Energy Biosciences Institute. Thanks to EBI for putting food on my table and a QCM on my lab bench.

Personal

I first need to thank my mother, Deirdre DeAngelis; my boyfriend, Jeff Johnson; and my two best friends, Mitra Lohrasbpour and Shana Roth-Gormley. These four, working together, have been the pillars of my life, providing much-needed support on the many occasions when it seemed like the roof was about to fall in. God only knows where I'd be without them.

Other than that, I'd like to recognize all the treasured friends I've made over the years I've spent in Harrisburg, Boston, and San Francisco. There are so many people whose friendship has led me to this point in my life that I could never list them all without accidentally omitting someone. Thanks also to family (of the DeAngelis, Maurer, and Castro-going varieties).

Spiritual

I'd like to further thank the rainstorm that passed over Glacier National Park on July 17th, 2011, for reminding me that the sky is powerful and life is fragile; Heidi Swanson, for teaching me how to nourish the body and soul with natural cuisine; and Sufjan Stevens, for releasing *The Age of Adz* at just the right time.

Chapter 1

Introduction

1.1. Production of Biofuels from Lignocellulosic Feedstocks

As humanity depletes worldwide supplies of fossil fuels, biofuels derived from the deconstruction of large-scale agricultural crops offer a renewable alternative for numerous applications.[1 2 3] Although carbon-dioxide output of biofuel combustion relative to fossil fuels is an open question currently addressed by life-cycle analysis,[4 5] it is clear that fuel from agricultural feedstocks offers a renewable source of energy, while dwindling supplies of coal, natural gas, and oil are extracted from the Earth by increasingly destructive methods.[6] Currently, all industrial-scale biofuel production is accomplished by the enzymatic deconstruction of plant mass into glycans that are subsequently fermented to alcohols or processed to other fuel additives.[1 7] Typical large-scale biofuel efforts adopt a "one-pot" method, where microorganisms are contacted with an agricultural feedstock.[8 9] These microorganisms secrete enzymes to degrade the feedstocks, consume the glycans produced by their deconstruction, and produce desired fuel additives as a byproduct of this growth.[8]

Early efforts toward the production of fuels from plant sources used corn stover as a feedstock due to its wide availability.[10] However, corn is a water-intensive crop, and environmental concerns arose as arable agricultural land was used to grow feedstocks for biofuel production rather than food crops.[11] Current efforts focus on large-scale production of prairie grasses such as *Miscanthus x giganteus* and switchgrass (*Panicum virgatum)*.[12 13] These new crops grow tall, grow rapidly, require minimal input of water and fertilizer, and are resistant to disease.[14] As these sturdier crops can be grown on previously unusable land, agricultural land is no longer displaced.

With this advantage comes a tradeoff, as the increased rigidity and stability of these new feedstocks results in a higher resistance to degradation.[12] Prairie grasses such as *Miscanthus* consist primarily of three long-chain biopolymers—cellulose, hemicellulose, and lignin—thus coining the term "lignocellulosic feedstocks."[1 15] Separate suites of glycolytic enzymes are necessary to degrade each of these water-insoluble biopolymers.[16] Furthermore, these polymers are organized in extensive hydrogen-bonding networks that prohibit enzyme access.[15] Currently, feedstocks are pretreated using methods such as mechanical digestion,[17] acidification, or ammonia fiber-explosion[18] to disrupt the hydrogen-bonding superstructure and increase the enzyme-accessible surface area.[19]

Thus, there are many factors to consider in modeling industrial-scale biofuel production. The separate, simultaneous action of several classes of enzyme on the surface of several different water-insoluble biopolymers is necessary. Enzymatic deconstruction changes the surface area, degree of polymerization, and relative accessibility of these biopolymers. Oligosaccharides released into solution are known to be enzyme inhibitors.[20 21 22] Fermentation products and other desired compounds released into solution affect the stability of enzymes and microorganism cell walls.[23]

Of all factors, the fundamental rate-limiting step in the production of biofuels is the enzymatic deconstruction of cellulose into glycan oligomers that are subsequently processed into fuel additives.[1 2 3 6 24] Despite significant scientific effort and tremendous subsidy of biofuel production, the kinetics governing this fundamental surface reaction remain poorly understood. Current assays are limited, as most are performed in bulk solution, whereas the enzymatic deconstruction of cellulose is an interfacial interaction between an aqueous solution of enzymes and the surface of a solid, insoluble substrate.[25] This thesis utilizes surface-based assays to elucidate the kinetics of the principal interaction in biofuel production.

1.2. Enzymatic Deconstruction of Cellulose

Cellulose, the world's most abundant biopolymer, consists of long, nonbranching chains of glucose linked together by 1,4-β-glycosidic linkages.[26] These chains are then ordered together in a complex hydrogen-bonding network, typically in bundles of 36 – 42 known as microfibrils, which are further organized and bound with other biopolymers into rigid plant-cell-wall structures.[1 27] The strength of this hydrogen-bonding network makes cellulose insoluble in water and highly recalcitrant to enzymatic degradation.[26] Dissolving cellulose in water requires a temperature of 320 ºC and a pressure of 25 MPa.[28] Cellulose can also be dissolved and depolymerized in ionic liquids, although fuel production using this method has not been accomplished on an industrial scale.[29 30]

Enzymes that are active on cellulose are known as cellulases. Hundreds of distinct cellulases exist, synthesized by a variety of microorganisms including fungi, bacteria, and protozoa.[31] Complete degradation of cellulose requires the concerted action of two classes of enzyme on the cellulose surface.[32] Endoglucanases bind and complex nonspecifically on the cellulose surface and cleave 1,4-β-glycosidic linkages to produce chain ends that are lifted from the hydrogen-bonding network.[32] Cellobiohydrolases, sometimes known as exoglucanases, then complex with these chain ends and cleave individual bonds to produce oligosaccharides with degree of polymerization 2 – 6[33] that are subsequently released into aqueous solution.[32] Once in solution, these oligosaccharide products are further depolymerized by aqueous enzymes known as cellobiases or beta-glucosidases.[32]

Enzymes from both classes of surface-active cellulase (endoglucanases and cellobiohydrolases) typically consist of two domains, a larger catalytic domain (CD) and a smaller cellulose-binding domain (CBD), joined by a flexible glycosylated peptide linker.[34] Although there is considerable structural diversity among cellulases synthesized by different microorganisms,[31] enzymes from each class typically have some broad morphological similarities. The CD of endoglucanases resembles a cleft,[35] whereas the CD of cellobiohydrolases resembles a barrel.[36] The cellobiohydrolase barrel forms a complex with exposed chain-ends on the cellulose surface and cleaves the chain into oligosaccharides. A scission requires significant conformational change of the cellulose chain, induced by the interaction of at least four internal amino-acid residues with cellulose.[37] Once a cellobiohydrolase CD is complexed with a chain end, it typically works processively to degrade cellulose, keeping the cellulose chain in its binding barrel.[38 39] The CBD is the smaller of the two domains, and some surface-active cellulases lack a CBD entirely.[31 40] The mechanism of interaction between the CBD and the cellulose surface is not well-characterized. In many fungal cellulases, the interaction with the cellulose surface is known to be mediated by three critical tyrosine residues,[41 42] with possible involvement of tryptophan and glutamine residues.[43] The

interaction between the CBD and the cellulose surface has been described in different sources as both reversible[44] and irreversible.[42 45] Reversibility of the CBD-cellulose interaction may depend on the structure of the CBD and the identity of the cellulase.[31]

With hundreds of cellulases and cellulose feedstocks available for analysis, standardization of enzyme activity is necessary. Fungal cellulases, such as those from *T. reesei, T. longibrachiatum*, and *T. emersonii* are often used in studies of cellulase activity due to their high availability and applicability to industrial-scale production.[1 8 24 25 32 46] Avicel, a pure cellulose powder made from mechanically-ground steam-exploded spruce wood, is a laboratory standard for measuring cellulase activity, as observed degradation rates on Avicel typically correlate well with those measured on common industrial feedstocks.[32 47]

1.3. Challenges in Modeling Cellulose Deconstruction

Since cellulose is water-insoluble and cellulytic enzymes bind to its solid surface, the enzymatic deconstruction of cellulose is a surface-based process. However, until recently, only bulk assays were available to examine deconstruction kinetics.[25] Estimates of the enzyme-accessible surface area of Avicel range from 1 m^2 / g to 300 m^2 / g,[48 49] making it difficult to relate activity data measured in the bulk with surface activity.

The surface activity of an individual cellulase on the cellulose surface can be understood according to a four-step process:[32 50] (1) adsorption of the cellulase to the cellulose surface and interaction of the CBD with cellulose; (2) complexation of the enzyme CD with the cellulose surface; (3) enzyme activity, leaving the cellulase complexed; and (4) return of the cellulase to the adsorbed uncomplexed state. The cooperative activity of endoglucanases and cellobiohydrolases in creating and degrading cellulose chain ends can be further described from this basic framework. Extended kinetic models consider factors such as inhibition of cellulases by oligosaccharide products,[51 52] processive chain length of cellobiohydrolases,[53] 2-D surface diffusion of cellulases[54] and subsequent jamming of surface enzymes,[55] and the effect of crystallinity on cellulase activity.[56 57]

An outstanding problem in cellulose degradation is the phenomenon of kinetic slowdown.[58] After 12 – 24 h contact between the cellulase mixture and the cellulose surface, enzyme activity decreases significantly, often leaving large fractions of undegraded cellulose.[59] Low yield as a result of this kinetic slowdown is a major limitation in industrial biofuel production.[58] Several hypotheses exist for kinetic slowdown, including an increase in recalcitrance of the cellulose surface as cellulose is degraded,[60] denaturation/inactivation of surface cellulases,[61 62] or oligosaccharide product inhibition.[51] Surface-based assays are useful in evaluating each of these hypotheses.

1.4. Existing Surface-Based Research Into Cellulose Deconstruction

Recently, thin model films of cellulose adhered to glass and metal supports have become available.[63] These films offer a well-defined surface of known area on which cellulase adsorption and kinetics can be measured. A variety of synthesis methods are available to produce cellulose films of varying thickness and surface properties. Cellulose films can be synthesized via spin-coating of ionic-liquid-solvated cellulose[64] or trimethylsilylcellulose,[65] via Langmuir-Blodgett deposition from cellulose suspensions,[66 67] or by adhering high-crystallinity cellulose (*Valonia*, *Tunicin*, bacterial microcrystalline cellulose) directly to solid supports.[68]

These thin films of cellulose have been analyzed via ellipsometry,[69 70 71 72] quartz crystal microgravimetry,[73 74 75 76 77 78] atomic-force microscopy,[68 79 80] neutron reflectometry,[81] and Brewster-angle microscopy.[82]

Turon *et al*. utilized a quartz crystal microbalance (QCM) to measure enzyme activity on model cellulose films.[73] However, kinetic data were reported as a frequency shift and were not converted to a quantitative mass basis. Turon *et al*. do provide useful qualitative results for enzyme adsorption and cellulose deconstruction, as well as the impact of temperature on cellulase activity.[73] In a similar study, Josefsson *et al*. used QCM to explore the synergy between individual endoglucanases and cellobiohydrolases in degrading cellulose films.[74] These authors convert their results to a mass basis and report enzyme-adsorption data for endoglucanases. However, the remainder of their analysis is based on qualitative observation. Suchy *et al.* also use QCM to characterize endoglucanase and cellobiohydrolase activity on model amorphous cellulose films, finding degradation results to vary considerably with film preparation and crystallinity.[78] Gang *et al.* used QCM and neutron reflectometry in combination to explore qualitatively the penetration of fungal endoglucanases into amorphous cellulose films, finding that the CBD mediated film penetration.[81] Earlier, Erikkson *et al*. characterized enzyme activity via ellipsometry, studying the effect of pH, ionic strength, agitation, and temperature on cellulase reactivity. Again, their data are mainly qualitative and describe only total enzyme activity, not enzyme adsorption.[72] Ma *et al*. explored the relationship between cellobiohydrolase activity and irreversible binding.[83] Results, however, were limited to a single enzyme and did not explore the cooperative activity of endoglucanases and cellobiohydrolases.

1.5. Thesis

Despite progress in developing surface-based sensing techniques for cellulase activity, current literature results are preliminary. Surface-based assays offer continuous, non-invasive, inhibition-free tools for measuring enzyme kinetics. The goal of this thesis is to measure via surface-based assays the adsorption and cooperative activity of cellulases on a model cellulose surface and to devise a kinetic model for the cooperative enzymatic deconstruction of cellulose.

In Chapter 2, flow ellipsometry is used to quantify the adsorption and activity of a lyophilized mixture of cellulases from *T. reesei* on a model cellulose film. Enzyme activity on the model film is identical to that on the industry-standard Avicel, validating the quantitative results of the surface-based assay. Degradation rate and adsorption data are analyzed according to a single-enzyme kinetic model incorporating Langmuir kinetics to describe adsorption and Michaelis-Menten kinetics to describe the complexation and activity of adsorbed cellulase on the cellulose surface. This model is a coarse picture of cellulose deconstruction, as it considers all enzymes as having cellulytic activity and does not discriminate between endoglucanases and cellobiohydrolases. Further, the lyophilized mixture used to effect degradation is not well-characterized. Nevertheless, good agreement is shown between the transient kinetic model and measured ellipsometry data, thus establishing a "proof of concept" for the surface-based assay and modeling approach.

After demonstrating the viability of surface-based assays to measure, describe, and model cellulase activity on a cellulose surface, the cooperative action of isolated *T. longibrachiatum* cellobiohydrolase I (CBHI, Cel7A) and endoglucanase I (EGI, Cel7B) on model cellulose films is explored. As such isolated enzymes are commercially available only in much smaller quantities than the lyophilized mixture used in Chapter 2, a quartz crystal microbalance (QCM)

was used to measure degradation data. Due to a smaller flowcell, QCM study required 100 times less enzyme than ellipsometry study. Measured degradation rates were found to be identical between the two assays. This important finding confirms the viability of both assays, as ellipsometry is an optical technique that uses changes in the polarization and intensity of light to measure the mass of a thin film, while QCM is an acoustic technique that uses changes in the resonance of an oscillating quartz crystal to detect the mass and rigidity of a surface layer.

In Chapter 3, QCM is used to measure the competitive sorption of Cel7A and Cel7B on model cellulose films. Both enzymes show substantial fractions irreversibly bound on the cellulose surface after only 30 – 60 min of enzyme/surface contact. Sorption kinetics is analyzed according to a modified Langmuir adsorption model, where enzyme adsorbed to the cellulose surface can transition to an irreversibly bound state according to first-order kinetics. Although Cel7A has a higher affinity for the celluose surface, the first-order kinetic constants governing irreversible binding are identical. We hypothesize that irreversible adsorption is, therefore, a surface phenomenon mediated primarily by the interaction of the CBD with the cellulose surface.

In Chapter 4, these competitive sorption parameters are incorporated into the Langmuir-Michaelis-Menten kinetic model for enzyme activity. The cooperative activity of Cel7A and Cel7B on the cellulose surface, both at pseudo-steady-state and over short and long time scales is measured via QCM and described via this new kinetic model. Optimal ratios for Cel7A and Cel7B activity are determined. Again, good agreement is found between model and experiment. However, even this extended, two-enzyme kinetic model with irreversible adsorption remains a comparatively basic picture of cellulase activity on the cellulose surface, given the many factors affecting cellulose deconstruction listed in Section 1.3. Chapter 5 thus concludes by proposing future work to quantify other surface kinetic phenomena and thereby elucidate the activity of cellulases on the cellulose surface.

1.6. References

(1) Himmel, M.; Ding, S. Y.; Johnson, D. K.; Adney, W. S.; Nimlos, M. R.; Brady, J. W.; Foust, T.D. Biomass Recalcitrance: Engineering Plants and Enzymes for Biofuels Production. *Science* **2007**, *315,* 804-807.

(2) Kumar, R.; Singh, S.; Singh, O. V. Bioconversion of Lignocellulosic Biomass: Biochemical and Molecular Perspectives. *J Industrial Microbio and Biotech* **2008,** *35,* 377-391.

(3) Wyman, C. E. Ethanol from Lignocellulosic Biomass: Technology, Economics, and Opportunities. *Bioresource Technol*. **1994,** *50,* 3-16.

(4) Hill, J; Nelson, E.; Tilman, D; Polasky, S.; Tiffany, D. Environmental, Economic and Energetic Costs and Benefits of Biodiesel and Ethanol Biofuels. *Proc Nat Acad Sci USA* **2006,** *30,* 11206-11210.

(5) Von Blottnitz, G.; Curran, M. A. A Review of Assessments Conducted on Bio-ethanol as a Transportation Fuel from a Net Energy, Greenhouse Gas, and Environmental Life Cycle Perspective. *J Cleaner Production* **2007,** *15,* 607-619.

(6) Tester, J. W.; Drake E. M.; Golay M. W.; Driscoll, M. J.; Peters, W. A. Sustainable Energy: Choosing Among Options. Cambridge: MIT Press **2005**. Chapter 7.

(7) Taherzadeh, M. J.; Karimi, K. Enzyme-based Hydrolysis Processes for Ethanol from Lignocellulosic Materials: A review. *Bioresources* **2007,** *4,* 707-738.

(8) Lynd, L. R.; Weimer, P. J.; Van Zyl, W. H.; Pretorius, I. S. Microbial Cellulose Utilization: Fundamentals and Biotechnology. *Microbio and Mol Bio Rev* **2002,** *66,* 506-526.

(9) Houghton, J.; Weatherwax, S.; Ferrell, J. Breaking the Biological Barriers to Cellulosic Ethanol: A Joint Research Agenda. *US DOE,* DOE/SC-0095, **2005**.

(10) Bothast, R. J.; Schlicher, M. A. Biotechnological Processes for Conversion of Corn into Ethanol. *Appl Microbio Biotech* **2005,** *67,* 19-25.

(11) Pimentel, D.; Marklein, A.; Toth, M. A.; Karpoff, M. N.; Paul, G. S.; McCormack, R.; Kyriazis, J.; Krueger, T. Food Versus Biofuels: Environmental and Economic Costs. *Human Ecology* **2009,** *37,* 1-12.

(12) Heaton, A. E.; Dohleman, F. G.; Long, S. P. Meeting U.S. Biofuels with Less Land. *Global Change Biology* **2008,** *14,* 2000-2014.

(13) Somerville, C.; Youngs, H.; Taylor, C.; Davis, S. C.; Long, S. P. Feedstock for Lignocellulosic Biofuels. *Science* **2010,** *329,* 790-792.

(14) Parrish, D. J.; Fike, J. H. The Biology and Agronomy of Switchgrass for Biofuels. *Critical Reviews in Plant Sciences* **2005,** *24,* 423-459.

(15) Yoshida, M.; Liu, Y.; Uchida, S.; Kawarada, K.; Ukagami, Y.; Ichinose, H.; Kaneko, S.; Fukuda, K. Effects of Cellulose Crystallinity, Hemicellulose, and Lignin on the Enzymatic hydrolysis of Miscanthus Sinensis to Monosaccharides. *Biosci Biotech Biochem* **2008,** *72,* 805-810.

(16) Howard, R. L.; Abotsi, E.; Jansen van Rensburg, E. L.; Howard, S. Lignocellulose Biotechnology: Issues of Bioconversion and Enzyme Production. *Afr Journal Biotech* **2003,** *2,* 602-619.

(17) Mais, U.; Esteghlalian, A. R.; Saddler, J. N.; Mansfield, S. D. Enhancing the Enzymatic Hydrolysis of Cellulosic Materials Using Simultaneous Ball Milling. *Appl Biochem Biotech* **2002,** *98,* 815-832.

(18) Eggleman, T.; Elander, R. T. Process and Economic Analysis of Pretreatment Technologies. *Bioresource Tech* **2005,** *96,* 2019-2025.

(19) Yang, B.; Wyman, C. E. Pretreatment: the Key to Unlocking Low-Cost Cellulosic Ethanol. *Biofuels Bioprod Bioref* **2008,** *2,* 26-40.

(20) Xiao, Z. Z.; Zhang, X.; Gregg, D. J.; Saddler, J. N. Effect of Sugar Inhibition on Cellulases and beta-Glucosidase During Enzymatic Hydrolysis of Softwood Substrates. *App Biochem Biotech* **2004,** *113,* 1115-1126.

(21) Gruno, M.; Väljamäe, P.; Petterson, G.; Johansson, G. Inhibition of the *Trichoderma reesei* Cellulases by Cellobiose is Strongly Dependent on the Nature of the Substrate. *Biotech Bioeng* **2004,** *86,* 503-511.

(22) Qing, Q.; Yang, B.; Wyman, C. E. Xylooligomers Are Strong Inhibitors of Cellulose Hydrolysis by Enzymes. *Bioresource Tech* **2010,** *24,* 9624-9630.

(23) Zaldivar, J.; Nielsen, J.; Olsson, L. Fuel Ethanol Production from Lignocellulose: A Challenge for Metabolic Engineering and Process Integration. *App Microbio and Biotech* **2001,** *56,* 17-34.

(24) Macmillan, J. D. Bioethanol Production: Status and Prospects. *Renewable Energy* **1997,** *2-3,* 295-302.

(25) Bansal, P.; Hall, M.; Realff, M. J.; Lee, J. H.; Bommarius, A. S. Modeling Cellulase Kinetics on Lignocellulosic Substrates. *Biotech Advances* **2009,** *6,* 833-848.

(26) O'Sullivan, A. C. Cellulose*:* The Structure Slowly Unravels. *Cellulose* **1997,** *4,* 173-207.

(27) Pauly, M.; Albersheim, P.; Darvill, A.; York, W. S. Molecular Domains of the Cellulose/Xyloglucan Network in the Cell Walls of Higher Plants. *Plant Journal* **1999,** *20,* 629-639.

(28) Deguchi, S.; Tsujii, K.; Horikoshi, K. Cooking Cellulose in Hot and Compressed Water. *Chem Commun* **2006**, *31,* 3293-3295.

(29) Swatloski, R. P.; Spear, S. K.; Holbrey, J. D.; Rogers, R. D. Dissolution of Cellulose with Ionic Liquids. *J Am Chem Soc* **2002,** *18,* 4974-4975.

(30) Wang, Y.; Radosevich, M.; Hayes, D.; Labbe, N. Compatible Ionic Liquid-Cellulases System for Hydrolysis of. Lignocellulosic Biomass. *Biotech Bioeng* **2011,** *108,* 1042-1048.

(31) Beguin, P. Molecular-Biology of Cellulose Degradation. *Ann Rev Microbiol* **1990,** *44,* 219-248.

(32) Zhang, Y. H. P.; Himmel, M. E.; Mielenz, J. Outlook for Cellulase Improvement: Screening and Selection Strategies. *Biotech Advances* **2005,** *24,* 452-481.

(33) Gupta, R.; Lee, Y. Y. Mechanism of Cellulase Reaction on Pure Cellulosic Substrates. *Biotech Bioeng* **2008**, *102,* 1570-1581.

(34) Gilkes, N. R.; Henrissat, B.; Kilburn, D. G.; Miller, R. C.; Warren, R. A. J. Domains in Microbial Beta-1,4-Glycanases – Sequence Conservation, Function, and Enzyme Families. *Microbio Rev* **1991,** *55,* 303-315.

(35) Rouvinen, J.; Bergfors, T.; Teeri, T.; Knowles, J. K. C.; Jones, T. A. Three-Dimensional Structure of Cellobiohydrolase II from *Trichoderma reesei*. *Science* **1990,** *249,* 380-386.

(36) Divne, C.; Ståhlberg, J.; Reinikainen, T.; Ruohonen, L.; Pettersson, G.; Knowles, J. K. C.; Teeri, T. T.; Jones, T. A. The Three-Dimensional Crystal Structure of the Catalytic Core of Cellobiohydrolase I from *Trichoderma reesei*. *Science* **1994,** *265,* 524-528.

(37) André, G.; Kanchanawong, P.; Palma, R.; Cho, H.; Deng, X.; Irwin, D.; Himmel, M. E.; Wilson, D. B.; Brady, J. W. Computational and Experimental Studies of the Catalytic Mechanism of Thermobifida Fusca Cellulase Cel6A (E2). *Protein Eng* **2003,** *16*, 125-134.

(38) Kipper, K.; Väljamäe, P.; Johansson, G. Processive Action of Cellobiohydrolase Cel7A from *Trichoderma reesei* is Revealed as Burst Kinetics on Fluorescent Polymeric Model Substrates. *Biochem J*. **2005,** *385,* 527-535.

(39) Varrot, A.; Frandsen, T. P.; Von Ossowski, I.; Boyer, V.; Cottaz, S.; Driguez, H.; Schulein, M.; Davies, G. J. Structural Basis for Ligand Binding and Processivity in Cellobiohydrolase Cel6A from *Humicola insolens*. *Structure* **2003,** *11,* 855-864.

(40) Linder, M.; Teeri, T. T. The Roles and Function of Cellulose-Binding Domains. *J Biotech* **1997,** *57,* 15-28.

(41) Linder, M.; Mattinen, M. L.; Kontteli, M.; Lindeberg, G.; Stahlberg, J.; Drakenberg, T.; Reinikainen, T.; Pettersson, G.; Annila, A. Identification of Functionally Important Amino-Acids in the Cellulose-Binding Domain of *Trichoderma-reesei* Cellobiohydrolase I. *Protein Sci* **1995,** *4,* 1056-1064.

(42) Tavagnacco, L.; Mason, P. E.; Schnupf, U.; Pitici, F.; Zhong, L. H.; Himmel, M.E.; Crowley, M.; Cesaro, A.; Brady, J.W. Sugar-Binding Sites on the Surface of the Carbohydrate-Binding Module of Cel7A from *T. reesei*. *Carbohydrate Research* **2011,** *346,* 839-846.

(43) Bray, M. R.; Johnson, P. E.; Gilkes, N. R.; McIntosh, L. P.; Kilburn, D. G.; Warren, R. A. J. Probing the Role of Tryptophan Residues in a Cellulose-Binding Domain by Chemical Modification. *Protein Science* **1996,** *5,* 2311-2318.

(44) Linder, M.; Teeri, T. T. The Cellulose-Binding Domain of the Major Cellobiohydrolase of Trichoderma Reesei Exhibits True Reversibility and a High Exchange Rate on Crystalline Cellulose. *Proceedings of the National Academy of Sciences* **1996**, *93,* 12251-12255.

(45) Jung, H.; Wilson, D.B.; Walker, L.P. Binding and Reversibility of *Thermobifida fusca* Cel5A, Cel6B, and Cel48A and Their Respective Catalytic Domains to Bacterial Microcrystalline Cellulose. *Biotech Bioeng* **2003,** *84,* 151-159.

(46) Schuster, A.; Schmoll, M. Biology and Biotechnology of *Trichoderma*. *App Microbio and Biotech* **2010,** *87,* 787-799.

(47) Berlin, A.; Gilkes, N.; Kilburn, D.; Bura, R.; Markov, A.; Skomarovsky, A.; Okunev, O.; Gusakov, A.; Maximenko, V.; Gregg, D.; Sinitsyn, A.; Saddler, J. Evaluation of Novel Fungal

Cellulase Preparations for Ability to Hydrolyze Softwood Substrates – Evidence for the Role of Accessory Enzymes. *Enz Microb Tech* **2005,** *37,* 175-184.

(48) Lee, S.B; Shin, H.S.; Ryu, D. D. Y.; Mandels, M. Adsorption of Cellulase on Cellulose: Effect of Physicochemical Properties of Cellulose on Adsorption and Rate of Hydrolysis. *Biotechnol Bioeng* **1982**, *24,* 2137-2153.

(49) Abdmziem, K.; Passas, R.; Belgacem, M. N. Inverse Gas Chromatography as a Tool to Characterize the Specific Surface Area of Cellulose Fibers. *Cell Chem Technol* **2006,** *40,* 199-204.

(50) Zhang, Y. H. P.; Lynd, L. R. Toward An Aggregated Understanding of Enzymatic Hydrolysis of Cellulose: Noncomplexed Cellulase Systems. *Biotech Bioeng* **88,** *7,* 797-824.

(51) Holtzapple, M.; Cognata, M.; Shu, Y.; Hendrickson, C. Inhibition of *Trichoderma-reesei* Cellulase by Sugars and Solvents. *Biotech Bioeng* **1990,** *36,* 275-287.

(52) Gruno, M.; Väljamäe, P.; Pettersson, G.; Johansson, G. Inhibition of *Trichoderma reesei* Cellulases by Cellobiose is Strongly Dependent on the Nature of the Substrate. *Biotech Bioeng* **2004,** *86,* 503-511.

(53) Levine, S. E.; Fox, J. M.; Blanch, H. W.; Clark, D. S. A Mechanistic Model of the Enzymatic Hydrolysis of Cellulose. *Biotech Bioeng* **2010,** *107,* 37-51

(54) Liu, Y. S.; Zeng, Y. N.; Luo, Y. H.; Xu, Q.; Himmel, M. E.; Smith, S. J.; Ding, S. Y. Does the Cellulose-Binding Module Move on the Cellulose Surface? *Cellulose* **2009,** *16,* 587-597.

(55) Xu, F.; Ding, H. S. A New Kinetic Model for Heterogeneous (or Spatially Confined) Enzymatic Catalysis: Contributions from the Fractal and Jamming (Overcrowding) Effects. *App Cat A General* **2007,** *317,* 70-81.

(56) Hall, M.; Bansal, P.; Lee, J. H.; Realff, M. J.; Bommarius, A. S. Cellulose Crystallinity – a Key Predictor of the Enzymatic Hydrolysis Rate. *Febs Journal* **2010,** *277,* 1571-1582.

(57) Zhu, L.; O'Dwyer, J. P.; Chang, V. S.; Granda, C. B.; Holtzapple, M. T. Multiple Linear Regression Model for Predicting Biomass Digestibility from Structural Features. *Bioresource Tech* **2010,** *13,* 4971-4979.

(58) Bansal, P.; Vowell, B. J.; Hall, M.; Realff, M. J.; Lee, J. H.; Bommarius, A. S. Elucidation of Cellulose Accessibility, Hydrolysability and Reactivity as the Major Limitations in the Enzymatic Hydrolysis of Cellulose. *Bioresource Tech* **2012,** *107,* 243-250.

(59) Bommarius A. S.; Katona A.; Chebe S. E.; Patel, A. S.; Ragauskas, A. J.; Knudson, K.; Pu, Y. Cellulase Kinetics as a Function of Cellulose Pretreatment. *Metabol Eng* **2008**, *10,* 370-381.

(60) Chen, Y.; Stipanovic, A. J.; Winter, W. T.; Wilson, D. B.; Kim, Y. J. Effect of Digestion by Pure Cellulases on Crystallnity and Average Chain Length for Bacterial and Microcrystalline Celluloses. *Cellulose* **2007,** *14,* 283-293.

(61) Eriksson, T.; Karlsson, J.; Tjerneld, F. A Model Explaining Declining Rate in Hydrolysis of Lignocellulose Substrates with Cellobiohydrolase I (Cel7A) and Endoglucanase I (Cel7B) of *Trichoderma reesei*. *Appl Biochem Biotech* **2002,** *101,* 41-60.

(62) Zhang, Y.; Xu, J. L.; Xu, H. J.; Yuan, Z. H.; Guo, Y. Cellulase Deactivation Based Kinetic Modeling of Enzymatic Hydrolysis of Steam-Exploded Wheat Straw. *Bioresource Tech* **2010,** *101,* 8261-8266.

(63) Kontturi, E.; Tammelin, T.; Österberg, M. Cellulose—Model Films and the Fundamental Approach. *Chem Soc Rev* **2006,** *35,* 1287-1313.

(64) Gunnars S.; Wågberg L.; Stuart M. A. C. Model Films of Cellulose: I. Method Development and Initial Results. *Cellulose* **2002,** *9,* 239-249.

(65) Rehfeld, F.; Tanaka, M. Hydration Forces in Ultrathin Films of Cellulose. *Langmuir* **2003,** *19,* 1467-1473.

(66) Tammelin, T.; Saarinen, T.; Österberg, M.; Laine, J. Preparation of Langmuir/Blodgett-Cellulose Surfaces by Using Horizontal Dipping Procedure. Application for Polyelectrolyte Adsorption Studies Performed with QCM-D. *Cellulose* **2006,** *13,* 519-535.

(67) Habibi, Y.; Foulon, L.; Véronique, A. B.; Molinari, M.; Douillard, R. Langmuir-Blodgett Films of Cellulose Nanocrystals: Preparation and Characterization. *J Colloid Interface Sci* **2007,** *316,* 388-397.

(68) Nishiyama, Y.; Langan, P.; Chanzy, H. Crystal Structure and Hydrogen-Bonding System in Cellulose IB from Synchrotron X-ray and neutron Fiber Diffraction. *J Am Chem Soc* **2002,** *174,* 9074-9082.

(69) Maurer, S. A.; Bedbrook, C. N.; Radke, C. J. Cellulase Adsorption and Reactivity on a Cellulose Surface from Flow Ellipsometry. *I&ECR* **2012**. Under review.

(70) Gunnars S.; Wågberg L.; Stuart M. A. C. Model Films of Cellulose: I. Method Development and Initial Results. *Cellulose* **2002,** *9,* 239-249.

(71) Falt, S.; Wågberg, L.; Vesterlind, E. L.; Larsson, P. T. Model Films of Cellulose II - Improved Preparation Method and Characterization of the Cellulose Film. *Cellulose* **2004,** *11,* 151-162.

(72) Eriksson J.; Malmsten, M.; Tiberg, F.; Callisen, T. H.; Damhus, T.; Johansen, K. S. Enzymatic Degradation of Model Cellulose Films. *J Colloid Interface Sci* **2005,** *284,* 99-106.

(73) Turon X.; Rojas, O. J.; Deinhammer, R. S. Enzymatic Kinetics of Cellulose Hydrolysis: A QCM-D Study. *Langmuir* **2008,** *24,* 3880-3887.

(74) Josefsson P.; Henriksson G.; Wågberg L. The Physical Action of Cellulases Revealed by a Quartz Crystal Microbalance Study Using Ultrathin Cellulose Films and Pure Cellulases. *Biomacromolecules* **2008,** *9,* 249-254.

(75) Ahola, S.; Turon, X.; Österberg, M.; Laine, J.; Rojas, O J. Enzymatic Hydrolysis of Native Cellulose Nanofibrils and Other Cellulose Model Films: Effect of Surface Structure. *Langmuir* **2008,** 24, 11592 – 11599.

(76) Hu, G.; Heitmann, J. A.; Rojas, O. J. In Situ Monitoring of Cellulase Activity by Microgravimetry with a Quartz Crystal Microbalance. *J Phys Chem B*. **2009,** *113,* 14761-14768.

(77) Hu, G.; Heitmann, J. A.; Rojas, O. J. Quantification of Cellulase Activity Using the Quartz Crsytal Microbalance Technique. *Anal Chem* 2009, 81, 1872–1880.

(78) Suchy, M.; Linder, M. B.; Tammelin, T.; Campbell, J. M.; Vuorinen, T.; Kontturi, E. Quantitative Assessment of the Enzymatic Degradation of Amorphous Cellulose by Using a Quartz Crystal Microbalance with Dissipation Monitoring. *Langmuir* **2011,** *27,* 8819-8828.

(79) Andersen, M.; Johansson, L. S.; Tanem, B. S.; Stenius, P.; Properties and Characterization of Hydrophobized Microfibrillated Cellulose. *Cellulose* **2006,** *13,* 665-677.

(80) Mohan, T.; Kargl, R.; Doliska, A.; Vesel, A.; Kostler, S.; Ribitsch, V.; Stana-Kleinschek, K. Wettability and Surface Composition of Partly and Fully Regenerated Cellulose Thin Films from Trimethylsilyl Cellulose. *J Colloid Interface Sci* **2011,** *358,* 604-610.

(81) Cheng, G.; Datta, S.; Liu, Z.; Wang, C.; Murton, J.; Brown, P. A.; Jablin, M. S.; Dubey, M.; Majewski, J.; Halbert, C. E.; Browning, J. F.; Esker, A. R.; Watson, B. J.; Zhang, H.; Hutcheson, S. W.; Huber, D. L.; Sale, K. L.; Simmons, B. A.; Kent, M. S. Interactions of Endoglucanases with Amorphous Cellulose Films Resolved by Neutron Reflectometry and Quartz Crystal Microbalance with Dissipation Monitoring. *Langmuir* **2012.** In press.

(82) Habibi Y.; Foulon, L.; Aguie-Beghin, V.; Molinari, M.; Douillard, R. Langmuir-Blodgett Films of Cellulose Nanocrystals: Preparation and Characterization. *J Colloid Interface Sci* **2007,** *316,* 388-397.

(83) Ma, A.; Hu, Q.; Qu, Y.; Bai, Z.; Liu, W.; Zhuang, G. The Enzymatic Hydrolysis Rate of Cellulose Decreases with Irreversible Adsorption of Cellobiohydrolase I. *Enz Microb Tech* **2008**, *42(7)*, 543-547.

Chapter 2

Cellulase Adsorption and Reactivity on a Cellulose Surface from Flow Ellipsometry

2.1. Abstract

Enzymatic deconstruction of cellulose occurs at the aqueous/cellulose interface. Most assays to explore cellulase activity, however, are performed in bulk solution, and, hence, fail to elucidate surface-reaction kinetics. We use flow ellipsometry to quantify adsorption and surface reactivity of aqueous cellulase on a model cellulose-film substrate. The rate of cellulose digestion at the aqueous/solid interface increases with increasing bulk concentration of enzyme, but only up to a plateau corresponding to the maximum adsorption density of cellulase. Kinetic data are analyzed according to a modified Langmuir-Michaelis-Menten framework including both reversible adsorption of cellulase to the cellulose surface and complexation of surface cellulose chains with adsorbed cellulase. At ambient temperature, the molar turnover number is 0.57 ± 0.08 s^{-1}, commensurate with literature values, and the Langmuir adsorption equilibrium constant, characterizing the binding strength of the cellulase, is 0.086 ± 0.026 ppm^{-1}. The rate-determining step in the surface-reaction sequence is complexation of adsorbed cellulase with the solid-cellulose surface. Simultaneous knowledge of sorption and digestion kinetics is necessary to quantify cellulose deconstruction.

2.2. Introduction

Fuels derived from the decomposition of lignocellulosic biomass offer a renewable alternative to fossil fuels.[1 2 3 4 5] The accepted rate-determining step in the biological production of fuel from cellulosic feedstocks is the enzymatic cleavage of crystalline cellulose to produce sugars that are subsequently fermented to alcohols.[6 7] Despite the major economic and social impacts of biofuel deployment, kinetic parameters governing deconstruction of solid cellulose by aqueous cellulytic enzymes remain poorly characterized.[8 9]

Cellulose, a complex carbohydrate, is the most abundant biological polymer and a major building block of all plant life.[10] It is comprised of long, nonbranching chains of glucose monomers joined by 1,4-β-D-glycosidic linkages.[11] Elementary fibrils are comprised of approximately 40 of these chains held together by hydrogen bonds.[10] At least 6 possible conformations of cellulose chains within the elementary fibrils are possible depending on the conditions under which polymerization occurs.[10] Native cellulose found in plant-cell walls is composed of a heterogeneous mixture of at least two of these conformations.[10] Due to the strong internal hydrogen-bonded network, cellulose is highly crystalline in the center of its elementary fibrils, insoluble in water, and relatively intractable to enzymatic degradation.[7 10] The crystalline superstructure of cellulose is difficult to disrupt even under extreme reaction conditions: cellulose must be heated to 320 ºC at a pressure of 25 MPa to remove its crystallinity.[10] The complexity of the hydrogen bonding network within cellulose fibrils makes molecular modeling

difficult.[10] Recent studies have demonstrated successful solubilization and deconstruction of cellulose in ionic liquids.[12 13] Reaction in ionic liquid, however, appears economically infeasible given current technology.[14]

Presently, industrial-scale biofuel production employs cellulytic enzymes known as cellulases to deconstruct cellulose into fermentable sugars.[1] The term "cellulase" refers to any one of over 100 glucosidases that exhibit activity on cellulose or smaller glucose oligomers.[15] Cellulases are further classified into three major groups depending on their general function. Endoglucanases break hydrogen bonds and cleave glycosidic linkages within cellulose microfibrils, disrupting the crystal structure and exposing the ends of individual cellulose chains. Cellobiohydrolases hydrolyze the 1,4-β-D-glycosidic linkages that comprise the polymer backbone of cellulose, working at the ends of cellulose chains and producing oligomers consisting of 2-6 monosaccharides. Cellobiases then cleave the solubilized oligomeric reaction products completely into glucose monomers.[16] Mixtures of cellulases from all three classes work in concert to depolymerize solid cellulose completely into small aqueous oligomers and subsequently into glucose monomers.

Both endoglucanases and cellobiohydrolases consist of two primary domains: a catalytic domain (CD), where scission of cellulose bonds occurs, and a smaller cellulose binding domain (CBD) that attaches the cellulase to the cellulose surface. These two domains are connected by a flexible linker.[17] Cellulases have been synthesized with both deactivated catalytic sites and deactivated cellulose binding domains, allowing individual study of sorption and kinetic properties.[18]

Most kinetic studies of enzymatic-cellulose deconstruction utilize bulk assays,[8 16] and thus fail to recognize that cellulose cleavage occurs at the interface between the solid cellulose surface and an aqueous enzyme solution. Avicel, a steam-exploded, powdered microcrystalline cellulose produced from wood pulp, is a laboratory standard substrate for bulk assays, because its degradation rate is comparable to that of industrial cellulose feedstocks under similar reaction conditions[16]. Although numerous studies exist quantifying enzyme adsorption and reactivity on the surface of Avicel using solution depletion and other methods, [19 20 21 22] these measurements are limited because the surface of Avicel remains poorly defined. Estimates of the enzyme-accesible surface area of Avicel in water range from 1 m^2/g [23] to 300 m^2/g [24] and can change during digestion. A meaningful assay of enzyme kinetics at the aqueous/cellulose interface must operate on a well-defined and controlled surface.

Despite the importance of enzymatic cellulose degradation to biofuel production, relatively little is known about the actual mechanism of cellulase activity at the water/cellulose interface. Figure 2.1 portrays schematically a possible sequence of reaction steps. Cellulase, represented with its two domains separated by a linker, arrives at the surface by convective diffusion in series with sorption kinetics. It then complexes with cellulose surface chains and effects cleavage to produce scissioned oligomeric product. Thus, in addition to deconstruction kinetics, a complete picture of aqueous cellulase activity on a solid surface must consider enzyme adsorption, adsorption reversibility, possible surface-enzyme denaturation, and requisite changes in the surface area of the cellulose substrate during degradation. It is not possible to understand the detailed mechanism of cellulase catalysis of cellulose without considering surface behavior.

Some work is available describing the kinetics of cellulase activity via surface-based assays including quartz crystal microbalance (QCM),[18 25 26 27 28] ellipsometry,[29] and surface-plasmon resonance.[30] All cited studies, however, are qualitative in nature and do not separately

assess the role of enzyme adsorption equilibria and kinetics in the deconstruction process. We utilize flow ellipsometry to quantify adsorption and activity of cellulase on a flat, model cellulose surface.[25 26 27 28 29] Experimental isolation of enzymatic activity from adsorption on an insoluble cellulose substrate is challenging. By inhibiting the cellulytic enzyme, we ascertain adsorption/desorption kinetics independent from the reaction kinetics. Incorportation of adsorption kinetics leads to a Langmuir-Michaelis-Menten enzyme-catalysis model[31] for cellulose digestion. For the first time, we ascertain quantitative estimates of all kinetic parameters characterizing the reaction sequence pictured in Figure 2.1.

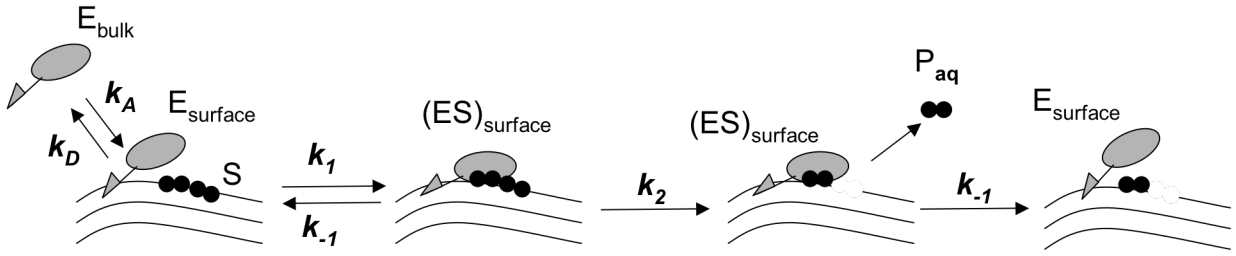

Figure 2.1. Illustration of the modified Langmuir-Michaelis-Menten kinetic sequence to describe the enzymatic degradation of cellulose. Cellulase is represented by an oval (active domain) and a triangle (cellulose binding domain). Light lines represent surface cellulose chains. Filled black circles represent monomeric subunits of the cellulose chain that are complexed with the cellulase active site and subsequently released from the cellulose surface as oligomeric products. Several degradation events (governed by k_2) can occur for each decomplexation event (governed by k_1). All surface-complexed enzymes, $(ES)_{surface}$, decomplex at the same rate, as illustrated on the far right of the figure.

2.3. Materials and Methods

2.3.1. Preparation of Cellulose Films

Several methodologies exist to produce isotropic model films of cellulose adhered to a variety of substrates.[32 33 34] These films offer well-defined, flat surfaces on which kinetic activity can be quantified. Here, thin cellulose films were deposited on silicon surfaces after the method of Gunnars *et al.*[33] A 5.28-g aliquot of powdered 4-methylmorpholine-N-oxide (4MMO; Sigma Aldrich #224286, 97% purity) was heated with 1.32 mL of distilled/deionized water (Millipore QGARD00R1, Billerica, MA, USA) in a round-bottom flask under magnetic stirring at 85 ºC until an opaque brown liquid formed. To this liquid mixture, 210 mg of Avicel microcrystalline cellulose (Sigma Aldrich #11363) were added, and the solution was heated at 103 ºC for 1 h. The solution was removed from heating, and 1.8 mL of dimethylsulfoxide (DMSO; Sigma Aldrich #D5879, 99.5%) were added to reduce solution viscosity. As noted in Falt *et al.*, decreasing the

viscosity of the cellulose solution decreased the coating thickness of the subsequent thin cellulose films.[34] After the addition of DMSO, the solution was cooled to ambient temperature.

Standard Test Grade Silicon wafers, 475 - 575 μm in thickness, were obtained from International Wafer Services (Colfax, CA, USA). Wafers were cut into 17 mm x 17 mm squares, dried under nitrogen flow, and plasma-cleaned (Harrick PDC-32G; Pleasantville, NY, USA) to remove surface organic residue. The wafers were subsequently soaked for 30 min in a 0.5% w/w solution of poly-diallyl-dimethyl-ammonium chloride (PDADMAC; Sigma-Aldrich #409030, sold as a 20% w/w aqueous solution), which functioned as a cationic polymer anchor between the silicon surface and the cellulose film. After deposition of the anchor polymer layer, wafers were washed in distilled/deionized water for 15 min and subsequently dried.

The cooled cellulose solution was deposited on the prepared silicon wafers by spin coating (Laurel Technologies WS-400B-6NPP/LITE; North Wales, PA, USA) at 5000 rpm for 1 min. Coated wafers were further washed in distilled/deionized water for 12 h without agitation and dried under nitrogen flow.

2.3.2. Cellulases

We utilized a lyophilized mixture of cellulases from the fungus *Trichoderma reesei* (Sigma Aldrich #C8546) consisting of endoglucanases, cellobiohydrolases, and cellobiases. This mixture exhibits approximately equal endoglucanase and cellobiohydrolase activity.[35] The endoglucanses and cellobiohydrolases in this mixture have similar domain structures, molecular weights of 55 ± 10 kDa, and dimensions of approximately 15 x 5 x 10 nm.[36 37] Accordingly, in this work, we treat the cellulase mixture as pseudo-single component. Because disappearance of the cellulose is measured rather than appearance of oligomeric product, the presence of cellobiase plays no active role in the resulting deconstruction kinetics.

2.3.3. Flow Ellipsometry for Cellulose Degradation

The thickness and refractive index of the thin cellulose films were measured with a single-wavelength ellipsometer (Sentech SE-400; Berlin, Germany) utilizing a helium-neon laser operating at a wavelength of 623.8 nm and a 70-degree angle of incidence. This configuration is typical for ellipsometric measurement of polymeric films.[38] A cellulose-coated silicon wafer was placed into a custom-built flow cell. The dimensions of this flowcell are given by Foose *et al*.[31] The flow cell was subsequently filled with a 9.5-mM NaH_2PO_4 buffer solution (pH 5.5; Sigma-Aldrich #S9638). The cellulose film swelled upon exposure to buffer solution; a steady-state thickness was reached after approximately 3 h, typically at 2 – 3 times the thickness of the dry film.

In a typical kinetic-degradation experiment, after swelling, a buffered cellulase solution of desired concentration was flowed over the cellulose-coated wafer for two or more hours, during which time the thickness and refractive index of the cellulose film were measured continuously. Nascent buffer was then flowed over the wafer to remove remaining surface enzyme and loosely bound scission products. A nominal flow rate of 8 mL / min was used, corresponding to a surface shear rate of about 0.25 s^{-1}. All experiments were performed at 25 °C.

Raw transient ellipsometry data (psi and delta)[38] were processed by Sentech SE401 modeling software on a two-layer optical model. The PDADMAC anchor layer was set at a thickness of 2 nm and a refractive index of 1.520, ascertained from the average of several dry ellipsometry measurements. For the outer layer, consisting of cellulose and adsorbed cellulase, thickness and refractive index were calculated continuously for each data point. In a typical

experiment, the refractive index varied by less than 1% from its initial value throughout enzyme adsorption and film degradation.

2.3.4. Flow Ellipsometry for Cellulase Adsorption

To measure cellulase adsorption dynamics independent of cellulose degradation, D-(+)-Glucose (Sigma Aldrich #G5767) was added to the aqueous enzyme solutions. Glucose is an inhibitor of cellulase, preventing not only deconstruction activity, but also complexation with the cellulose substrate.[39] For inhibition studies, lyophilized cellulase was added to a 6000-ppm aqueous solution of glucose in NaH_2PO_4 buffer solution, a ratio of approximately 100 to 1000 parts glucose to 1 part enzyme by mass. Various ratios of glucose inhibitor to aqueous cellulase were tested; the ratio of 100 parts glucose to 1 part cellulase was the lowest glucose concentration at which no enzyme activity was observed. Higher glucose concentrations produced identical cellulase adsorption histories. As with the non-inhibited assay, cellulose films were allowed to swell to a steady-state thickness in 6000-ppm glucose solution before the cellulase-glucose solution was injected into the cell.

2.3.5. Sulfuric-Acid Assay

To validate the ellipsometric surface-kinetic assay, comparison was made to the well-established sulfuric-acid assay.[40] Samples of a 350-ppm suspension of powdered Avicel cellulose were prepared by mixing 3.5 mg of cellulose with 10 mL of 9.5-mM NaH_2PO_4 buffer solution and agitating mechanically in a vortexer for 24 h. Concentrated 1000- to 6000-ppm aqueous solutions of *T. reesei* cellulase in buffer were added to achieve the desired bulk cellulase concentration. The resulting reaction mixture was stirred for 90 min at 360 rpm (ca. 0.1 s^{-1} shear rate based on a nominal particle diameter). Unreacted cellulose was then removed by centrifuging at 2500 rpm for 90 s and decanting the clear supernatant comprised of buffer, enzyme, and aqueous reaction products.

A 500-μL aliquot of each supernatant mixture was collected in a scintillation vial, after which 2 mL of concentrated sulfuric acid (Sigma-Aldrich #435589) and 500 μL of phenol (Sigma-Aldrich #P3653, 99% purity) were added. The solution was agitated for 20 min and transferred to a spectrophotometer cuvette. Under these reaction conditions, all oligomeric products of cellulose degradation are depolymerized into monomeric glucose and functionalized into an aromatic derivative that absorbs at 490 nm. To quantify the aqueous reaction products liberated from the cellulose surface over the 90-min reaction time, absorbance was measured and compared with a calibration curve prepared from aqueous glucose solutions of known concentrations.

2.4. Results

2.4.1. Characterization of Cellulose Films

Typical cellulose films prepared for this study exhibited an average dry thickness of 137.2 ± 2.7 nm and an average refractive index of 1.64 ± 0.02, commensurate with the values described by Gunnars *et al.*[33] Films swell to approximately twice their dry thickness when exposed to buffer, suggesting penetration of buffer solution into the matrix of the cellulose-film coating. As discussed below, the increased film water content does not, however, permit cellulase penetration into the cellulose film. The average refractive index of buffer-swollen films was 1.41 ± 0.01.

Figure 2.2 displays atomic-force-microscopy images of two typical cellulose films. The micrograph in Figure 2.2a shows an initially prepared dry film prior to degradation by cellulose. Nascent films exhibit features on the order of 300 nm in width, whereas the size of a cellulose microfibril is 30 nm.[10] This suggests that the dissolution in 4MMO and subsequent deposition of cellulose preserves features of the superstructure of cellulose. The film pictured in Figure 2.2b was exposed to a 12-ppm aqueous solution of cellulase for 4 h at ambient temperature. Degraded films display a loss in resolution of the 300-nm features and a rougher surface filled with crevasses. The calculated RMS roughness of the film increased from 24.3 ± 3.1 nm before enzymatic degradation to 47.2 ± 2.2 nm after enzymatic degradation. Both roughness values are an order of magnitude smaller than the wavelength of the laser used for ellipsometric measurement (632.8 nm), confirming the viability of ellipsometry as an assay tool for these cellulose films.[41]

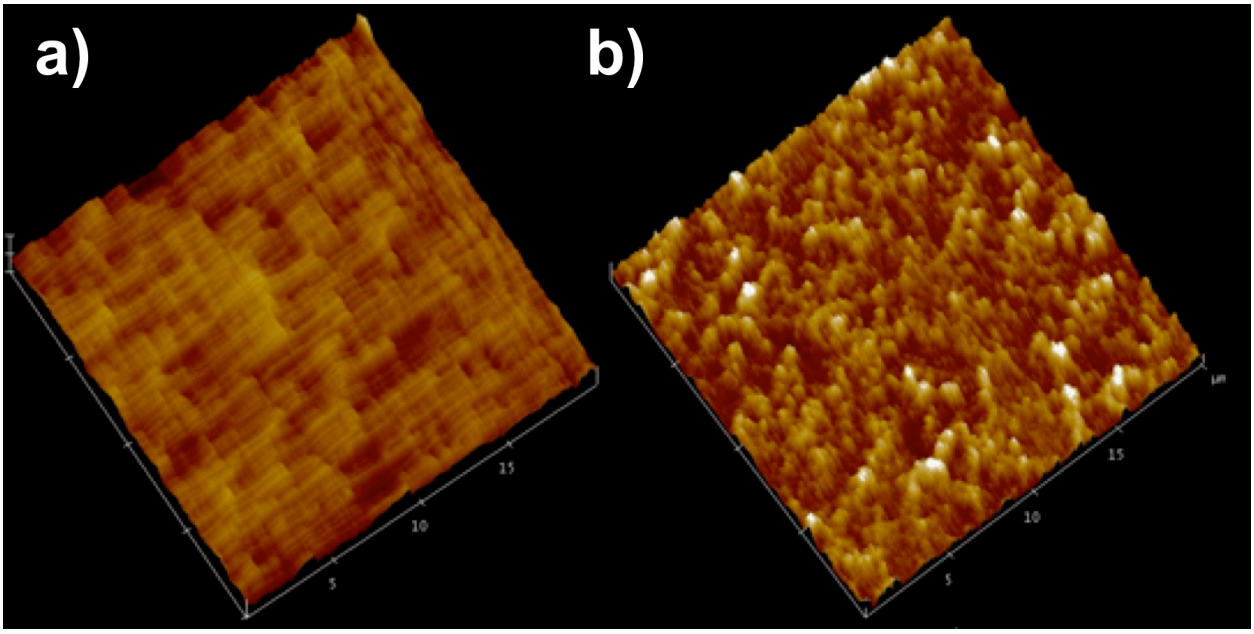

Figure 2.2. Atomic-force-microscopy (AFM) images of cellulose films in tapping mode. a) before degradation; b) after 2 h degradation by 12-ppm lyophilized cellulase from *T. reesei*. Width = 20 μm x 20 μm. Height scale = 200 nm.

Following Gollapalli *et al.*,[42] the index of crystallinity for cellulose, CI, was quantified via x-ray diffraction according to

$$CI = \frac{I_{002} - I_{am}}{I_{am}} \times 100 \quad , \qquad (2.1)$$

where I_{002} and I_{am} represent the absorbances of the material at angles of incidence of $2\Theta = 18°$ and 22.5°, respectively, and correspond to the scattering angles for crystalline and amorphous

cellulose.[42] The crystallinity index of Avicel was 58 ± 2%, whereas the crystallinity index of the cellulose films was 42 ± 4%. The crystallinity index of films exposed to cellulase for 2 h was 42 ± 3%. Accordingly, enzymatic degradation of cellulose films over this time scale did not preferentially degrade crystalline cellulose versus amorphous cellulose. The constant crystallinity throughout degradation suggests that the *T. reesei* enzymes digest the cellulose film at the external surface and not throughout the film interior.

2.4.2. Deconstruction Kinetics

Figure 2.3 shows a typical thickness history of a thin cellulose film, as measured by continuous-flow ellipsometry, during deconstruction over a period of 3 h in a 62-ppm solution of cellulase in NaH_2PO_4 buffer. Following Figure 2.1, stages of enzyme adsorption, film degradation, and enzyme desorption upon washing with buffer are labelled. Film thickness initially increases as the cellulases adsorb to and complex with the cellulose substrate surface. Following adsorption and complexation, degradation of the film is evident. During the degradation stage, the slope of the thickness reaches a constant negative value, indicating a constant rate of film deconstruction. Crevasses in the AFM image shown in Figure 2.2b suggest that enzyme reactivity is not perfectly isotropic. Rather, the degradation rate represents an average over the surface area measured by the ellipsometer, approximately 1 mm x 1 mm. After 2 h of degradation, buffer solution was flowed over the film, desorbing surface enzyme and washing away remaining surface deconstruction products. The amount of enzyme desorbed during washout is close to that initially adsorbed.

The slope of the linear portion of Figure 2.3 represents the overall rate of cellulose degradation in nm / h for a constant surface enzyme concentration at a given bulk cellulase concentration (62 ppm in Figure 2.3). Experiments performed with shear rate increased by a factor of five showed no discernable effect of increased flow rate. Thus, mass-transfer resistance pictured in Figure 2.1 is minimal in the ellipsometric flow cell. This conclusion was confirmed by comparing the overall rate of degradation to that predicted by Lévêque theory for the mass transfer coefficient[43] using the known shear rate in the ellipsometry flow cell (0.25 s^{-1}) and an estimated enzyme diffusion coefficient (10^{-6} cm^2/s) Thus, the linear-period slope of the thickness history quantifies the surface kinetics of cellulose deconstruction.

Kinetic rates of cellulose degradation were measured for varying bulk cellulase concentrations and converted from a thickness basis (nm / h) to a mass basis (mg cellulose / m^2 h) using an assumed density of 1.46 g / cm^3.[33] Our cellulose films degrade completely, leaving only the PDADMAC anchor layer, after exposure to cellulase for 24 – 48 h. This observation contradicts the work of Turon *et al.*, who suggest that a layer of intractable cellulose remains after degradation of spin-coated cellulose films.[18]

Figure 2.4 plots the measured mass-basis cellulose degradation rates as a function of bulk cellulase concentration (open squares). Degradation rates initially increase with bulk cellulase concentration, but eventually reach a plateau. Increasing cellulase concentration beyond 60 ppm no longer increases the rate of cellulose degradation. In contrast to the results in Figure 2.4, the classical Michaelis-Menten kinetic model predicts a strict linear rise with bulk enzyme concentration.[44] The asymptotic behavior shown in Figure 2.4 is consistent with surface-controlled enzyme reactivity on a solid substrate, where surface-coverage limitations restrict enzyme availability.[31]

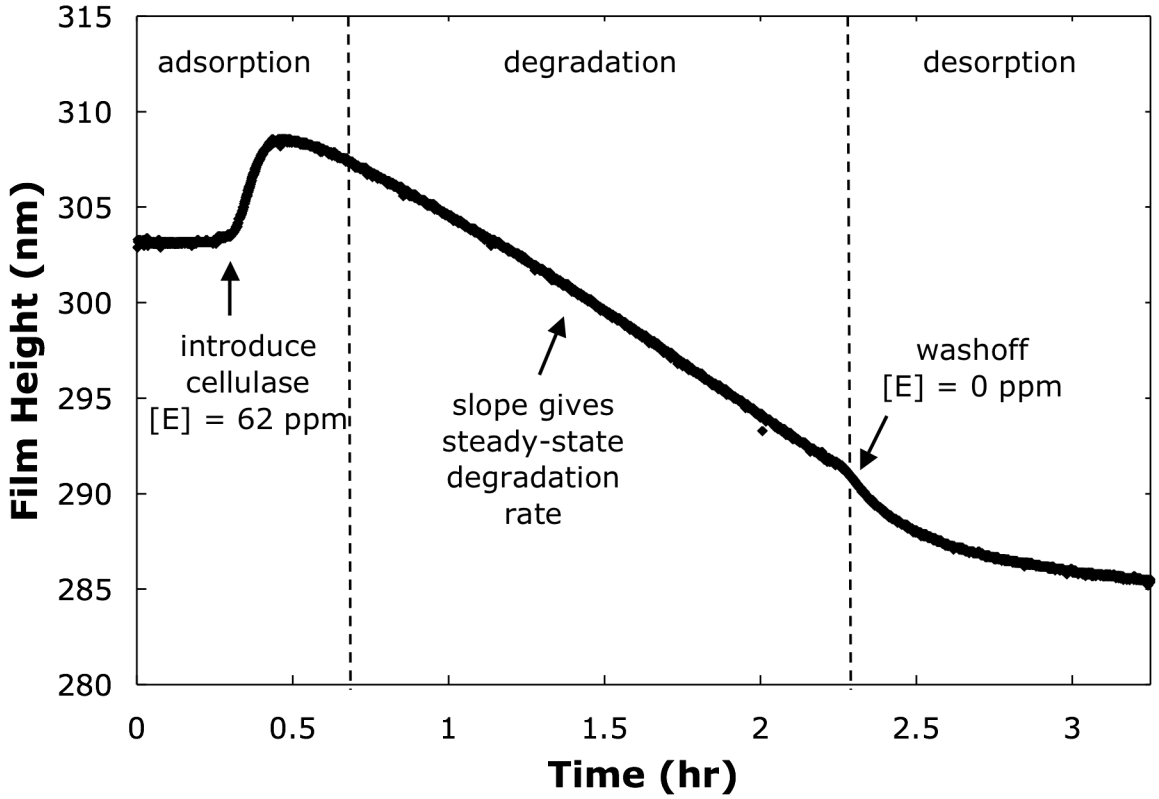

Figure 2.3. Enzyme adsorption, degradation, and desorption, measured via flow ellipsometry with 62- ppm lyophilized cellulase from *T. reesei* at 25 ºC.

To assess specifically the validity of our flow-elipsometry deconstruction rates for spin-coated cellulose films, the bulk sulfuric-acid assay was also used to measure enzymatic degradation of Avicel, in mg / h, at several aqueous bulk enzyme concentrations. Possible mass-transfer rate limitations in the bulk assay were assessed by varying stirring speeds over a factor of five (300 – 1500 rpm), which produced no discernible effect on degradation rate. Thus, mass transport to and from the cellulose surface was not rate limiting in either assay.

Degradation rates from the sulfuric-acid assay were converted to a per-unit-area basis, using an average surface area of 3.4 m^2 / g Avicel, measured via BET analysis. These values were then plotted against the bulk concentration of cellulase. Figure 2.4 compares the mass-per-unit-area degradation rates measured by the sulfuric-acid assay (filled circles) to those measured by ellipsometry (open squares). It is important to distinguish between the fundamental quantities measured by the two assays. The sulfuric-acid assay measures the appearance of reaction products in solution, whereas the flow-ellipsometric assay measures disappearance of the solid substrate. Nevertheless, the two assays are in excellent agreement when compared on a per-unit-area basis. This result not only validates the surface assay, but also confirms that the deconstruction reaction occurs at the external cellulose interface. We find no evidence for penetration of the enzymes into the spin-coated cellulose film. Results in Figure 2.4 mean that our spin-coated cellulose films degrade at rates identical to those of Avicel, the accepted

substrate standard. The bulk sulfuric-acid assay, however, provides no information on enzyme surface concentration and kinetics, and does not allow continuous measurement.

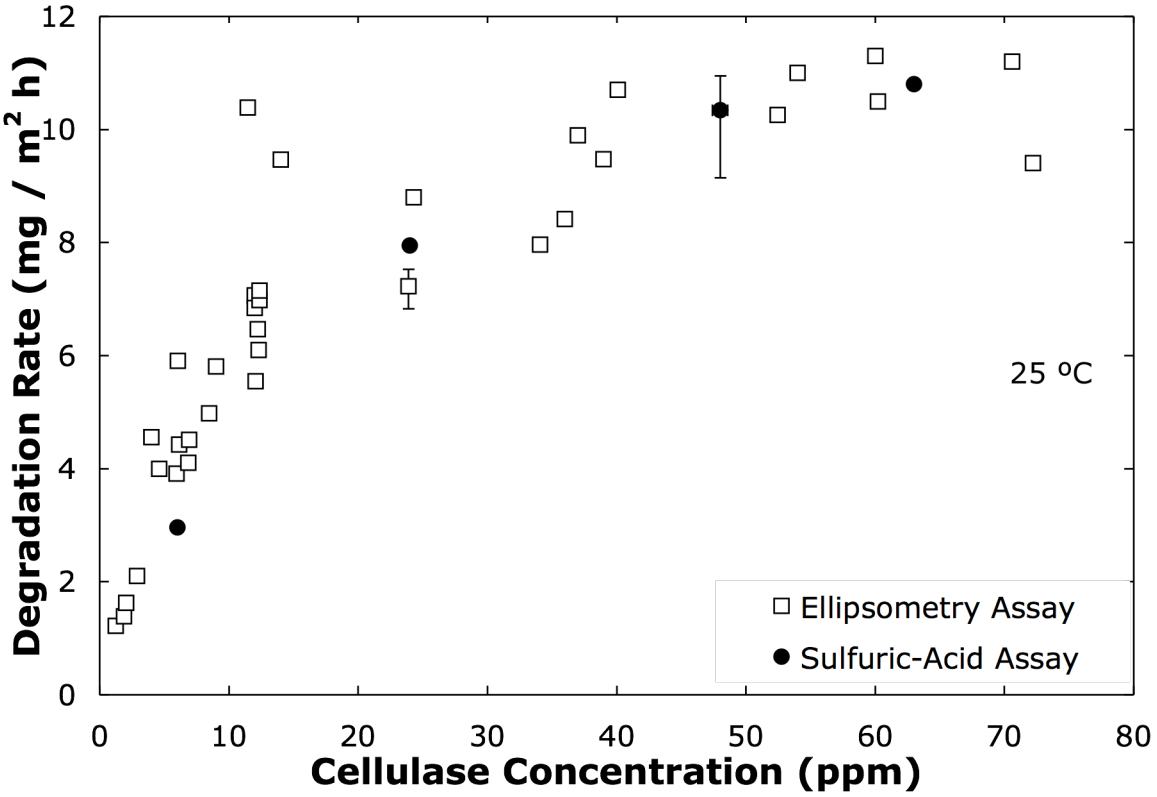

Figure 2.4. Cellulose degradation rate in mg / m^2 h as measured by flow ellipsometry on a thin cellulose film (open squares) and by sulfuric-acid assay on Avicel (closed circles) plotted against bulk enzyme concentration. Lyophilized cellulase from *T. reesei* at 25 ºC. Typical error bars shown.

2.4.3. Adsorption Kinetics

A typical flow-ellipsometric result for enzyme adsorption under glucose inhibition is shown in Figure 2.5. Adsorption of lyophilized cellulase to the model cellulose film substrate reaches equilibrium after about 1 h. Return of the film to its initial thickness after washing with buffer also establishes the reversibility of the adsorption process when total exposure time to the surface is 2 h or less.

Figure 2.6 compares transient adsorption measured under glucose inhibition to transient adsorption and degradation measured in the absence of glucose at 24-ppm enzyme concentration in buffer. Both curves follow identical adsorption trajectories over the first 0.25 h of measurement. We did observe glucose adsorbing from 6000-ppm solution to the cellulose film

surface, producing a height response of about 0.2 nm. However, the important result in Figure 2.6 indicates that glucose does not compete with cellulase for surface sites, prevent cellulase from adsorbing to the surface, or otherwise affect the adsorption properties of cellulase when deployed as an inhibitor to cellulase complexation and activity. Thus, glucose inhibition of the active site of cellulase does not affect the sorption properties, apparently because the binding domain primarily controls adsorption. Deviation of the two curves thereafter is attributed to cellulose degradation, which occurs when no glucose is present in solution (see discussion of Figure 2.3). Leveling of the adsorbed amount for the deactivated cellulase over the time frame of 0.5 h further confirms the inability of the enzyme to penetrate the coated-cellulose film.

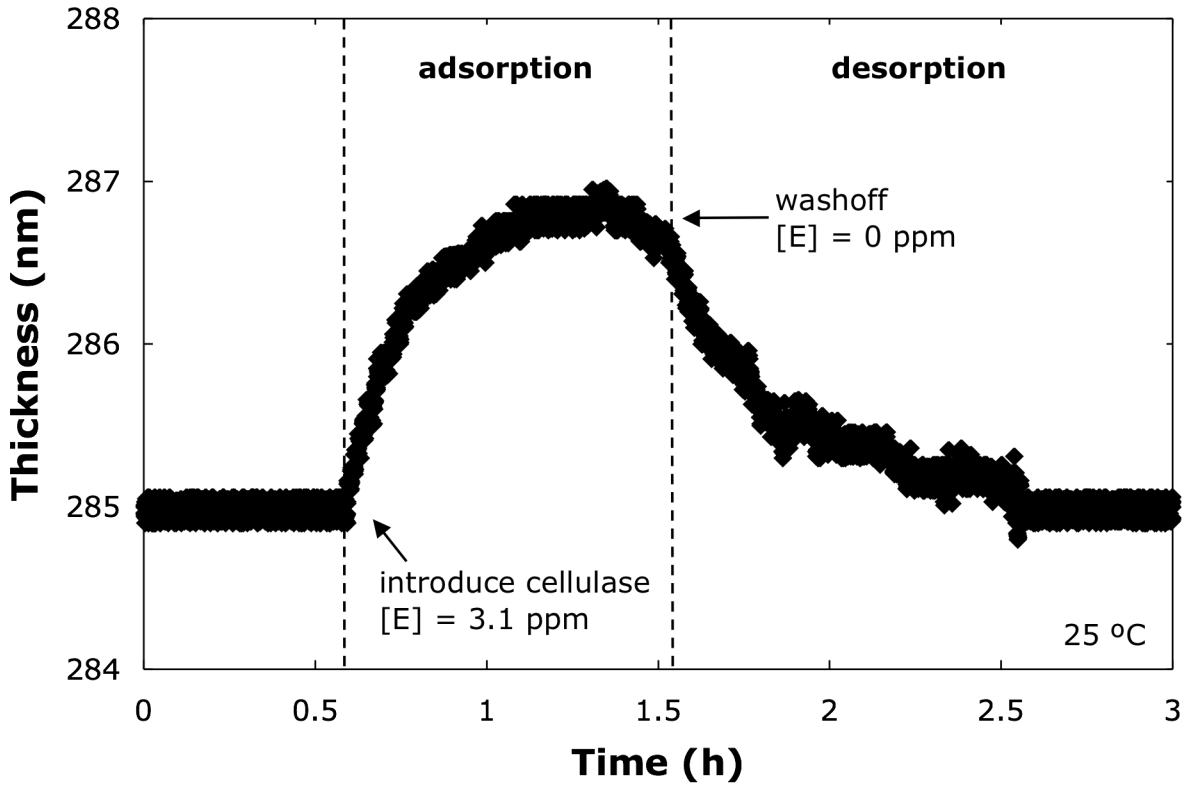

Figure 2.5. Adsorption and desorption kinetics of cellulase, as measured by ellipsometry. 3.1-ppm lyophilized cellulase from *T. reesei* under inhibition by 6000-ppm glucose at 25 ºC.

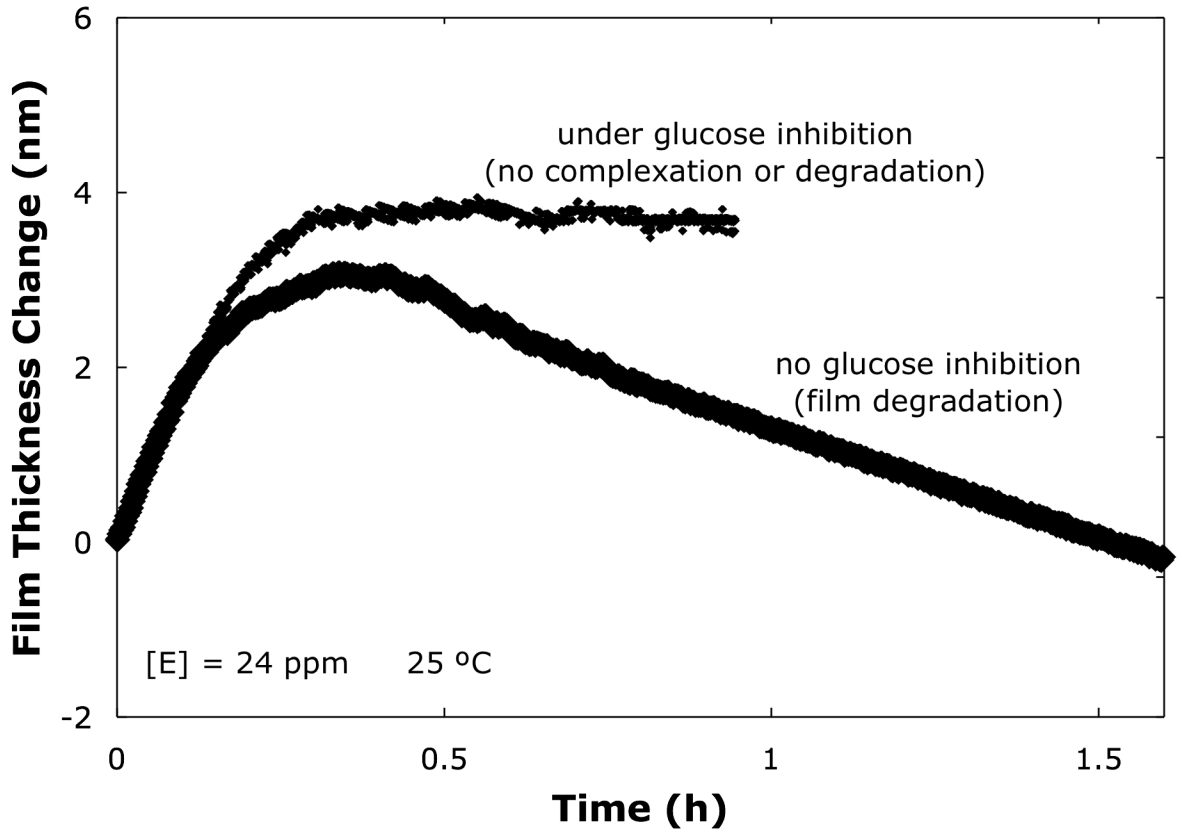

Figure 2.6. Adsorption of cellulase measured under 6000 ppm glucose inhibition compared to adsorption and activity of noninhibited cellulase, measured by flow ellipsometry. Data represent film-thickness deviations from two separate baselines established in two separate experiments. 24-ppm lyophilized cellulase from *T. reesei* under inhibition by 6000-ppm aqueous glucose at 25 ºC.

Enzyme surface concentration, in units of enzyme mass per substrate surface area, was quantified from the thickness histories using the formula of de Feijter:[45]

$$\Gamma = \frac{h(n_f - n_w)}{dn/dc} \quad , \tag{2.2}$$

where h and Γ represent the adsorbed-enzyme thickness and surface concentration of enzyme, while n_f and n_w, respectively, represent the indices of refraction of the film and aqueous solution. The refractive index of the film was taken as 1.410, and the ambient refractive index for the buffer solution was 1.333, equal to that of water. The "de Feijter constant", dn/dc, a property of the enzyme in bulk solution, was set at 0.183 cm^3 / g, typical for aqueous-enzyme systems.[45]

Figure 2.7 displays the equilibrium cellulase adsorption isotherm on solid cellulose. Similar to the cellulose degradation rates in Figure 2.4, these data show that cellulase equilibrium adsorption increases linearly with bulk enzyme concentration for small concentrations, but eventually reaches an asymptote. In the plateau region, increasing bulk cellulase concentration

no longer increases cellulase adsorption. This finding is consistent with a surface-based model of cellulase activity where cellulose adsorption is limited by a fixed density of surface sites. Thus, degradation rates reach an upper limit in Figure 2.4 as adsorption reaches maximum coverage. In the adsorption-plateau region, higher solution concentrations of enzyme do not increase deconstruction rates because the surface is fully occupied by enzyme. Thus, enzyme bulk concentration does not control the deconstruction rate. Rather, the surface concentration of enzyme dictates that rate. Based on the geometry of a cellulase molecule (15 x 5 x 10 nm)[36], monolayer coverage corresponds to approximately 9.8 mg / m^2. Observation of submonolayer coverage is inconsistent with significant cellulose penetration into the deposited cellulose film.

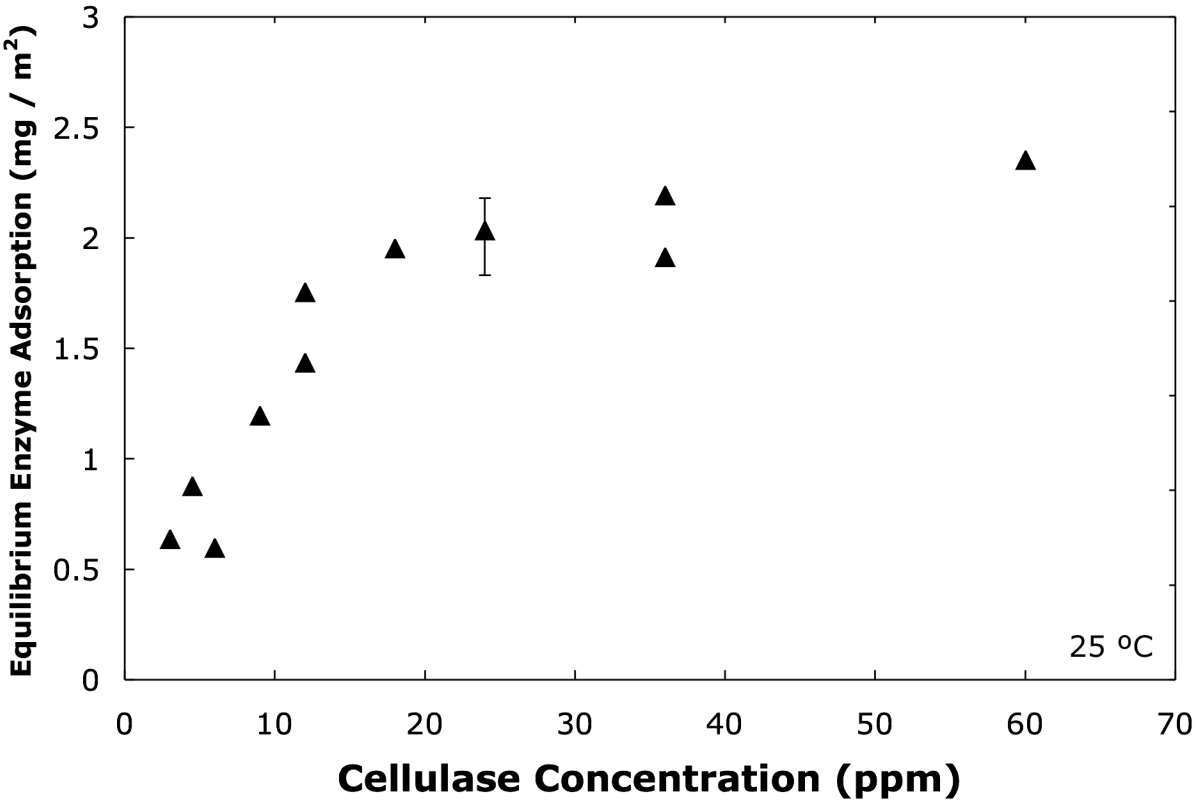

Figure 2.7. Equilibrium adsorption isotherm of cellulase on solid cellulose plotted against bulk cellulase concentration. Lyophilized cellulase from *T. reesei* under inhibition by 6000-ppm aqueous glucose at 25 ºC. Typical error bar is shown.

2.5. Theory

The kinetic data presented in Figure 2.4 demonstrate that enzyme activity on a solid cellulose surface reaches a plateau corresponding to the adsorption plateau in Figure 2.7. In traditional Michaelis-Menten kinetics[44], substrate concentration, not enzyme concentration, limits activity. Although considerable effort has been directed towards kinetic modeling of enzymatic deconstruction of cellulose,[8 39 46 47 48 49 50 51 52 53] with few exceptions[54 55], current models of cellulase activity on cellulose do not quantify the observed surface-coverage limitation of rate.

2.5.1. Kinetic Model

To quantify the results in Figures 2.4 and 2.7, we present a modified Michaelis-Menten rate expression for enzymatic degradation of cellulose including Langmuir adsorption behavior. Based on the experimental findings discussed above, we neglect diffusion into and enzymatic deconstruction within the cellulose film. Since external mass-transfer resistance is negligible, our proposed Langmuir-Michaelis-Menten (LMM) kinetic model, illustrated in Figure 2.1, accounts for four processes in the interaction between aqueous enzyme and a digestible solid substrate: (1) adsorption of aqueous enzyme to the solid surface; (2) formation of an enzyme-substrate complex between an adsorbed enzyme molecule and the solid substrate; (3) surface reaction liberating product from the solid surface into solution; and (4) return of the complexed enzyme to the uncomplexed adsorbed state. Measured degradation kinetics are areal. Based on the constancy of degradation rate and surface roughness during continued digestion, we assume that new underlying substrate is unveiled to the aqueous/cellulose surface during deconstruction. We do not account for molecular-weight change of the surface chains during reaction,[47 54 56] nor do we discriminate between endoglucanases and cellobiohydrolases.

Figure 2.1 summarizes the proposed cellulose-deconstruction model. The first step is the adsorption of cellulase to the cellulose surface, shown in Figure 2.5 and in the literature to be reversible for low exposure times.[57] Thus, provided exposure time to the surface is small, the cellulose-binding domain reversibly attaches to and detaches from the cellulose surface. We characterize sorption kinetics according to the Langmuir model,[58]

$$E_{bulk} + [open\ site] \underset{k_D}{\overset{k_A}{\rightleftarrows}} E_{surface} \quad . \tag{2.3}$$

Thus, the rate of adsorption, r_A, is proportional to the bulk cellulase concentration, $[E]$, and to the surface concentration of open adsorption sites, Γ_O, according to an adsorption rate constant, k_A:

$$r_A = k_A[E]\Gamma_O \quad . \tag{2.4}$$

Likewise, the rate of desorption, r_D, is proportional to the surface concentration of adsorbed cellulase, Γ_E, according to a rate constant, k_D,

$$r_D = k_D\Gamma_E \quad . \tag{2.5}$$

Once adsorbed to the cellulose substrate surface, cellulase has the potential to draw a cellulose chain into its active site, forming an enzyme/substrate complex. This step requires the interaction of several functional groups within the cellulase reaction barrel with the cellulose

chain, forcing significant conformational change in the substrate. We assume this step is reversible, as in the typical Michaelis-Menten kinetic model:

$$E_{surface} + S \underset{k_{-1}}{\overset{k_1}{\rightleftharpoons}} ES_{surface} \quad , \tag{2.6}$$

where S is a surface cellulose chain end available for complexation with cellulase enzyme. The rate of complexation, r_C, is proportional to the surface concentration of cellulase, Γ_E, and to the surface concentration of available cellulose chains, Γ_S, according to the complexation rate constant, k_1:

$$r_C = k_1 \Gamma_E \Gamma_S \quad , \tag{2.7}$$

where the surface concentration of the cellulose chains is assumed constant, as discussed above. Similarly, the rate of decomplexation is first-order in the surface concentration of complexed enzyme, Γ_{ES}, according to the decomplexation rate constant k_{-1}.

$$r_{DC} = k_{-1} \Gamma_{ES} \quad . \tag{2.8}$$

Cleavage occurs within the enzyme/substrate complex and a glucose oligomer is released from the cellulose surface. Once released, oligomeric cleavage products enter into the aqueous phase. Any re-adsorption of cleavage products is neglected. The rate of cleavage for this process, r_{CL}, is proportional to the surface concentration of enzyme-substrate complex, Γ_{ES}, according to the rate constant k_2:

$$ES_{surface} \xrightarrow{k_2} ES_{surface} + P \quad , \tag{2.9}$$

with

$$r_{CL} = k_2 \Gamma_{ES} \quad . \tag{2.10}$$

Note in Equation 2.9 and in Figure 2.1 that we do not distinguish between surface-complexed cellulase states with different chain lengths in the active site. All surface-complexed cellulase states have equal probability of returning to the uncomplexed state. After cleavage, the enzyme remains complexed with the cellulose chain. Later, it reverts to the adsorbed uncomplexed state in obedience to Equation 2.8. Finally, adsorption site conservation demands that

$$\Gamma_{\max} = \Gamma_E + \Gamma_{ES} + \Gamma_O \quad , \tag{2.11}$$

where $\Gamma_{\max}$ is the maximum surface concentration of adsorbed enzyme.

Three mass balances describe the change in the surface concentrations of enzyme and enzyme-substrate complex and the rate of release of oligosaccharide products from the cellulose surface. Equations 2.4, 2.5, 2.7, 2.8, 2.10, and 2.11 provide the rate laws for these balances:

$$\frac{d\Gamma_E}{dt} = k_A [E](\Gamma_{\max} - [\Gamma_E + \Gamma_{ES}]) - k_D \Gamma_E - k_1 \Gamma_E \Gamma_S + k_{-1} \Gamma_{ES} \quad , \tag{2.12}$$

$$\frac{d\Gamma_{ES}}{dt} = k_1\Gamma_E\Gamma_S - k_{-1}\Gamma_{ES} \quad , \qquad (2.13)$$

and

$$\frac{dP}{dt} = k_2\Gamma_{ES} \quad . \qquad (2.14)$$

In Equation 2.14, *dP/dt* represents the mass rate of aqueous product formation per unit area, which is necessarily equal to the mass rate of degradation of cellulose per unit area. Once parameters k_A, k_D, $k_1\Gamma_S$, $k_{-1,}$ k_2, and Γ_{max} are specified, Equations 2.12 – 2.14 are solved numerically by a Runge-Kutta algorithm to predict aqueous cellulase adsorption onto and reactivity with the solid cellulose surface.

2.5.2. Kinetic Parameters

The proposed modified LMM kinetic model was applied to the data obtained from our surface-based flow-ellipsometric assay to determine values for the kinetic parameters appearing in Equations 2.12 – 2.14 above. First, adsorption and desorption rate constants, k_A and k_D, were determined from equilibrium and kinetic adsorption data obtained under glucose inhibition, as in Figures 2.5 – 2.7. As glucose inhibits not only cellulase activity but also the formation of the enzyme-substrate complex,[39] these data represent the processes of cellulase adsorption to and desorption from the cellulose surface unencumbered by complex formation and cellulose deconstruction. Accordingly, Equation 2.12 reduces to Langmuir kinetics of adsorption and desorption,

$$\frac{d\Gamma_E}{dt} = k_A[E](\Gamma_{\max} - \Gamma_E) - k_D\Gamma_E \quad . \qquad (2.15)$$

The Langmuir equilibrium constant is defined as $K_L = k_A / k_D$. Thus, the equilibrium surface concentrations of cellulase, $\Gamma_{E,eq}$, at each bulk cellulase concentration were fit to the Langmuir isotherm in Figure 2.7 ,

$$\frac{\Gamma_{E,eq}}{\Gamma_{\max}} = \frac{K_L[E]}{1 + K_L[E]} \quad , \qquad (2.16)$$

to give $K_L = 0.086 \pm 0.026$ ppm^{-1} and the maximum adsorption of cellulase as $\Gamma_{max} = 2.9 \pm 0.2$ x 10^{-3} g / m^2.

Transient desorption data, such as those shown in Figure 2.5, were then used in conjunction with Equation 2.15 (upon setting *[E]* = 0) to determine the desorption rate constant $k_D = 0.14 \pm 0.05$ h^{-1}. Consequently, given the value of K_L, the adsorption rate constant was specified as $k_A = 1.7 \pm 0.4$ ppm^{-1} h^{-1}.

It remains to determine the surface kinetic rate constants. The typical flow-ellipsometry result shown in Figure 2.3 illustrates that the cellulose-degradation rate is constant after approximately 45 min of contact between cellulase and the cellulose film, corresponding to the pseudo-steady-state rate of oligomeric product formation $[dP/dt]_{PSS}$. Equation 2.14 reveals that the rate of cellulose degradation is constant in time only when the surface concentration of enzyme-substrate complex, Γ_{ES}, is also constant in time. Equation 2.13 then demands that the

surface enzyme concentration, Γ_E, is also constant. Consequently, Equations 2.12 – 2.14 yield in the pseudo-steady state

$$\left[\frac{dP}{dt}\right]_{PSS} = \frac{k_2 k_1 \Gamma_S \Gamma_{\max} K_L [E]}{k_{-1} + K_L [E](k_{-1} + k_1 \Gamma_S)} \quad . \qquad (2.17)$$

This expression represents the rate of cellulose degradation at equilibrium cellulase adsorption as a function of bulk cellulase concentration, *[E]*, corresponding to the measured deconstruction rates in Figure 2.4. The pseudo-steady-state LMM kinetic model of Equation 2.17 successfully predicts the trends in the experimental kinetic data in Figure 2.4. For small values of bulk cellulase concentration, the rate of cellulose degradation increases linearly with bulk cellulase concentration. Conversely, for large values of bulk cellulase concentration, the cellulose degradation rate reaches an upper limit. In this limit, increasing bulk concentration of cellulase no longer increases the corresponding enzyme surface concentration, and, hence, no longer increases the rate of deconstruction. Using surface concentration in the digestion kinetics therefore explains the observed leveling of kinetic rate at higher solution enzyme concentration.

Remaining kinetic parameters were then determined from Equation 2.17 in the limits of low bulk enzyme concentration and of high bulk enzyme concentration, respectively:

$$\left(\left[\frac{dP}{dt}\right]_{PSS}\right)_{[E]\Rightarrow 0} = k_2 \left(\frac{k_1 \Gamma_S}{k_{-1}}\right) K_L \Gamma_{\max} [E] \qquad (2.18)$$

and

$$\left(\left[\frac{dP}{dt}\right]_{PSS}\right)_{\max} = k_2 \frac{\left(\frac{k_1 \Gamma_S}{k_{-1}}\right)}{1 + \left(\frac{k_1 \Gamma_S}{k_{-1}}\right)} \Gamma_{\max} \quad . \qquad (2.19)$$

We obtain two lumped kinetic parameters, shown in parentheses on the right of Equations 2.19 and 2.20: the turnover number, $k_{cat} = k_2$, representing the rate of cellulose cleavage per unit mass enzyme attached to the surface; and the complexation equilibrium constant $K_C = k_1 \Gamma_S / k_{-1}$. Equations 2.19 and 2.20 were fit to the experimental rate data to give the mass-basis turnover number for cellulase $k_{cat} = 4.2 \pm 0.6 \times 10^{-3}$ s^{-1} and the cellulase complexation equilibrium constant $K_C = 0.54 \pm 0.05$. Table 2.1 summarizes the fit parameters obtained by applying our single-enzyme modified LMM kinetic model to the flow-ellipsometry data. The physical significance of these parameters is discussed in the following section.

2.5.3. Comparison to Experiment

Given the fit parameters, Equations 2.16 and 2.17 predict the cellulase equilibrium adsorption and the pseudo-steady-state cellulose degradation rate as functions of bulk enzyme concentration. Figure 2.8 compares the predicted behaviors with experimental data. The proposed LMM model shows good agreement with experimental data, both for the kinetics of digestion and the adsorption amounts. Again the direct correlation between deconstruction rate and surface concentration of enzyme is clear in Figure 2.8.

Table 2.1. Kinetic parameters for the Langmuir-Michaelis-Menten kinetic model.

k_A	$ppm^{-1}\ h^{-1}$	1.7 ± 0.4
k_D	h^{-1}	0.14 ± 0.05
K_L	ppm^{-1}	0.086 ± 0.026
Γ_{max}	g / m^2	$2.9 \pm 0.2 \times 10^{-3}$
K_C	[unitless]	0.54 ± 0.05
$K_1\Gamma_S$	h^{-1}	1.6 ± 0.3
k_{-1}	h^{-1}	3.0 ± 0.4
$K_2 = k_{cat}$	(g product) / (g cellulose s)	$4.2 \pm 0.6 \times 10^{-3}$
$k_{cat,mol}$	(mol cellobiose) / (mol cellulase s)	0.57 ± 0.08

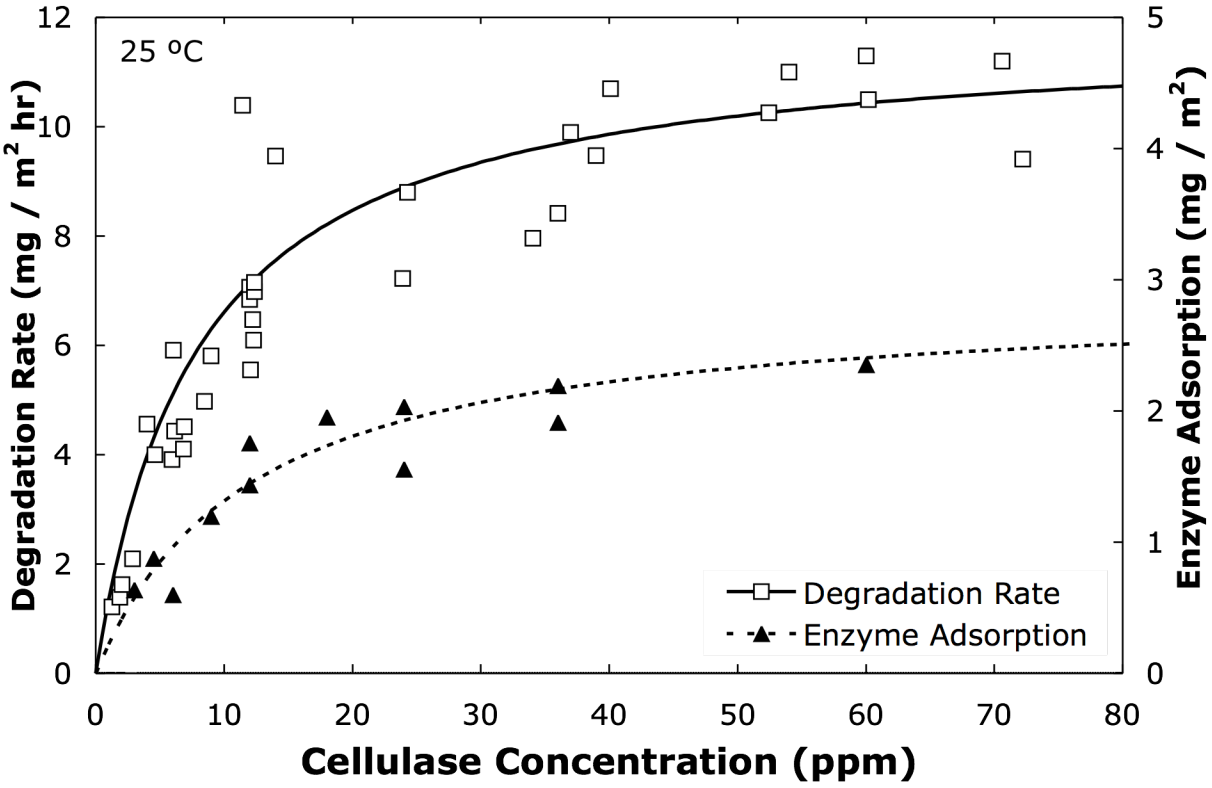

Figure 2.8. Degradation rate of cellulose (open squares, left axis, mg deconstructed / m^2 hr) and equilibrium surface adsorption of cellulase (filled triangles, right axis, mg adsorbed / m^2) plotted against bulk cellulase concentration. Modified LMM kinetic model shown as lines. Lyophilized cellulase from *T. reesei* at 25 ºC. Adsorption measured in a 6000-ppm solution of glucose.

We also used our modified-LMM framework and the associated kinetic parameters to predict complete transient cellulase reactivity on a solid model cellulose film. In this case, it is necessary to estimate $k_1\Gamma_S$ and k_{-1} separately, not only their ratio. Due to the major conformational change of both enzyme and substrate necessary to effect degradation, cellulases are slow to decomplex from cellulose chains.[59] Many chain scissions occur before the active site decomplexes. We assume a processive length of 50 cellobiose units; that is, 50 chain scissions occur before a chain-decomplexation occurs. This means that $k_{-1} = k_2 / 50$. Typical estimates in the literature range from 10 – 100 units.[60] Figure 2.9 compares a typical flow-ellipsometry result with a cellulose film thickness calculated from the full transient kinetic model. The extended LMM model shows good agreement with the transient flow-ellipsometry data, particularly from 0 – 0.5 h where transient adsorption and film degradation occur simultaneously. Thus, the proposed LMM kinetic model successfully describes cellulase adsorption and activity at a cellulose surface in both pseudo-steady-state and transient regimes. Note that the ratio k_2 / k_{-1} is the only condition imposed upon our model. All other parameters come from independent experiments; no chosen parameters are necessary to achieve this good agreement between experiment and model. Furthermore, the model is not sensitive to the choice of ratio between k_2 and k_{-1}. Selecting nominal values of 10, 50, 100, and 1000 units produced equivalent results.

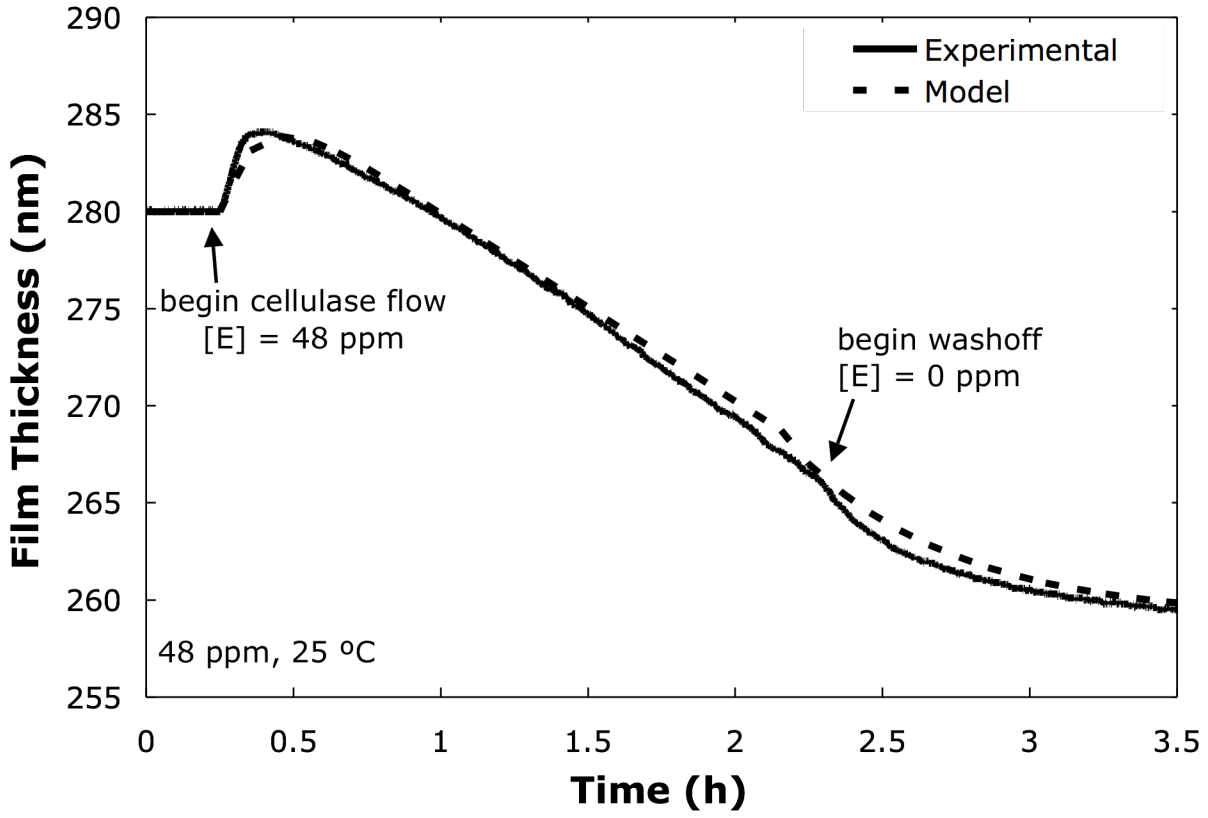

Figure 2.9. Comparison of experimental cellulose-film-degradation flow-ellipsometry data (solid line) to transient prediction of Langmuir-Michaelis-Menten kinetic model (dashed line), at 48.0-ppm bulk enzyme concentration. Lyophilized cellulase from *T. reesei* at 25 ºC.

2.6. Discussion

Based on agreement with the well-established sulfuric-acid assay, cellulase activity on our model thin cellulose films measured by flow ellipsometry is commensurate with activity on Avicel, which is the literature standard for cellulase activity. Our flow-ellipsometry data also show good agreement with the preliminary work completed by Eriksson *et al.*,[29] where a similar ellipsometry technique employed thin cellulose films synthesized according to the same protocol. Similar cellulose films were utilized in the work of Turon *et al.*[18] and Hu *et al.*[27] who presented similar qualitative results. No quantitative comparison can be made to our work, as the quartz-crystal-microbalance data presented in those studies were not converted to a mass basis. Our model cellulose films degrade completely after exposure to high concentrations of cellulase for 24 – 48 h, leaving only the PDADMAC anchor layer. Ahola *et al.* report a similar finding for spin-coated cellulose films.[28]

It is difficult to compare directly the results of our kinetic analysis to those found in the literature, as little effort has been made to quantify simultaneous cellulase adsorption and reactivity on a cellulose substrate. Some work, however, has been completed using bulk assays to establish a turnover number for cellulase. Our mass-basis turnover number, $k_{cat} = 4.2 \pm 0.6 \times 10^{-3}\ s^{-1}$, was transformed to a molar basis by assuming an average cellulase molecular weight of 55000 g / mol and degradation of the cellulose film only into cellobiose dimers (molecular weight 343 g / mol). The resulting value, $k_{cat,mol} = 0.57 \pm 0.08\ s^{-1}$, represents the average number of cellulose chain cleavages by a single bound cellulase molecule per second, and is commensurate with values obtained for other enzymes such as chymotrypsin ($k_{cat,mol} = 0.17\ s^{-1}$)[61]. Our turnover-number result is also on the same order of magnitude as those of Holtzapple *et al.* ($k_{cat,mol} = 0.43\ s^{-1}$)[39] and Bommarius *et al.* ($k_{cat,mol} = 0.22\ s^{-1}$)[19]. These studies do not separately account for adsorption. Therefore, if an enzyme is attached to the cellulose surface only via its binding domain, it is counted as "complexed" according to the criteria used in these studies. Here, binding-domain attachment is attributed to adsorption and not complexation. This distinction might account for the higher turnover number in our study, since fewer cellulase molecules on the surface are defined as complexed.

The maximum surface enzyme concentration, $\Gamma_{max} = 2.9 \pm 0.2 \times 10^{-3}\ g / m^2$ falls within physical bounds for cellulase adsorption based on the assumed geometry of the cellulase molecule (15 x 5 x 10 nm)[36 37]. As a lower bound, a sparsely packed "excluded rod" configuration was considered, where each cellulase molecule, upon reaching the surface, occupies a 15 nm-diameter circle that no other cellulases can occupy. The surface concentration of cellulase in this configuration was $\Gamma_{max,excluded} = 0.8 \times 10^{-3}\ g / m^2$. As an upper bound, a densely packed "2-D liquid crystal" configuration was assumed, with cellulases completely covering the cellulose surface. The cellulase surface coverage in this configuration was $\Gamma_{max,crystal} = 9.8 \times 10^{-3}\ g / m^2$. The experimentally determined maximum surface coverage thus falls between these two bounds. Our maximum cellulase surface density is also commensurate with Josefsson *et al*, who report a maximum surface concentration of $\Gamma_{max} = 3.7 \times 10^{-3}\ g / m^2$ for an inactivated endoglucanase.[25]

From the rate constants listed in Table 2.1, we find that complexation of adsorbed cellulase with cellulose chains is the rate-limiting step in enzymatic cellulose deconstruction. Once the enzyme-substrate complex is formed, the enzyme works efficiently to degrade the cellulose surface. Although this rate-limiting step has been acknowledged in recent cellulose

degradation literature,[60] our work represents the first major step to quantify the relative rates of each surface process via a surface-based assay.

2.7. Conclusions

A surface-based flow-ellipsometry assay for cellulase activity is established to quantify enzymatic degradation kinetics on a solid cellulose substrate. New deconstruction kinetic data are analyzed according to an extended Langmuir-Michaelis-Menten kinetic model pertinent to cellulose digestion at the aqueous/solid interface. Obtained kinetic constants agree with those for similar enzymes; the obtained turnover number is also similar to those obtained via other kinetic models. Raw kinetic data are in excellent agreement with cellulose-degradation data obtained from the standard sulfuric-acid assay as well as from similar assays conducted in the literature. The extended LMM kinetic theory accurately predicts the degradation of a thin cellulose film as measured by ellipsometry. We, thus, demonstrate the validity of the surface-based flow-ellipsometry assay for quantifying cellulase adsorption and activity on solid cellulose films. This exercise accentuates the need for simultaneous measurement of digestion and sorption kinetics to quantify enzymatic deconstruction rates of cellulose.

The LMM kinetic model presented, however, remains a coarse description of molecular cellulase activity on a cellulose surface. We have lumped all cellulases into a single representative enzyme acting on cellulose to produce oligosaccharide products. In reality, the concerted action of endoglucanases and cellobiohydrolases to create and degrade chain ends is necessary to depolymerize fully the cellulose surface. Effort should be directed towards establishing the kinetics of separate cellulases individually and in known mixtures.

2.8. List of Symbols

h : Film thickness, nm
n : Refractive index
dn/dc : Refractive index increment, cm^3 / g
$[E]$: Bulk enzyme concentration, ppm
Γ_S : Surface concentration of cellulose, g / m^2
Γ_E : Surface concentration of adsorbed, uncomplexed cellulase, g / m^2
$\Gamma_{E,eq}$: Surface concentration of adsorbed, uncomplexed cellulose at equilibrium, g / m^2
Γ_{ES} : Surface concentration of adsorbed, complexed cellulose, g / m^2
Γ_{max} : Maximum enzyme adsorption, g / m^2
Γ_T : Total surface concentration for all enzyme, g / m^2
Γ_O : Surface concentration of open enzyme adsorption sites, g / m^2
P : Oligomeric product produced per unit area, g / m^2
k_A : Adsorption rate constant, ppm^{-1} h^{-1}
k_D : Desorption rate constant, h^{-1}
K_L : Langmuir equilibrium constant, ppm^{-1}
k_1 : Complexation rate constant, m^2 / mg h
k_{-1} : Decomplexation rate constant, h^{-1}
K_C : Michaelis-Menten equilibrium constant, m^2 / mg
k_2 : Activity rate constant, h^{-1}
k_{cat} : Turnover number, h^{-1}

r_A : Rate of adsorption to the cellulose surface, g / m^2 h
r_D : Rate of desorption from the cellulose surface, g / m^2 h
r_C : Rate of complexation with the cellulose surface, g / m^2 h
r_{DC} : Rate of decomplexation from to the cellulose surface, g / m^2 h
r_{CL} : Rate of chain scission by complexed cellulase, g / m^2 h

2.9. References

(1) Himmel, M.; Ding, S. Y.; Johnson, D. K.; Adney, W. S.; Nimlos, M. R.; Brady, J. W.; Foust, T.D. Biomass Recalcitrance: Engineering Plants and Enzymes for Biofuels Production. *Science* **2007**, *315,* 804-807.

(2) Houghton, J.; Weatherwax, S.; Ferrell, J. Breaking the Biological Barriers to Cellulosic Ethanol: A Joint Research Agenda. *US DOE,* DOE/SC-0095, 2005.

(3) Wyman, C. E. Ethanol from Lignocellulosic Biomass: Technology, Economics, and Opportunities. *Bioresource Technol*. **1994,** *50,* 3-16.

(4) Taherzadeh, M. J.; Karimi, K. Enzyme-based Hydrolysis Processes for Ethanol from Lignocellulosic Materials: A review. *Bioresources* **2007,** *4,* 707-738.

(5) Beguin, P.; Aubert, J. P. The Biological Degradation of Cellulose. *Fems Microbio Rev* **1994,** *13,* 25-58.

(6) Macmillan, J. D. Bioethanol Production: Status and Prospects. *Renewable Energy* **1997,** *2-3,* 295-302.

(7) Pauly, M.; Keegstra, K. Cell-wall Carbohydrates and Their Modification as a Resource for Biofuels. *Plant Journal* **2008,** *54,* 559-568.

(8) Bansal, P.; Hall, M.; Realff, M. J.; Lee, J. H.; Bommarius, A. S. Modeling Cellulase Kinetics on Lignocellulosic Substrates. *Biotech Advances* **2009,** *6,* 833-848.

(9) Gan, Q.; Allen, S. J.; Taylor, G. Kinetic Dynamics in Heterogeneous Enzymatic Hydrolysis of Cellulose: An Overview, an Experimental Study and Mathematical Modelling. *Process Biochem* **2003,** *38,* 1003-1018.

(10) O'Sullivan, A. C. Cellulose*:* The Structure Slowly Unravels. *Cellulose* **1997,** *4,* 173-207.

(11) Teeri, T. T. Crystalline Cellulose Degradation: New Insight into the Function of Cellobiohydrolases. *Trends Biotechnol* **1997,** *15,* 160-167.

(12) Yang, B.; Wyman, C. E. Pretreatment: the Key to Unlocking Low-Cost Cellulosic Ethanol. *Biofuels Bioprod Bioref* **2008,** *2,* 26-40.

(13) Wang, Y.; Radosevich, M.; Hayes, D.; Labbe, N. Compatible Ionic Liquid-Cellulases System for Hydrolysis of. Lignocellulosic Biomass. *Biotech Bioeng* **2011,** *108,* 1042-1048.

(14) Lynd, L. R.; Laser, M. S.; Brandsby, D.; Dale, B. E.; Davison, B.; Hamilton, R.; Himmel, M.; Keller, M.; McMillan, J. D.; Sheehan, J.; Wyman CE. How Biotech Can Transform Biofuels. *Nature Biotechnol* **2008,** *26,* 169-172.

(15) Beguin, P. Molecular-Biology of Cellulose Degradation. *Ann Rev Microbiol* **1990,** *44,* 219-248.

(16) Zhang, Y. H. P.; Himmel, M. E.; Mielenz, J. Outlook for Cellulase Improvement: Screening and Selection Strategies. *Biotech Advances* **2005,** *24,* 452-481.

(17) Gilkes, N. R.; Henrissat, B.; Kilburn, D. G.; Miller, R. C.; Warren, R. A. J. Domains in Microbial Beta-1,4-Glycanases – Sequence Conservation, Function, and Enzyme Families. *Microbio Rev* **1991,** *55,* 303-315.

(18) Turon X.; Rojas, O. J.; Deinhammer, R. S. Enzymatic Kinetics of Cellulose Hydrolysis: A QCM-D Study. *Langmuir* **2008,** *24,* 3880-3887.

(19) Bommarius A. S.; Katona A.; Chebe S. E.; Patel, A. S.; Ragauskas, A. J.; Knudson, K.; Pu, Y. Cellulase Kinetics as a Function of Cellulose Pretreatment. *Metabol Eng* **2008**, *10,* 370-381.

(20) Borjesson, J.; Engqvist, M.; Sipos, B.; Tjerneld F. Effect of Poly(Ethylene Glycol) on Enzymatic Hydrolysis and Adsorption of Cellulase Enzymes to Pretreated Lignocellulose. *Enzyme and Microbial Technol* **2007,** *41,* 186-195.

(21) Kumar, R..; Wyman, C. E. Cellulase Adsorption and Relationship to Features for Corn Stover Solids Produced by Leading Pretreatments. *Biotech Bioeng* **2009**, *103,* 252-267.

(22) Lee, S.B; Shin, H.S.; Ryu, D. D. Y.; Mandels, M. Adsorption of Cellulase on Cellulose: Effect of Physicochemical Properties of Cellulose on Adsorption and Rate of Hydrolysis. *Biotechnol Bioeng* **1982**, *24,* 2137-2153.

(23) Abdmziem, K.; Passas, R.; Belgacem, M. N. Inverse Gas Chromatography as a Tool to Characterize the Specific Surface Area of Cellulose Fibers. *Cell Chem Technol* **2006,** *40,* 199-204.

(24) Ardizzone, S.; Dioguardi, F. S.; Mussini, T.; Mussini, P. R.; Rondinini, S.; Vercelli, B.; Vertova, A. Microcrystalline Cellulose Powders: Structure, Surface Features and Water Sorption Capability. *Cellulose* **1999,** *6,* 57-69.

(25) Josefsson P.; Henriksson G.; Wågberg L. The Physical Action of Cellulases Revealed by a Quartz Crystal Microbalance Study Using Ultrathin Cellulose Films and Pure Cellulases. *Biomacromolecules* **2008,** *9,* 249-254.

(26) Suchy M.; Linder M. B.; Tammelin T.; Campbell J. M.; Vuorinen T.; Kontturi E. Quantitative Assessment of the Enzymatic Degradation of Amorphous Cellulose by Using a Quartz Crystal Microbalance with Dissipation Monitoring. *Langmuir* **2011,** *27,* 8819-8828.

(27) Hu, G.; Heitmann, J. A.; Rojas, O. J. In Situ Monitoring of Cellulase Activity by Microgravimetry with a Quartz Crystal Microbalance. *J Phys Chem B*. **2009,** *113,* 14761-14768.

(28) Ahola, S.; Turon, X.; Österberg, M.; Laine, J.; Rojas, O J. Enzymatic Hydrolysis of Native Cellulose Nanofibrils and Other Cellulose Model Films: Effect of Surface Structure. *Langmuir* **2008,** 24, 11592 – 11599.

(29) Eriksson J.; Malmsten, M.; Tiberg, F.; Callisen, T. H.; Damhus, T.; Johansen, K. S. Enzymatic Degradation of Model Cellulose Films. *J Colloid Interface Sci* **2005,** *284,* 99-106.

(30) Ma, A.; Hu, Q.; Qu, Y.; Bai, Z.; Liu, W.; Zhuang, G. The Enzymatic Hydrolysis Rate of Cellulose Decreases with Irreversible Adsorption of Cellobiohydrolase I. *Enz Microb Tech* **2008**, *42(7)*, 543-547.

(31) Foose, L. L.; Blanch, H. W.; Radke, C. J. Kinetics of Adsorption and Proteolytic Cleavage of a Multilayer Ovalbumin Film by Subtilisin Carlsberg. *Langmuir* **2008**, *24(14)* 7388-7393.

(32) Kontturi, E.; Tammelin, T.; Österberg, M. Cellulose—Model Films and the Fundamental Approach. *Chem Soc Rev* **2006,** *35,* 1287-1313.

(33) Gunnars S.; Wågberg L.; Stuart M. A. C. Model Films of Cellulose: I. Method Development and Initial Results. *Cellulose* **2002,** *9,* 239-249.

(34) Falt, S.; Wågberg, L.; Vesterlind, E. L.; Larsson, P. T. Model Films of Cellulose II - Improved Preparation Method and Characterization of the Cellulose Film. *Cellulose* **2004,** *11,* 151-162.

(35) Semedo, L. T. A. S.; Gomes, R. C.; Bon, P. S.; Soares, R. M. A.; Linhares, L. F.; Coelho, R. R. R. Endocellulase and Exocellulase Activities of Two Streptomyces Strains Isolated from a Forest Soil. *Appl Biochem Biotechnol* **2000,** *84-86,* 267-286.

(36) Receveur V.; Czjzek M.; Schulein M.; Panine P.; Henrissat, B. Dimension, Shape, and Conformational Flexibility of a Two Domain Fungal Cellulase in Solution Probed by Small Angle X-ray Scattering. *J Bio Chem* **2002,** *277,* 40887-40892.

(37) Pereira J. H.; Sapra R.; Volponi J. V.; Kozina C. L.; Simmons B.; Adams P. D. Structure of endoglucanase Cel9A from the thermoacidophilic Alicyclobacillus acidocaldarius. *Acta Crystallographica Section D* **2009,** *D65,* 744-750.

(38) Fujiwara, H. *Spectroscopic Ellipsometry*. Wiley: Hoboken, 2007.

(39) Holtzapple, M.; Cognata, M.; Shu, Y.; Hendrickson, C. Inhibition of Trichoderma-Reesei Cellulase by Sugars and Solvents. *Biotech Bioeng* **1990,** *36,* 275-287.

(40) Wood, T. M.; Bhat, K. M. Methods for Measuring Cellulase Activities. *Method Enzymol* **1988,** *160,* 87-112.

(41) Tompkins, H. G. *A User's Guide to Ellipsometry*. Academic Press, Inc.: San Diego, 1993.

(42) Gollapalli, L. E.; Dale, B. E.; Rivers, D. M. Predicting Digestibility of Ammonia Fiber Explosion (AFEX)-Treated Rice Straw. *App Biochem Biotech* **2002,** *98,* 23-35.

(43) Lok, B. K.; Cheng, Y.; Robertson, C. R. Protein Adsorption on Crosslinked Polydimethylsiloxane Using Total Internal Reflection Fluorescence. *J. Colloid Interface Sci.* **1983,** 91, 104–116.

(44) Clark, D. S.; Blanch, H. W. *Biochemical Engineering*. Marcel Dekker: New York, 1996.

(45) De Feijter, J. A.; Benjamins, J.; Veer, F. A. Ellipsometry as a Tool to Study the Adsorption Behavior of Synthetic and Biopolymers at the Air–Water Interface. *Biopolymers* **1978,** *17,* 1759-1772.

(46) Howell, J. A.; Stuck, J. D. Kinetics of Solka Floc Cellulose Hydrolysis by Trichoderma Viride Cellulase. *Biotech Bioeng* **1975,** *17(6)*, 873-893.

(47) Okazaki M, Mooyoung M. Kinetics of Enzymatic Hydrolysis of Cellulose: Analytical Description of a Mechanistic Model. *Biotech Bioeng* **1978,** *20,* 637-663.

(48) Wald, S.; Wilke, C. R.; Blanch, H. W. Kinetics of the Enzymatic Hydrolysis of Cellulose. *Biotech Bioeng* **1984,** *26,* 221-230.

(49) Brown, R. F.; Holtzapple, M. T. A Comparison of the Michaelis–Menten and HCH-1 Models. *Biotech Bioeng* **1990,** *36,* 1151-1154.

(50) Bezerra R. M. F.; Dias, A. A. Discrimination Among Eight Modified Michaelis-Menten Kinetics Models of Cellulose Hydrolysis with a Large Range of Substrate/Enzyme Ratios. *Appl Biochem Biotech* **2004,** *112,* 173-184.

(51) Peri, S.; Karra, S.; Lee, Y. Y.; Karim, M. N. Modeling Intrinsic Kinetics of Enzymatic Cellulose Hydrolysis. *Biotech Progress* **2007,** *23,* 626-637.

(52) Zheng, Y.; Pan, Z. L.; Zhang, R. H., Jenkins, B. M. Kinetic Modeling of Enzymatic Hydrolysis of Pretreated Creeping Wild Ryegrass. *Biotech Bioeng* **2009,** *102,* 1558-1569.

(53) Hall, M.; Bansal, P.; Lee, J. H.; Realff, M. J.; Bommarius, A. S. Cellulose Crystallinity – a Key Predictor of the Enzymatic Hydrolysis Rate. *Febs Journal* **2010,** *277,* 1571-1582.

(54) Levine, S. E.; Fox, J. M.; Blanch, H. W.; Clark, D. S. A Mechanistic Model of the Enzymatic Hydrolysis of Cellulose. *Biotech Bioeng* **2010,** *107,* 37-51

(55) Daoud, F. B. O; Kaddour, S.; Sadoun, T. Adsorption of Cellulase Aspergillus Niger on a Commercial Activated Carbon: Kinetics and Equilibrium Studies. *Colloids and Surfaces B* **2010,** *75,* 93-99.

(56) Zhang, Y. H. P.; Lynd, L. R. A Functionally Based Model for Hydrolysis of Cellulose by Fungal Cellulase. *Biotech Bioeng* **2006,** *94(5),* 888-898

(57) Linder, M.; Teeri, T. T. The Cellulose-Binding Domain of the Major Cellobiohydrolase of Trichoderma Reesei Exhibits True Reversibility and a High Exchange Rate on Crystalline Cellulose. *Proceedings of the National Academy of Sciences* **1996**, *93,* 12251-12255.

(58) Fogler, H. S. *Elements of Chemical Reaction Engineering*, fourth ed. Pearson: Westford, 2006.

(59) Andre, G.; Kanchanawong, P.; Palma, R.; Cho, H.; Deng, X.; Irwin, D.; Himmel, M. E.; Wilson, D. B.; Brady, J. W. Computational and Experimental Studies of the Catalytic Mechanism of Thermobifida Fusca Cellulase Cel6A (E2). *Protein Eng* **2003,** *16,* 125-134.

(60) Fox, J. M.; Levine, S. E.; Blanch, H. W.; Clark, D. S. Initial- and Processive-Cut Products Reveal Cellobiohydrolase Rate Limitations and the Role of Companion Enzymes. *Biochemistry*. **2012**, *51(1)*, 442-452.

(61) Voet, D.; Voet, J. G. *Biochemistry*. Wiley and Sons: Hoboken, 2004.

Chapter 3

Competitive Sorption Kinetics of Inhibited Endo- and Exo-glucanases on a Model Cellulose Substrate

3.1. Abstract

For the first time, competitive adsorption of inhibited cellobiohydrolase I (Cel7A, an exoglucanase) and endoglucanase I (Cel7B) from *T. longibrachiatum* is studied on cellulose. Using quartz crystal microgravimetry (QCM), sorption histories are measured for individual types of cellulases and their mixtures adsorbing to and desorbing from a model cellulose surface. We find that Cel7A has a higher adsorptive affinity for cellulose than does Cel7B. Adsorption of both cellulases becomes irreversible on time scales of 30 – 60 min, much shorter than those typically used for industrial cellulose hydrolysis. A multicomponent Langmuir kinetic model including first-order irreversible binding is proposed. Although adsorption and desorption rate constants differ between the two enzymes, the rate at which each surface enzyme irreversibly binds is identical. Due to the higher affinity of Cel7A for the cellulose surface, when Cel7A and Cel7B compete for surface sites, a significantly higher bulk concentration of Cel7B is required to achieve comparable surface enzyme concentrations. Since cellulose deconstruction benefits significantly from the cooperative activity of endoglucanases and cellobiohydrolases on the cellulose surface, accounting for competitive adsorption is crucial to developing effective cellulase mixtures.

3.2. Background

As humanity depletes worldwide supplies of fossil fuels, lignocellulosic biofuels offer an alternate, renewable energy source.[1 2 3 4] The rate-limiting step in lignocellulosic biofuel production is the depolymerization of biomass to form simple sugars and their oligomers that are subsequently fermented and processed to form fuel additives or other chemicals.[5 6 7] Currently, all industrial-scale biofuel production deploys cellulytic enzymes known as cellulases to effect depolymerization.[8] Despite a significant industrial effort toward production of biofuels from various carbon sources, the mechanisms and kinetics that govern aqueous enzymatic deconstruction remain poorly characterized.

To develop a broader understanding of deconstruction mechanisms, we utilize a surface-based technique to measure the interfacial interaction between aqueous cellulytic enzymes and the solid cellulose surface. Most current assays of cellulase activity are performed in the bulk and, therefore, fail to characterize surface phenomena. Thin model films of cellulose[9] adhered to metal supports offer a well-defined surface of known area for measuring surface kinetics, whereas estimates of the enzyme-accessible surface area of the laboratory-standard cellulose Avicel can span several orders of magnitude. [10 11] Surface-based sensing techniques, such as ellipsometry,[12 13 14 15] quartz crystal microbalance,[16 17 18 19 20 21] atomic force microscopy,[22 23]

Brewster angle microscopy,[24] and neutron reflectometry[25] are then available to elucidate the mechanisms and kinetics of cellulase activity.

Cellulose is insoluble in water and recalcitrant to enzymatic degradation due to strong internal hydrogen bonding between long, nonbranching polymer chains.[26] [27] [28] Complete deconstruction of solid cellulose benefits from the concerted activity of two classes of enzyme. First, endoglucanases disrupt the hydrogen-bonding structure of cellulose and dislodge individual cellulose chain ends from the surface. Subsequently, cellobiohydrolases complex with the released chain ends, cleaving them into glucose oligomers, which are then released into aqueous solution.[29] Surface-active cellulases from these two classes each consist of a catalytic domain (CD) joined to a cellulose-binding domain (CBD) by a flexible linker. The activity of any individual cellulase can be understood according to a four-step model: (1) adsorption from bulk solution to the cellulose surface, with binding of the CBD to cellulose; (2) complexation of the active site with a cellulose chain; (3) catalytic activity within the active site; and (4) return of the cellulase to the uncomplexed adsorbed state.[12] Extended models of cellulase activity consider cellulose chain length,[30] processive activity of cellobiohydrolases,[31] and surface diffusion of adsorbed enzymes, among other parameters.[32]

In this work, kinetic rate constants are quantified that govern sorption of inhibited *T. longibrachiatum* cellobiohydrolase I (CBHI, Cel7A) and endoglucanase I (EGI, Cel7B) on the cellulose surface. Interaction of the CBD of these fungal cellulases with the cellulose surface, mediated by three critical tyrosine residues,[33] [34] has been characterized by different sources as reversible[35] or irreversible.[36] We adopt modified Langmuir adsorption kinetics after Cascao Pereira *et al.*,[37] where enzymes first adsorb reversibly from bulk solution to the cellulose surface, followed by slower irreversible attachment. This adsorption scheme is illustrated in Figure 3.1.

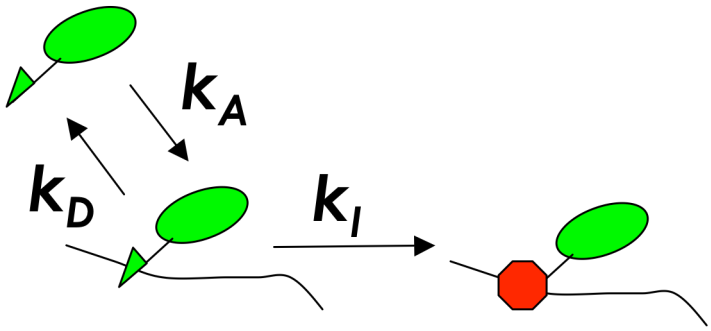

Figure 3.1. Schematic of cellulase sorption and irreversible binding on a cellulose surface. Cellulase catalytic domain is represented by an ellipse, and the cellulose binding domain (CBD) is shown as a triangle. Cellulase freely adsorbs and desorbs from bulk solution until it irreversibly binds, as indicated by the change of the binding domain to an octagon shape. Eventually, all adsorbed enzyme is attached irreversibly to the surface.

To measure sorption kinetics, we implement quartz crystal microgravimetry (QCM), as it allows characterization of small quantities of aqueous enzyme. QCM has been used previously as a continuous, non-invasive, inhibition-free, surface-oriented assay of cellulase activity. Turon *et al*. first utilized QCM to measure enzymatic degradation of cellulose films.[16] Josefsson *et al.* studied the synergy between endoglucanases and cellobiohydrolases on the cellulose surface and generated a qualitative portrait of enzyme activity on model cellulose films.[17] Ahola *et al*. explored the activity of enzymes on cellulose surfaces with various deposition techniques. They fit endoglucanase adsorption kinetics to a three-parameter model.[18] Work by Hu *et al.* similarly explored the interaction of cellulase with several different cellulose surfaces, including the effect of concentration on degradation rate.[19] [20] Finally, Suchy *et al*. measured the activity of endoglucanase I on spin-coated cellulose films.[21] Despite growing interest in the use of QCM, the extent of this work is preliminary and qualitative. We provide a quantitative assessment of cellulase sorption kinetics from QCM, tracking the sorption of individual cellulases both singly and in binary mixtures.

3.3. Materials and Methods

3.3.1. Cellulases

Isolated *T. longibrachiatum* cellulases were obtained from Megazyme (Bray, Ireland). These fungal cellulases are typical for kinetic studies of cellulytic activity.[38] [39] Cellobiohydrolase I (Cel7A; Megazyme E-CBHI, MW 65,000 Da) was obtained at a concentration of 10,000 ppm in a suspension of 3.2-M ammonium sulfate/0.02 wt% ammonium azide. *Endo*-cellulase contaminant was minimal; the enzyme mixtures show 0.003 U/mg *endo*-cellulase activity in comparison to 0.1 U/mg Cel7A activity. Endoglucanase I (Cel7B; Megazyme E-CELTR, MW 57,000 Da) was obtained at a concentration of 9,400 ppm in a solution of 3.2-M ammonium sulfate/0.02 wt% ammonium azide, again with minimal glucosidase contaminants. Enzymes were used as supplied after dilution to concentrations of 1 – 100 ppm in an aqueous solution of sodium dihydrogen phosphate buffer and glucose.

3.3.2. Coating and Characterization of Cellulose Films

Gold-coated QCM sensors (Q-Sense QSX-401, Västra Frölunda, Sweden) were plasma-cleaned (Harrick PDC-32G; Pleasantville, NY, USA) for 10 min to remove surface organic residue. The sensors were subsequently cleaned for 5 min in a solution of distilled/deionized water, hydrogen peroxide (Sigma-Aldrich H1009, sold as 30% w/w aqueous solution) and ammonia (Sigma-Aldrich AX1303, sold as 30% w/w aqueous solution) mixed in a 5:1:1 volume ratio and heated to 75 ºC. After rinsing in distilled/deionized water, the sensors were again plasma-cleaned for 10 min to remove residual organic debris.

Thin cellulose films were deposited on the cleaned gold-coated sensors by a modification of the method of Gunnars *et al*..[13] Cellulose is dissolved in 4-methylmorpholine-N-oxide (4MMO; Sigma Aldrich #224286, 97% purity) and dimethyl sulfoxide (DMSO; Sigma Aldrich #D5879, 99.5%), and spin-coated onto a gold sensor coated with the cationic anchor polymer poly-diallyl-dimethyl-ammonium chloride (PDADMAC; Sigma-Aldrich #409030, sold as a 20% w/w aqueous solution). The cellulose film is subsequently soaked in water to remove remaining 4MMO and DMSO. The detailed procedure is available elsewhere,[12] with the following changes in solution composition. A 20-mg quantity of Avicel microcrystalline cellulose (Sigma Aldrich #11363) was added to a mixture of 503 mg powdered 4MMO and 880 mL distilled/deionized

water; after dissolution, 2 mL DMSO was added to adjust solution viscosity. These changes permitted the deposition of thinner, more rigid cellulose films suitable for QCM analysis. The proportion of DMSO in the coating mixture controls the viscosity of the spin-coated cellulose solution and, therefore, the mass and thickness of the adsorbed film.[12 14]

The QCM frequency response of PDADMAC-coated sensor crystals was measured before and after cellulose deposition. From the difference in frequency response, film mass and film thickness were ascertained. The cellulose films have an approximate dry mass of 69.5 μg and an approximate dry thickness of 42.9 ± 1.6 nm. In previous work, cellulose films prepared using this method were found to have a crystallinity of 42 ± 4%, in comparison to a crystallinity of 58 ± 2% for Avicel.[12] Our previous work also established that cellulytic deconstruction kinetics of the model cellulose films is identical to that of their cellulose source Avicel, an industry standard for measuring enzyme activity on cellulose.[12]

3.3.3. Measurement of Adsorption via Quartz Crystal Microbalance

A cellulose-coated gold wafer was placed into the flow cell of a quartz crystal microbalance (QCM; Q-Sense E4, Västra Frölunda, Sweden). The flow cell was subsequently filled with a 9.5-mM NaH_2PO_4 aqueous buffer solution (pH 5.5; Sigma-Aldrich #S9638) containing glucose (Sigma Aldrich #G5767) at a concentration of 6000 ppm. Glucose was added to the aqueous solution because it acts as an inhibitor not only of cellulase activity, but also of cellulase complexation with cellulose, thus allowing measurement of enzyme adsorption absent these factors.[12 40] Aqueous glucose at this concentration does not significantly affect the mass of the model cellulose films nor does it inhibit adsorption of aqueous cellulase to the cellulose surface.[12]

The cellulose film was allowed to swell in the buffer/glucose solution until a constant frequency shift was reached, typically 1 – 2 h after exposure to the solution. Following swelling, a solution of cellulase at the desired concentration in the same buffer/glucose mixture was flowed over the cellulose-coated wafer at a flowrate of 100 μL/min, typically for 15 – 120 min, during which time the frequency shift and dissipation response of the cellulose film were measured continuously. Although endoglucanase penetration into amorphous cellulose films has been reported,[25] cellulases do not penetrate the partially-crystalline films used in this work, even in conjunction with cellulytic enzyme activity.[12] Thus, only external surface sorption is measured. Following the sorption step, nascent buffer/glucose solution was flowed over the wafer to remove reversibly adsorbed surface enzyme. All sorption experiments were conducted at 25 ºC.

3.3.4. QCM Frequency and Dissipation Shift Result

Figure 3.2 shows a typical frequency-shift (ΔF) and energy-dissipation (ΔD) response for a solution of 10-ppm cellobiohydrolase I (Cel7A) in glucose/buffer solution. Data for the third overtone are shown, as response on the fundamental frequency was typically noisy. When the film is exposed to Cel7A, the frequency shift decreases, indicating adsorption of the enzyme to the cellulose surface. After 30 min of exposure to enzyme, buffer/glucose solution is flowed across the cellulose film ($[E]_{bulk} = 0$). The frequency shift then increases, indicative of enzyme washoff. Energy dissipation, which varies with the rigidity of the film, correspondingly increases during the adsorption phase and decreases during the washoff phase, i.e., the film becomes less rigid as cellulase adsorbs to the surface. However, the magnitude of the energy dissipation is small compared to the frequency-shift response.

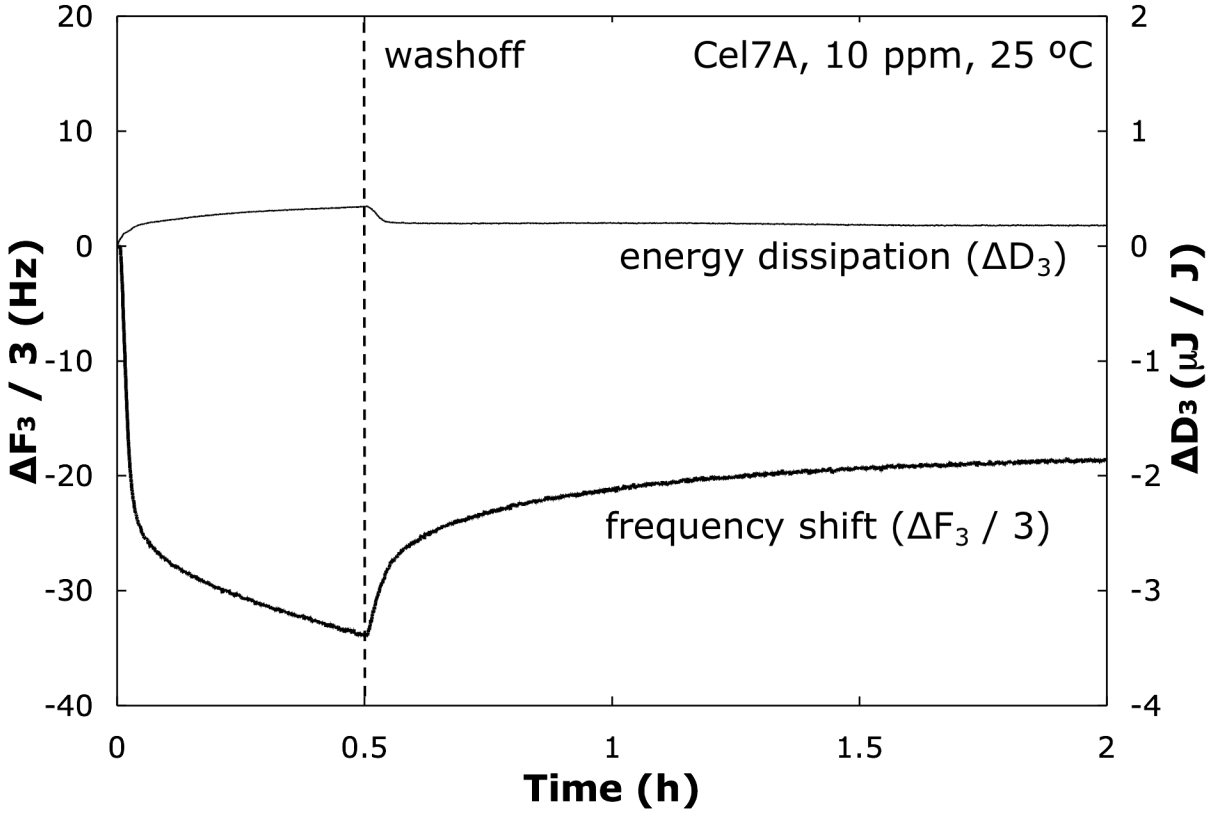

Figure 3.2. Typical frequency shift (Δ*F*, thick line) and dissipation (Δ*D,* thin line) histories for an enzyme loading/washoff experiment. Data shown were measured on the third overtone of a Q-Sense QCM operating at 5 MHz. Washoff after 30 min is indicated by a vertical dashed line. 10-ppm *T. longibrachiatum* Cel7A with 6000-ppm glucose in aqueous buffer at 25 ºC.

For rigid films with sufficiently low dissipation response, the Sauerbrey equation[41] relates change in mass of the resonating film to the frequency-shift response:

$$\Delta F = -\frac{2 f_0^2}{A\sqrt{\rho_q G_q}} \Delta m \quad , \tag{3.1}$$

where ΔF is the frequency shift measured by the QCM; Δm is the change in resonating mass associated with the cellulose-film surface; f_0 represents the resonant frequency of the quartz crystal; (5 MHz); A denotes the area of the gold-coated sensor; ρ_q is the density of quartz (2.648 g / cm^3); and G_q represents the shear modulus of quartz (29.47 GPa).[41] Thus, the change in mass of a sufficiently rigid thin film varies linearly with observed frequency shift. In this study, frequency-shift results were converted to adsorbed mass density (mg / m^2) using the QTools 3.01 software package included with the Q-Sense instrument. The $\Delta D / \Delta F$ ratio was 0.01 – 0.05 in all experiments, validating use of the Sauerbrey equation.[41]

Increasing flowrate up to a factor of 10 had no effect on enzyme adsorption histories, verifying that mass transfer was not rate-limiting. This experimental result was confirmed by using Lévêque theory to calculate the mass-transfer resistance[12] given the geometry of the QCM flowcell,[42] the flowrate of 100 μL/min (a shear rate of 0.4 s^{-1}), and an estimated enzyme diffusion coefficient of 10^{-6} cm^2/s.

Control experiments were conducted without glucose inhibition to confirm that glucose does not alter the rate of adsorption for Cel7A or Cel7B. For small adsorption times ($t < 5$ min), both frequency and dissipation response were identical for cellulose films exposed to identical concentrations of both enzymes, with or without the presence of glucose inhibitor. After the short-time exposure, enzyme complexation and degradation were observed in experiments without inhibitor. Thus, we confirm our previous findings obtained with ellipsometry: dissolved glucose, used as an inhibitor of complexation, does not affect Cel7A or Cel7B adsorption on the cellulose surface.[12] Both inhibited-enzyme adsorption and cellulytic mass-degradation rates (measured in the absence of inhibitor) agreed well when independently determined from ellipsometry[12] and here from QCM.

3.4. Results

Figure 3.3 depicts typical enzyme adsorption histories for cellobiohydrolase I (Cel7A) in glucose/buffer solution at selected concentrations from 5 – 100 ppm. In each experiment, Cel7A adsorbed for 30 min before washoff with glucose/buffer solution. Higher concentrations of cellulase give higher surface loading prior to washoff. Following elution, extensive flushing of the cellulose surface did not completely remove the enzyme. Rather, a sizeable fraction remained irreversibly bound. For the initial 30-min exposure time, about 75% remained bound to the surface for all Cel7A concentrations studied.

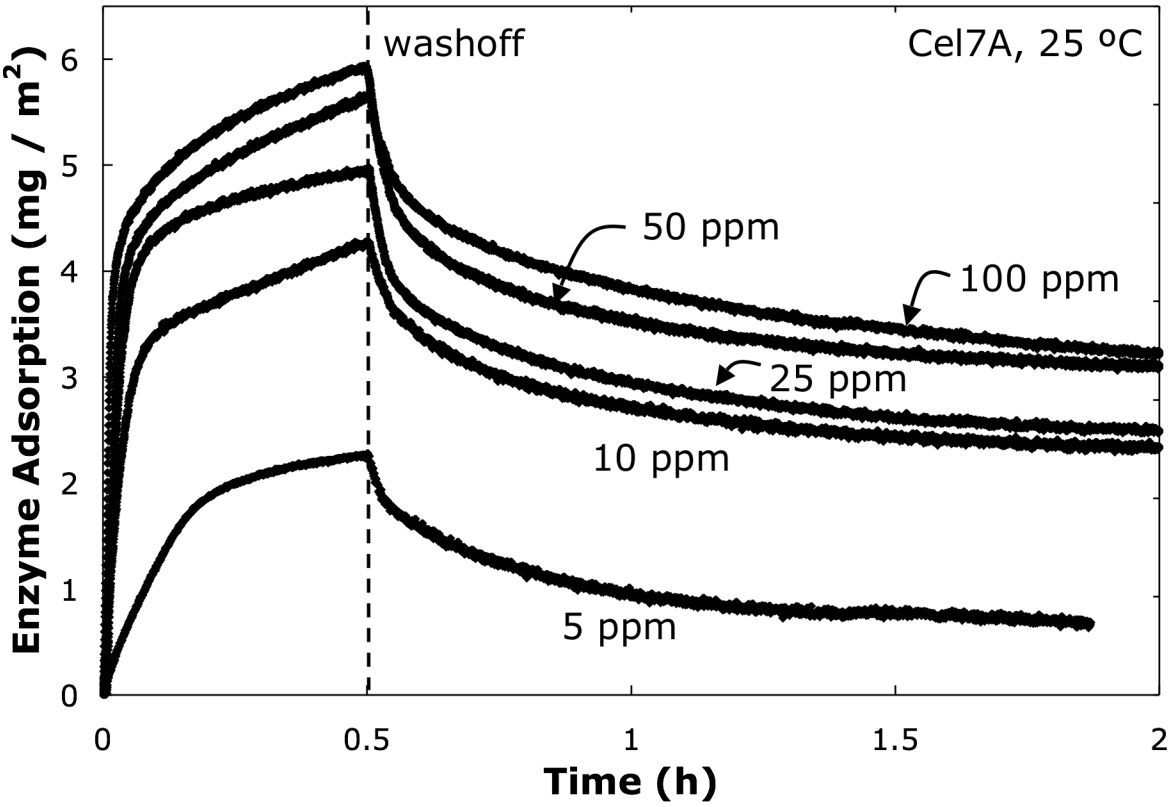

Figure 3.3. Loading/washoff histories for *T. longibrachiatum* Cel7A. Washoff after 30 min is indicated by a vertical dashed line. Enzyme concentrations from bottom to top are 5, 10, 25, 50, and 100 ppm, respectively. Enzyme with 6000-ppm glucose in aqueous buffer at 25 ºC.

Figure 3.4 shows similar adsorption histories for endoglucanase I (Cel7B) in glucose/buffer solution with washoff after 30 min and for bulk enzyme concentrations of 5 – 100 ppm. Again, higher Cel7B concentrations exhibit larger 30-min surface loading, and elution only partially desorbs Cel7B. For Cel7B, about 50% remains irreversibly bound after washoff, independent of enzyme concentration. Comparison of Figures 3.3 and 3.4 indicates that the affinity of Cel7B for the cellulose surface is smaller than that of Cel7A. At 100 ppm, an adsorption of 2.4 mg / m^2 for Cel7B is reached at t = 30 min, compared to 5.9 mg / m^2 for Cel7A. Although not seen on the scales of Figures 3.3 and 3.4, the initial rates of adsorption, shown in Figure 3.5, are linear in bulk-solution concentration for both Cel7A and Cel7B. Figure 3.5 confirms the faster adsorption kinetics for Cel7A seen in Figures 3.3 and 3.4.

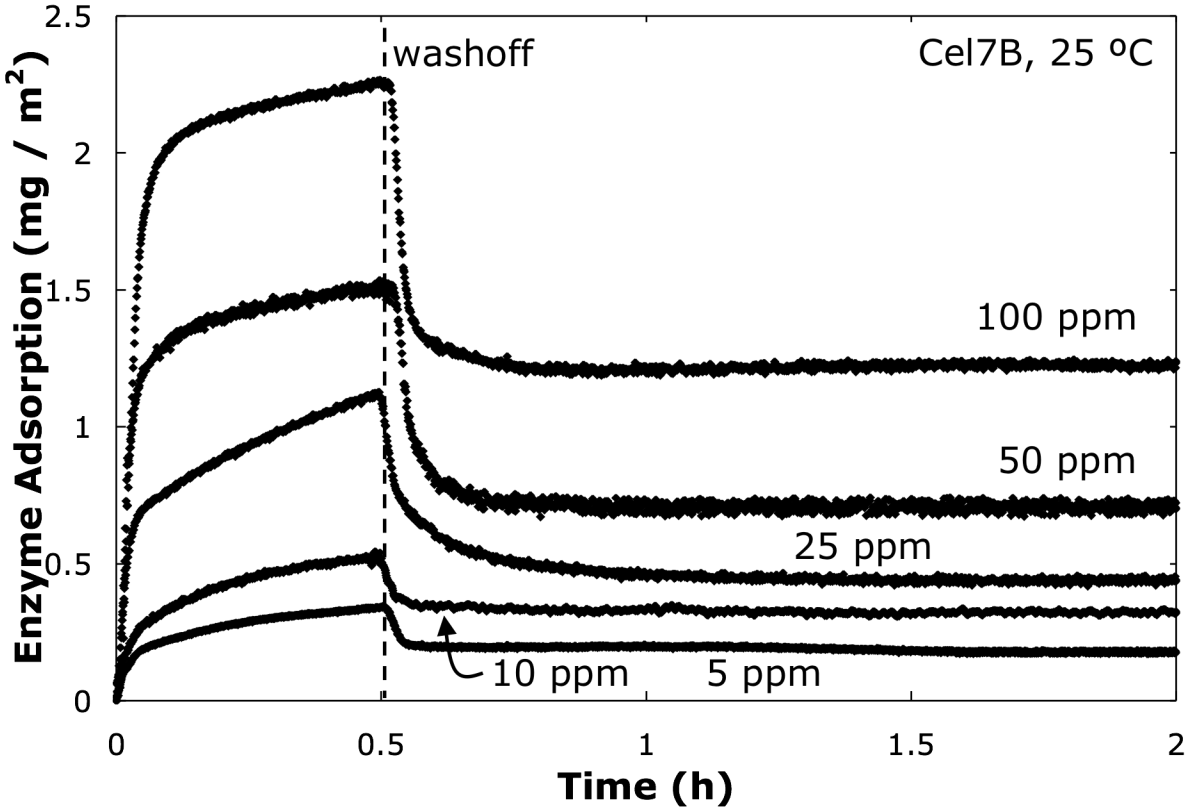

Figure 3.4. Loading/washoff histories for *T. longibrachiatum* Cel7B. Washoff after 30 min is indicated by a vertical dashed line. Enzyme concentrations from bottom to top are 5, 10, 25, 50, 100 ppm, respectively. 6000-ppm glucose in aqueous buffer at 25 ºC.

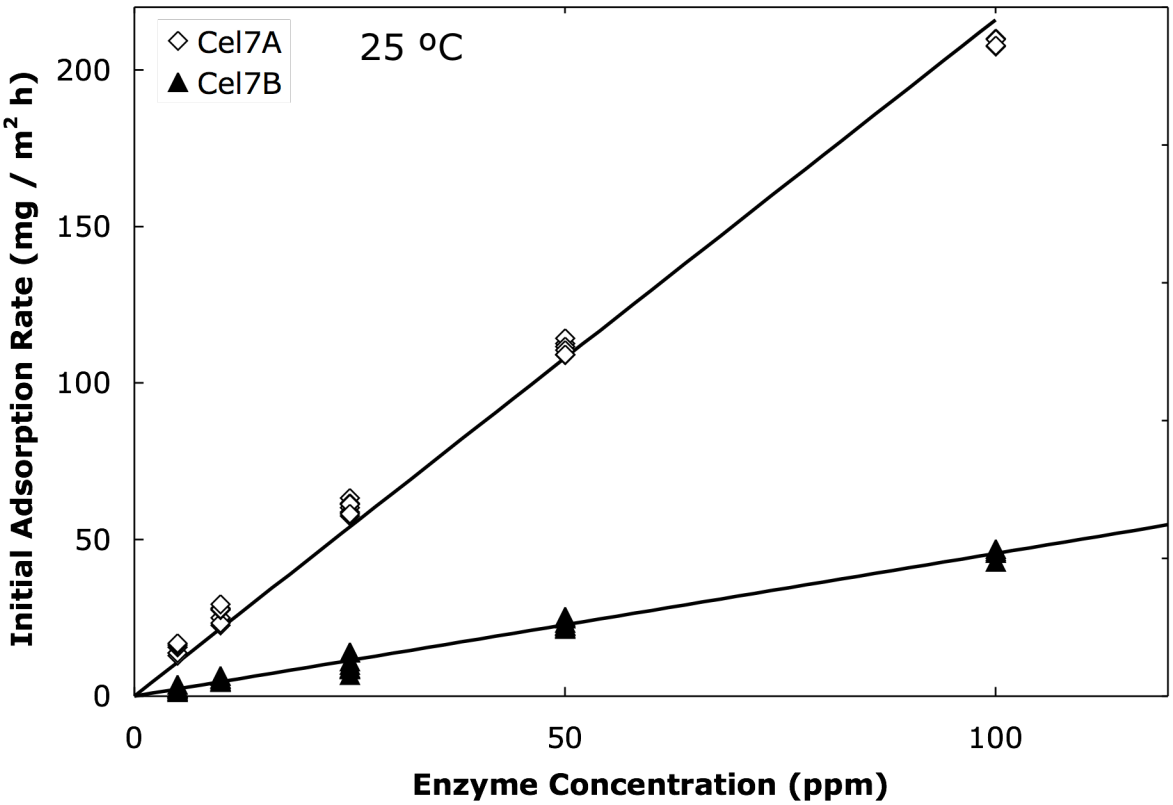

Figure 3.5. Initial cellulase adsorption rate (t < 3 min) on model cellulose films. *T. longibrachiatum* Cel7A (open diamonds) and Cel7B (black triangles) with 6000-ppm glucose in aqueous buffer at 25 ºC. Lines correspond to linear adsorption kinetics.

To elucidate the dynamics of irreversible adsorption, loading/elution histories of Cel7A and Cel7B were measured for differing washoff times. Figures 3.6 and 3.7 present sorption histories for single Cel7A and Cel7B enzymes at 25 ppm in glucose/buffer solution for washoff times of 3, 15, 30, and 60 min. For both enzymes, loading kinetics follows the identical trajectory for all washoff times. The longer that enzyme is in contact with the surface before washoff, the larger is the amount of enzyme that remains irreversibly bound to the surface.

Figure 3.8 shows adsorption kinetics of Cel7A and Cel7B over 12 h contact with the cellulose surface, while the inset shows the same data plotted only up to t = 1 h. Figures 3.6, 3.7, and the inset in Figure 3.8 suggest that cellulose adsorption is mainly irreversible and at a maximum level after about 2 h of exposure to the cellulose surface. The long-time adsorption kinetics shown in Figure 3.8, however, illustrate that binding of the irreversibly adsorbed cellulase is prolonged and not complete even after 12 h. Smooth solid and dashed lines in this figure, and in those to follow, reflect the kinetic model described below. Figure 3.8 confirms the faster adsorption of Cel7A relative to Cel7B at the same concentration. Noteworthy, however, is the finding that the maximum uptake of each cellulase is essentially the same, approximately 6.8 mg / m^2.

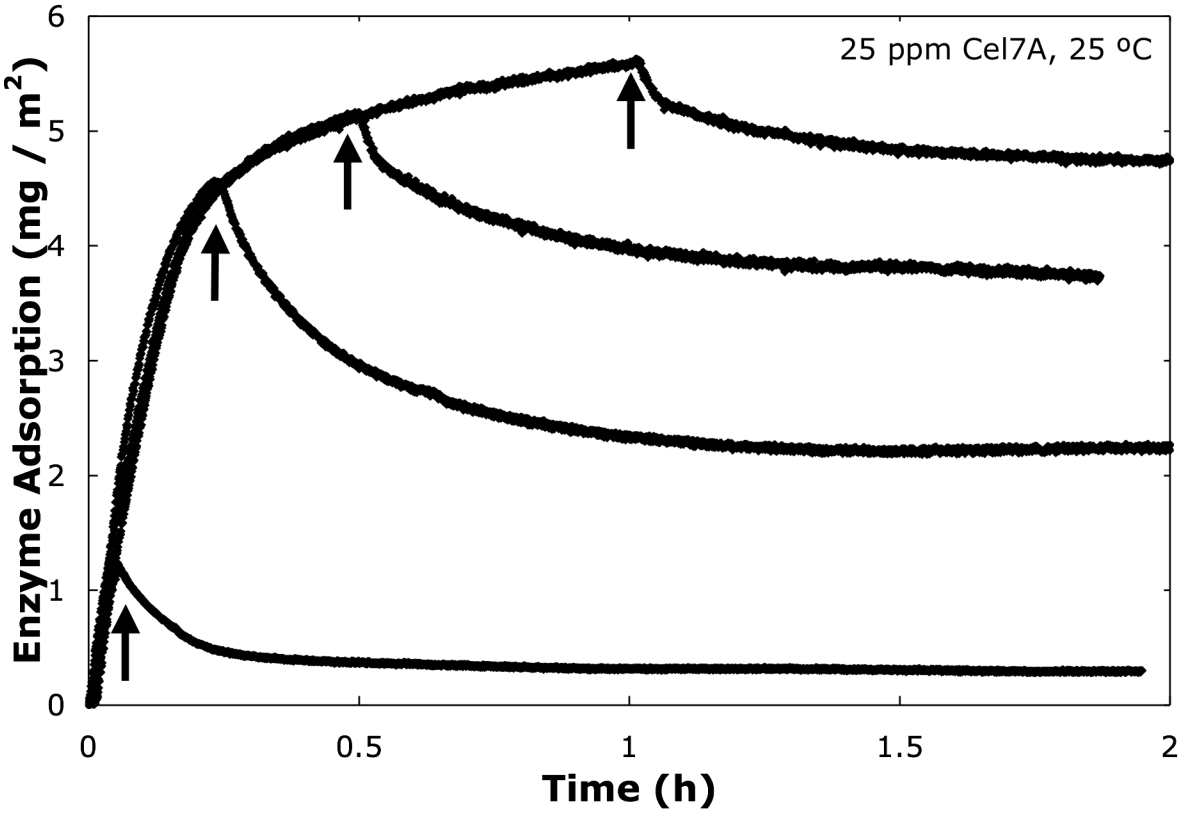

Figure 3.6. Loading/washoff histories for *T. longibrachiatum* Cel7A on a model cellulose film. Washoff after 3, 15, 30, and 60 min indicated by vertical arrows. 25-ppm Cel7A with 6000-ppm glucose in aqueous buffer at 25 ºC.

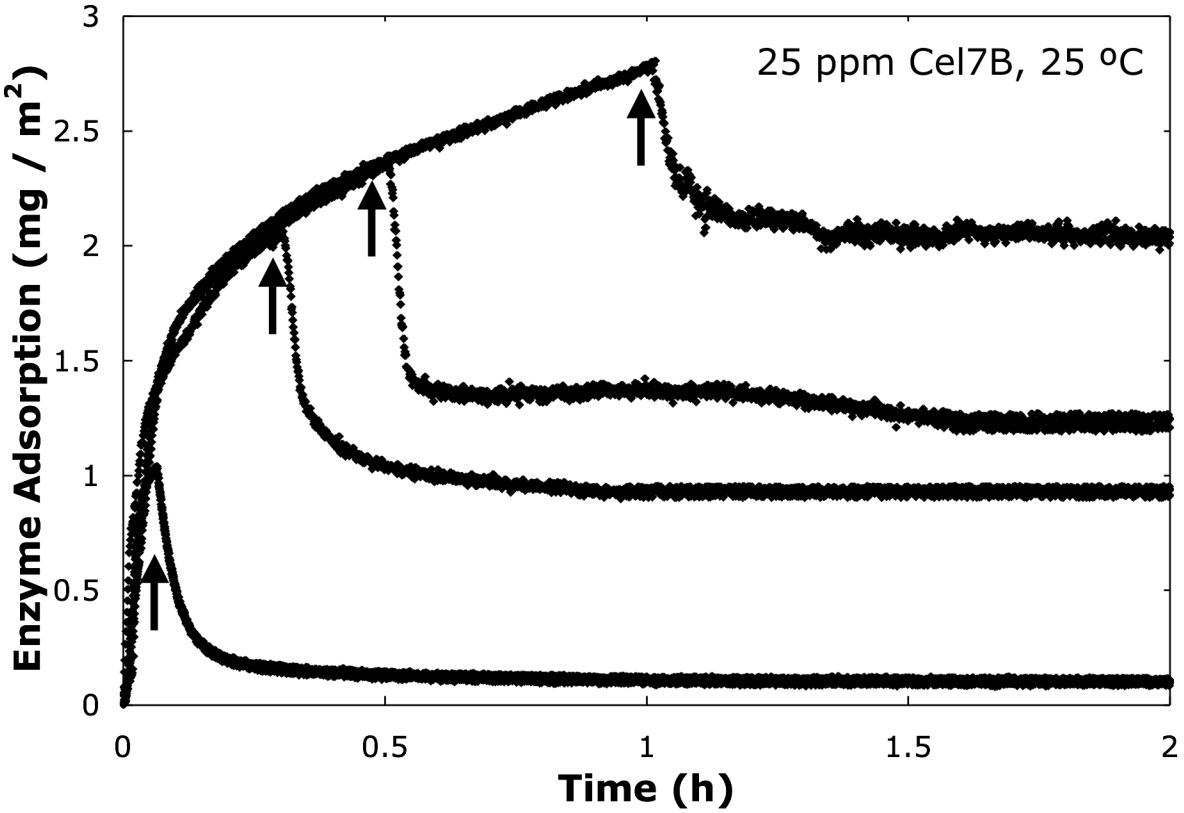

Figure 3.7. Loading/washoff histories for *T. longibrachiatum* Cel7B on a model cellulose film. Washoff after 3, 15, 30, and 60 min indicated by vertical arrows. 25-ppm Cel7B with 6000-ppm glucose in aqueous buffer at 25 ºC.

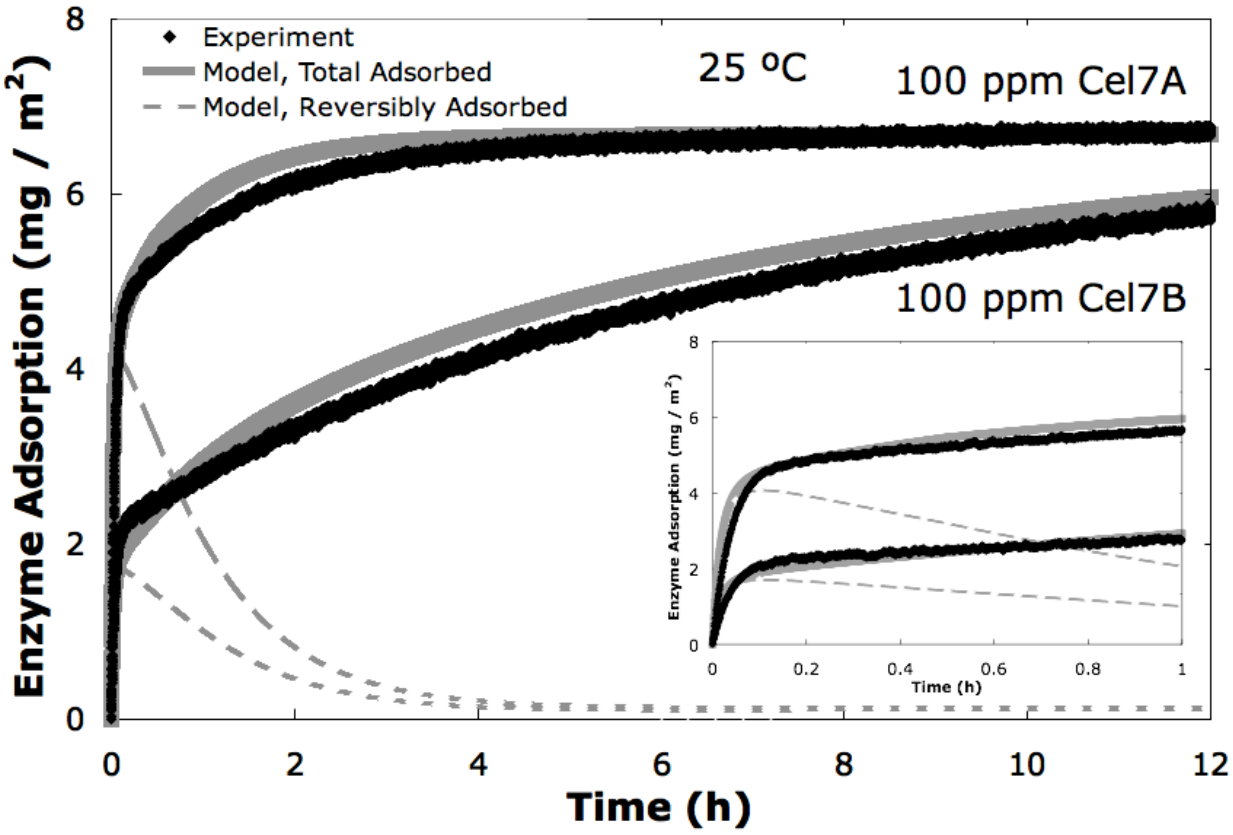

Figure 3.8. Adsorption histories for *T. longibrachiatum* Cel7A and Cel7B at 100 ppm with 6000-ppm glucose in aqueous buffer for times up to 12 h. Inset shows the identical data plotted over a time scale of 1 h. Smooth lines correspond to theory for total enzyme adsorption (thick gray) and reversible adsorption (dashed gray).

Figure 3.9 shows the fraction of Cel7A and Cel7B remaining irreversibly bound to the surface after washoff as a function of loading time before washoff. Lines in this figure are predicted from our proposed kinetic model described below. Data in Figures 3.8 and 3.9 are consistent with a framework where enzyme first binds to the surface reversibly and laterinexorably transitions to an irreversibly bound state. Figure 3.9 also shows that the final irreversibly bound fraction for Cel7B is smaller than that for Cel7A. This is consistent with the lower affinity of Cel7B for the cellulose surface, shown in Figures 3.6 – 3.8. With a lower surface affinity, Cel7B desorbs more quickly than does Cel7A. Therefore, a larger proportion is washed off before it irreversibly binds.

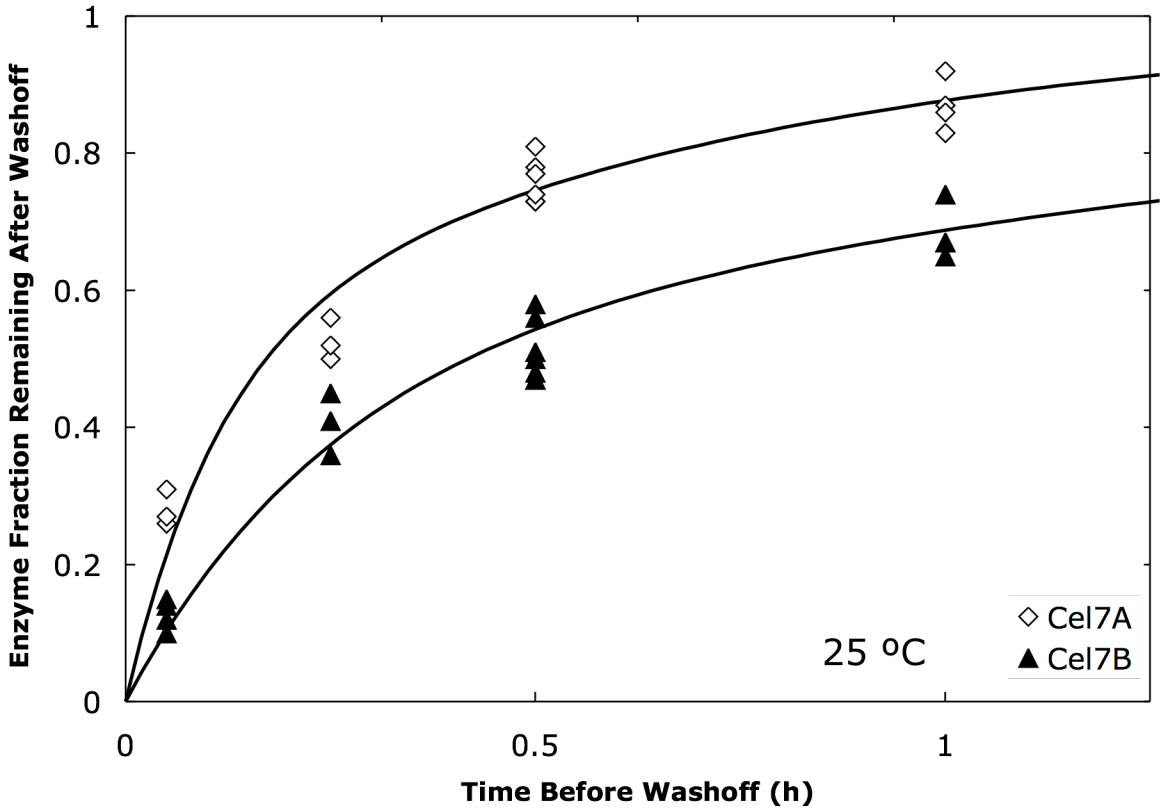

Figure 3.9. Fraction of cellulase irreversibly bound to a model cellulose film after washoff as a function of the time bulk cellulase solution was in contact with the surface before washoff. *T. longibrachiatum* Cel7A (open diamonds) and Cel7B (black triangles) 25-ppm enzyme with 6000-ppm glucose in aqueous buffer at 25 ºC. Lines correspond to theory.

Figure 3.10 plots the enzyme adsorption at 30 min of loading as a function of bulk enzyme concentration for solutions of Cel7A alone, Cel7B alone, and a 50:50 w/w mixture of Cel7A and Cel7B. Again, lines on this figure correspond to theory. This graph is similar in shape to a Langmuir isotherm. However, the resemblance is only apparent. The data do not

truly follow a Langmuir isotherm, because irreversible adsorption prevents the system from reaching an equilibrium balance between adsorption and desorption rates. In Figure 3.10, Cel7A exhibits an apparent higher adsorption affinity for the cellulose surface than does Cel7B, with a much larger amount adsorbed after 30 min for all bulk cellulase concentrations. Accordingly, adsorption of the 50:50 Cel7A:Cel7B mixture is nearer to that of single Cel7A than to adsorption of single Cel7B. Figure 3.8, however, shows that over long time scales, the final irreversibly adsorbed amount of each enzyme is the same. Thus, the results in Figure 3.10 arise from faster sorption kinetics for Cel7A compared to Cel7B. A kinetic model is necessary to quantify these observations.

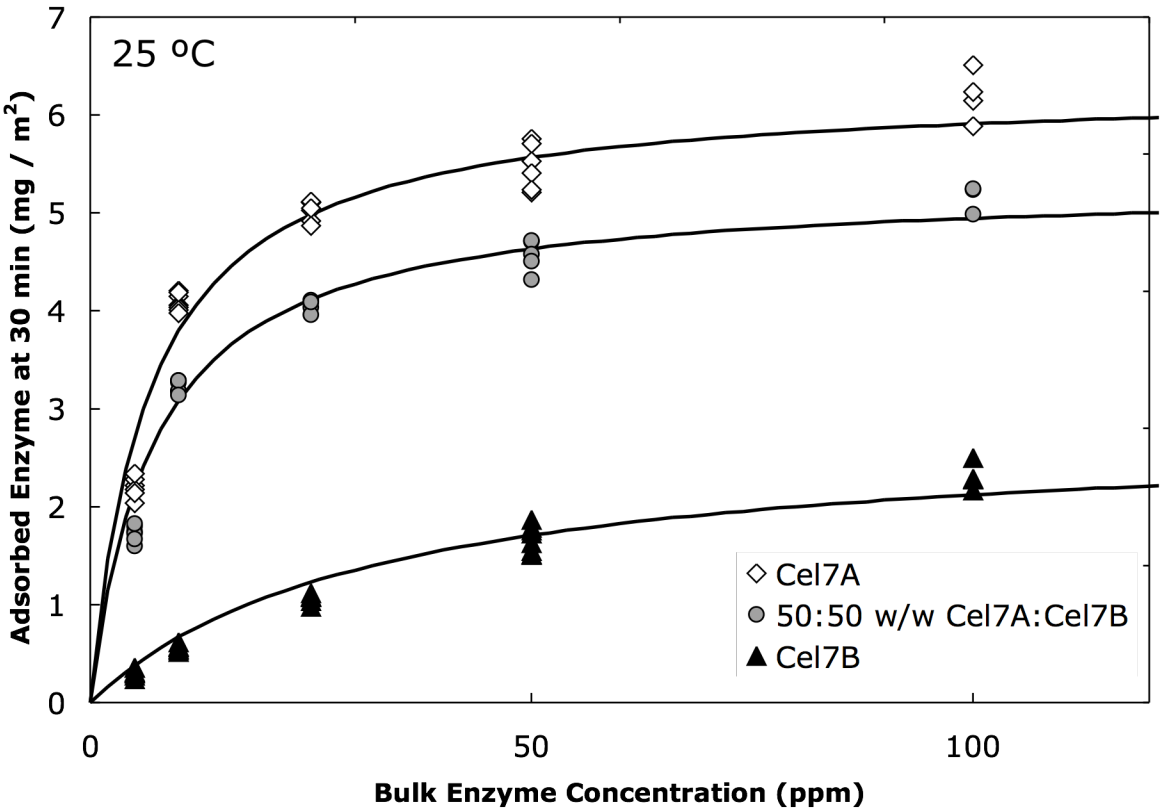

Figure 3.10. Adsorbed amount at 30 min for *T. longibrachiatum* single Cel7A (open diamonds), single Cel7B (black triangles), and a 50:50 w/w mixture of the two enzymes (gray circles) as a function of bulk concentration. Enzyme with 6000-ppm glucose in aqueous buffer at 25 ºC. Lines correspond to kinetic theory.

3.5. Kinetic Model

3.5.1 Single-Enzyme Sorption Kinetics

To explain the results in Figures 3.3 – 3.10, we adopt a Langmuir sorption kinetic model after Cascao Pereira *et al*.[37] Single-enzyme data are analyzed to obtain sorption rate constants for Cel7A and Cel7B. These rate constants are then utilized to predict sorption kinetics of the mixed enzymes.

Details of the kinetic model, illustrated in Figure 3.1, are available elsewhere.[37] For each single cellulase, we establish transient mass balances for the surface concentration of reversibly and irreversibly adsorbed enzyme. Using these rate expressions and the associated adsorption site balance, we establish mass balances for the surface concentration of reversibly and irreversibly adsorbed enzyme:

$$\frac{d\Gamma_E}{dt} = k_A[E]_{bulk}(\Gamma_{\max} - \Gamma_E - \Gamma_I) - k_D\Gamma_E - k_I\Gamma_E \quad , \tag{3.2}$$

$$\frac{d\Gamma_I}{dt} = k_I\Gamma_E \quad , \tag{3.3}$$

and

$$\Gamma_{\max} = \Gamma_E + \Gamma_I + \Gamma_O \quad ; \tag{3.4}$$

where Γ_E and Γ_I are the surface concentrations of reversibly adsorbed and irreversibly bound enzyme, respectively; $[E]_{\text{bulk}}$ is the constant bulk enzyme concentration; $\Gamma_{\max}$ is the maximum surface enzyme concentration; Γ_O is the surface concentration of open sites available for enzyme binding; and k_A, k_D, and k_I, are rate constants for adsorption, desorption, and irreversible binding, respectively. The first two terms on the right of Equation 3.2 specify Langmuir adsorption and desorption rates, respectively. We assume that irreversible adsorption occurs by transformation of the adsorbed enzyme and, hence, incorporate first-order kinetics for irreversible sorption in Equations 3.2 and 3.3.

3.5.2 Single-Enzyme Kinetic Parameters

To determine k_A, the rate constant governing adsorption of cellulase to the cellulose surface, initial rates of adsorption of cellulase to the cellulose surface are obtained immediately after the cellulose surface is exposed to enzyme (t < 2 min). Figure 3.5 reports measured initial enzyme adsorption amounts in the absence of prior adsorbed or irreversibly bound cellulase ($\Gamma_E \approx 0$, $\Gamma_I \approx 0$). In this case, Equation 3.1 reduces to

$$\left.\frac{d\Gamma_E}{dt}\right|_{t\approx 0} = k_A[E]_{bulk}\Gamma_{\max} \quad . \tag{3.5}$$

Accordingly, slopes of the lines fit to the data in Figure 3.5 give $k_A\Gamma_{\max}$ for single Cel7A and single Cel7B initial adsorption. From Figure 3.8, we observe a maximum adsorption of Γ_{max} = 6.8 mg / m^2 for both Cel7A and Cel7B. It is then simple to ascertain the Cel7A and Cel7B adsorption rate constants as $k_{A,Cel7A} = 0.28 \pm 0.05$ h^{-1} ppm^{-1} and $k_{A,Cel7B} = 0.070 \pm 0.013$ h^{-1} ppm^{-1}, respectively.

Kinetic parameters k_D and k_I, describing desorption and irreversible binding of cellulase on the cellulose surface, are obtained in the following manner. The total surface concentration of all states of cellulase on the cellulose surface, either reversibly adsorbed or irreversibly bound, is $\Gamma_T = \Gamma_E + \Gamma_I$. Let t_0 be the time at which washoff commences ($[E]_{bulk} = 0$), and let $\Gamma_{E,0}$, $\Gamma_{I,0}$ and $\Gamma_{T,0}$ represent the corresponding surface concentrations of adsorbed cellulase, irreversibly bound cellulase, and total adsorbed cellulase. Similarly, we define $\Gamma_{E,\infty}$, $\Gamma_{I,\infty}$ and $\Gamma_{T,\infty}$ as the corresponding surface concentrations of adsorbed cellulase, irreversibly bound cellulase, and total cellulase, once washoff is complete. At infinite time, only irreversibly bound cellulase remains on the surface. Thus, by definition, $\Gamma_{T,\infty} = \Gamma_{I,\infty}$ and $\Gamma_{E,\infty} = 0$. Figure 3.11 defines the pertinent variables used in ascertaining k_D and k_I.

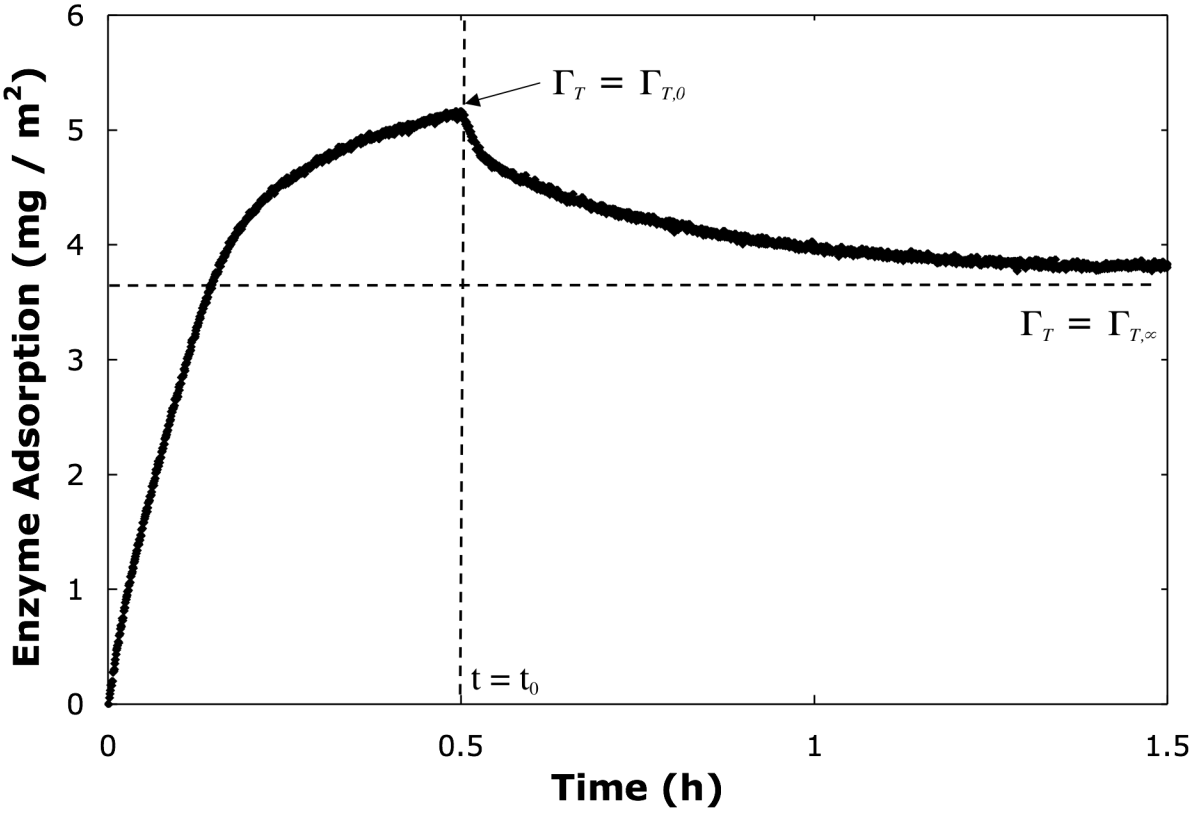

Figure 3.11. Definitions of t_0, $\Gamma_{T,0}$, and $\Gamma_{T,\infty}$ on a typical loading/washoff history.

Beginning with Equations 3.2 and 3.4 applied during washoff ($[E]_{bulk} = 0$), Appendix 3.A specifies the total surface enzyme concentration as a function of time parameterized by the kinetic constants k_D and k_I:

$$\frac{\Gamma_T(t) - \Gamma_{T,\infty}}{\Gamma_{T,0} - \Gamma_{T,\infty}} = e^{-(k_D + k_I)(t - t_0)} \quad . \qquad (3.6)$$

Importantly, Equation 3.6 describes the total surface enzyme concentration Γ_T, and not the individual reversibly and irreversibly adsorbed concentrations Γ_E and Γ_I, which cannot be measured separately by QCM. Equation 3.6 is applied to the QCM-measured loading/elution histories to determine the washoff parameter: $k_D + k_I$. Averaged across all experiments, $k_{D,Cel7A} + k_{I,Cel7A} = 8.3 \pm 0.4$ s^{-1} for Cel7A and $k_{D,Cel7B} + k_{I,Cel7B} = 25.6 \pm 3.3$ s^{-1} for Cel7B. The value of the washoff parameter varies by less than 10% for Cel7A and 20% for Cel7B over all experiments, validating the irreversible adsorption model.

It is not possible to solve Equations 3.2 – 3.4 directly to obtain a closed-form expression for k_D and k_I individually. We, therefore, solve Equations 3.2 – 3.4 numerically via a Runge-Kutta algorithm to determine separate values for k_D and k_I by iterating over a limited range of values specified by experimental data. Details are discussed in Appendix 3.B.

Resulting best-fit rate constants are listed in Table 3.1. We find desorption and irreversible binding rate constants of $k_{D,Cel7A} = 6.6 \pm 1.2$ s^{-1} and $k_{I,Cel7A} = 1.7 \pm 0.8$ s^{-1} for endoglucanase and $k_{D,Cel7B} = 24.0 \pm 2.8$ s^{-1} and $k_{I,Cel7B} = 1.6 \pm 0.5$ s^{-1}. Example calculated loading/washoff histories for single Cel7A and single Cel7B are shown in Figure 3.12. All calculated histories fit the transient data well. We have also used the proposed kinetic model to predict the smooth lines shown in Figures 3.5, 3.8, 3.9, and 3.10. In all cases, excellent agreement is achieved for both transient data and data taken at single time points. In particular, note from the light dashed lines in Figure 3.8 the rate at which the adsorbed enzymes transform to irreversible attachment. Within 1 h, well over one-half of each adsorbed enzyme is permanently attached to the surface.

Table 3.1. Kinetic parameters for single Cel7A and Cel7B

	k_A ppm^{-1} h^{-1}	k_D h^{-1}	K_L ppm^{-1}	k_I h^{-1}
Cel7A	0.28 ± 0.05	6.6 ± 1.2	0.042 ± 0.013	1.7 ± 0.8
Cel7B	0.070 ± 0.013	24.0 ± 2.8	0.0029 ± 0.0009	1.6 ± 0.5

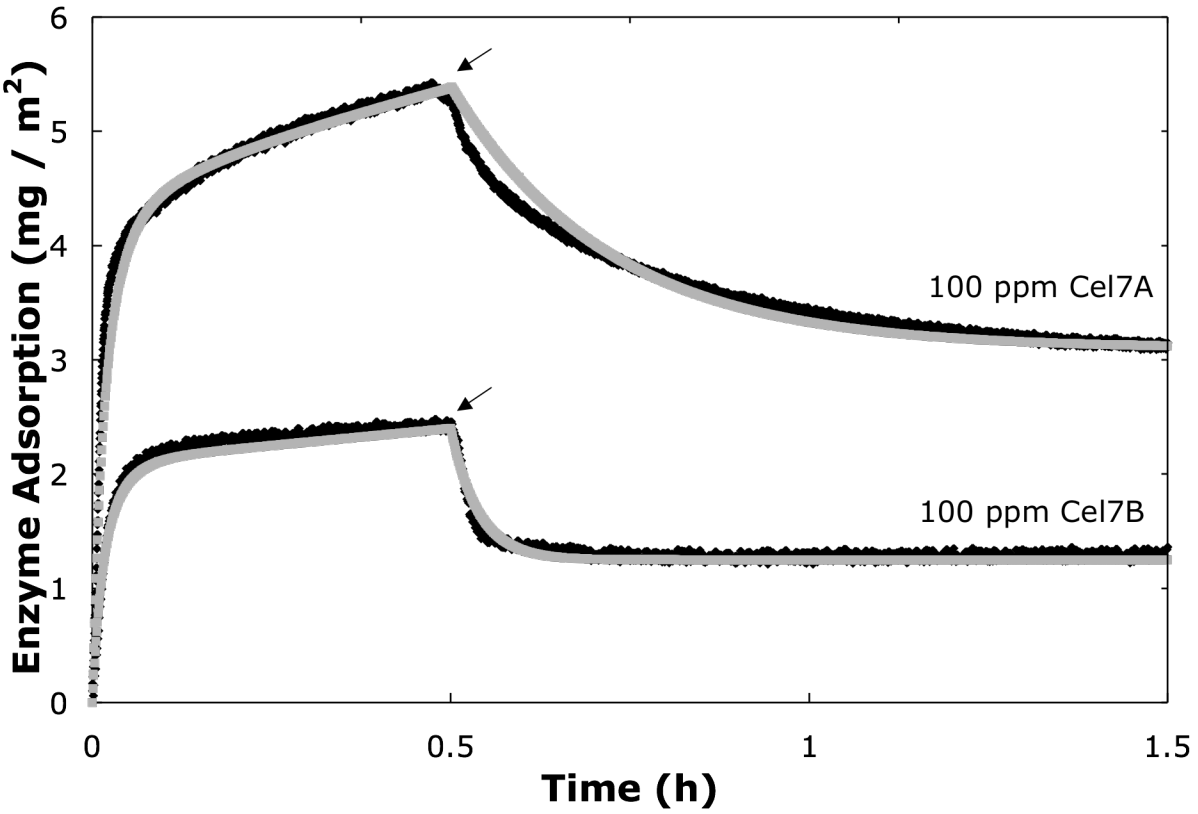

Figure 3.12. Example single-enzyme loading/washoff histories (black points) compared to theory (gray lines). Washoff after 30 min indicated by arrows. 100-ppm Cel7A and Cel7B from *T. longibrachiatum* with 6000-ppm glucose in aqueous buffer at 25 ºC. Single-enzyme kinetic constants from Table 3.1.

3.5.3. Mixed-Enzyme Sorption Kinetics

Extension of the kinetic model to predict competitive loading/washoff histories is important to its application. For a binary mixture of Cel7A and Cel7B, Equations 3.2 – 3.4 take the following forms:

$$\frac{d\Gamma_{E,Cel7A}}{dt} = k_{A,Cel7A}[Cel7A]_{bulk}\Gamma_O - k_{D,Cel7A}\Gamma_{E,Cel7A} - k_{I,Cel7A}\Gamma_{E,Cel7A} \quad , \qquad (3.8)$$

$$\frac{d\Gamma_{I,Cel7A}}{dt} = k_{I,Cel7A}\Gamma_{E,Cel7A} \quad , \qquad (3.9)$$

$$\frac{d\Gamma_{E,Cel7B}}{dt} = k_{A,Cel7B}[Cel7B]_{bulk}\Gamma_O - k_{D,Cel7B}\Gamma_{E,Cel7B} - k_{I,Cel7B}\Gamma_{E,Cel7B} \quad , \qquad (3.10)$$

$$\frac{d\Gamma_{I,Cel7B}}{dt} = k_{I,Cel7B}\Gamma_{E,Cel7B} \quad , \qquad (3.11)$$

and

$$\Gamma_{\max} = \Gamma_{E,Cel7A} + \Gamma_{E,Cel7B} + \Gamma_{I,Cel7A} + \Gamma_{I,Cel7B} + \Gamma_O \quad . \qquad (3.12)$$

Equations 3.8 – 3.12 are readily solved numerically for the surface concentrations of reversibly adsorbed and irreversibly bound Cel7A and Cel7B in any given mixture. As a stringent test of our mixture kinetic model, we utilize the single-enzyme rate constants to predict the kinetic behavior of binary mixtures. Figure 3.13 graphs modeled total cellulase adsorption, Γ_T, for three such binary mixtures (45 ppm Cel7A:5 ppm Cel7B; 25 ppm Cel7A:25 ppm Cel7B; and 5 ppm Cel7A:45 ppm Cel7B) in comparison to experimental data. Excellent agreement is seen. Similar excellent agreement between model and experiment for the competitive adsorption data is also seen in Figure 3.10. The proposed kinetic sorption model well predicts loading/washoff in a multiple-enzyme system including competitive reduction of the lesser-adsorbing enzyme. All rate constants used in the extended multiple-enzyme model were obtained from single-enzyme experimental data. No additional adjustable parameters were employed in the predictions.

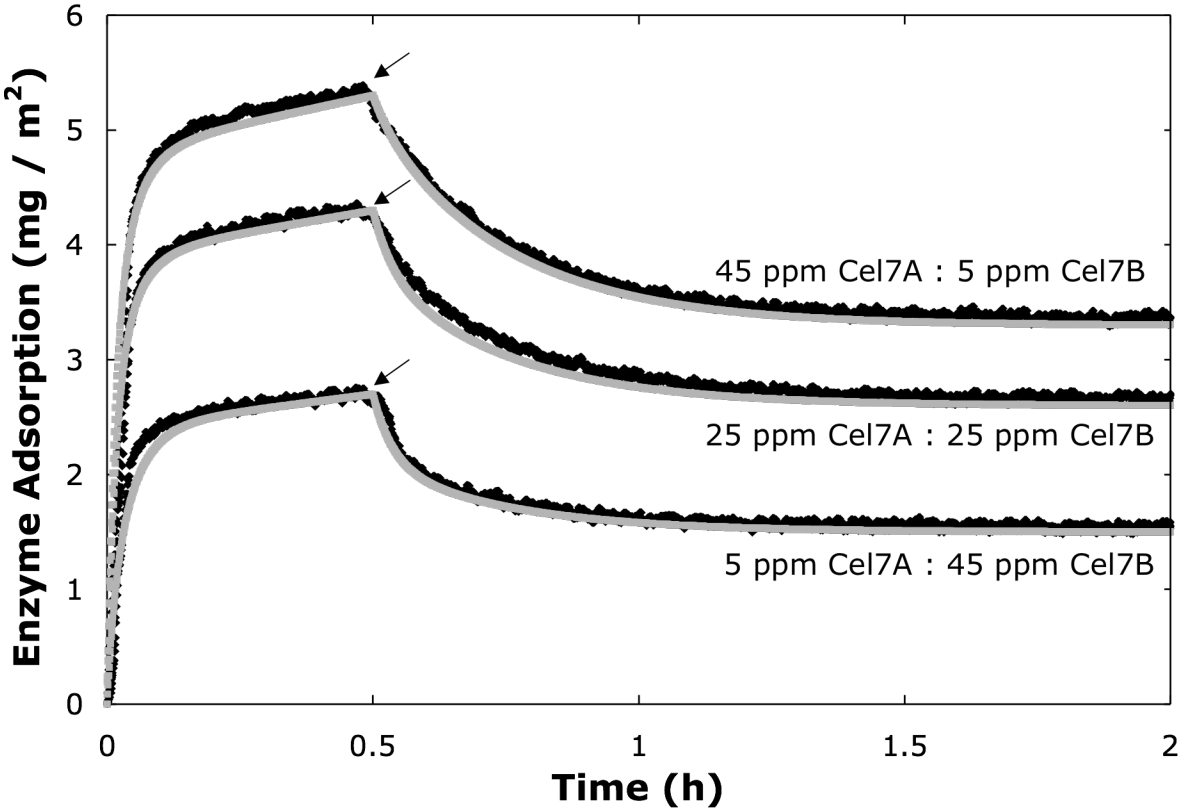

Figure 3.13. Loading/washoff histories (black data) for three *T. longibrachiatum* Cel7A and Cel7B mixtures on a model cellulose film compared to theory (grey lines). Washoff after 30 min, indicated by arrows. Enzyme in 6000-ppm glucose in aqueous buffer at 25 ºC. Single-enzyme kinetic constants from Table 3.1. No adjustable parameters were used.

3.6. Discussion

Rate constants k_A and k_D vary significantly between Cel7A and Cel7B, with k_A for Cel7A a factor of 4 higher and k_D a factor of 3.5 smaller. The Langmuir equilibrium constant $K_L = k_A / k_D$, a measure of cellulase affinity for the cellulose surface, is thus a factor of 14 larger for Cel7A. Cel7A adsorbs more readily to the cellulose surface than does Cel7B, and also desorbs more slowly.

However, as shown in Figure 3.8, when both enzymes are left in contact with the surface for long time periods (t = 10 – 12 h), they asymptote to the same adsorption maximum, Γ_{max} = 6.8 mg / m^2. Over short time scales (t = 0 – 2 h), as shown in the inset of Figure 3.8, adsorption is limited by an apparent Langmuir equilibrium where adsorption and desorption reach an approximate balance, with irreversible adsorption playing a comparatively small role. Thus, Cel7A initially appears to reach a higher adsorption maximum than does Cel7B. However, over longer time scales (t = 10 – 12 h), both enzymes continue to adsorb, while desorption is much slower, as a larger proportion of surface enzyme is converted to the irreversibly bound state. At long times, adsorption is controlled primarily by steric effects, up to the observed adsorption maximum. Although Cel7A and Cel7B have different molecular weights (65 and 57 kDa), this shared mass adsorption maximum suggests similar steric effects limit the adsorption of both cellulases. Josefsson *et al.* did not observe long-time adsorption, but calculated an enzyme adsorption of 8.3 mg / m^2 for Cel7A and 3.7 mg / m for endoglucanase V after one hour of surface contact at similar enzyme concentrations, confirming our observation of Cel7A having a higher surface affinity than a corresponding endoglucanase.[17] Thin films used in the work of Josefsson *et al.* were synthesized from dissolving pulp cellulose rather than Avicel. Differences in surface morphology may therefore account for the observed difference in maximum Cel7A adsorption. In previous work, we utilized ellipsometry and a similar adsorption method to calculate an adsorption maximum of Γ_{max} = 2.9 mg / m^2 for a lyophilized mixture of cellulases from *T. reesei*.[12] However, this mixture of cellulases also included non-surface active enzymes lacking cellulose binding domains (cellobiases) and other contaminants, and, therefore, may not have adsorbed as strongly as the isolated cellulases used in this work. The observed adsorption maximum remains below the monolayer adsorption level calculated from a typical cellulase geometry, Γ_{mono} = 9.8 x 10^{-3} g / m^2.[12]

Figures 3.3 and 3.4 show that for a given washoff time (t = 30 min) the proportion of enzyme remaining irreversibly bound on the cellulose surface remains constant, independent of bulk enzyme concentration and total surface adsorption. This important finding suggests that observed irreversible binding is not caused by cellulase aggregation either in bulk solution or on the cellulose surface, which requires an increase in irreversible binding rate at higher enzyme bulk and surface concentrations. Rather, the interactions of individual adsorbed cellulase molecules with the cellulose surface produce irreversible binding.

The first-order irreversible-binding rate constant (k_I) for Cel7A and Cel7B is approximately equal. The CBDs for Cel7A and Cel7B are structurally similar, to the extent that a recombinant protein consisting of a Cel7A catalytic domain attached to a Cel7B cellulose binding domain was shown to have identical activity with native Cel7A.[43] Given the similar binding sites and irreversible binding rate constants, we propose that irreversible binding is governed primarily by the interaction of the CBD with the cellulose film. Adsorption of the CBD both enzymes is mediated by the interaction of three tyrosine residues[33] with the cellulose surface, with possible involvement of tryptophan and glutamine residues.[44] Possible mechanisms

for irreversible binding include covalent interaction between aromatic CBD residues and free hydroxyl groups on the cellulose surface or morphological change/local partial surface denaturation[45 46] of the CBD. Changes in the character of tryptophan and glutamine interactions could also account for irreversible binding. Unfortunately, detailed mechanisms for adsorption for fungal cellulase CBD from solution to the cellulose surface are not well described. Both experimental studies[35 42 47] and molecular modeling[34 48] provide little direct, definitive characterization of the CBD-surface interaction.

Although the irreversible binding rate constants for Cel7A and Cel7B are identical, their adsorption and desorption rate constants (k_A, k_D) differ. Adsorption and desorption from bulk solution, however, is not dictated solely by the CBD but also by the geometry and morphological properties of the entire cellulase molecule. Cel7A and Cel7B have different molecular weights and catalytic-domain geometries. The catalytic domain of Cel7A is larger and resembles a binding barrel to draw in cellulose chains,[49] whereas the catalytic domain of Cel7B resembles a cleft.[50] Given the differing overall geometries of the molecules, it is possible that the CBD of Cel7A contacts the surface more readily due to the orientation of the enzyme in the surface region, producing an apparent higher adsorption rate and affinity of Cel7A for the cellulose surface. The exterior of the cellulase CD may also interact with the cellulose surface,[51] providing additional binding interactions and guiding binding of the CBD. Once adsorbed, both enzymes transition to an irreversibly bound state at the same rate, governed mostly by a change in the CBD/surface interaction.

To account for the apparent higher affinity of Cel7A for the cellulose surface despite identical binding domains and rates of irreversible adsorption, we consider the standard Gibbs free energy of enzyme adsorption to the surface,

$$\Delta G^0_{ads} = \Delta H^0_{CBD} + \Delta H^0_{CD} - T\Delta S^0_{CBD} - T\Delta S^0_{CD} \quad , \qquad (3.13)$$

where the standard enthalpies and entropies of adsorption for the cellulose binding and catalytic domains are taken as additive. Langmuir equilibrium constants in Table 3.1 ($K_{L,Cel7A} / K_{L,Cel7B} = 14$), indicate a difference in adsorption free energy of $\Delta G^0_{ads,Cel7A} - \Delta G^0_{ads,Cel7B} =$ -6.5 kJ / mol. By assuming that the standard enthalpies of adsorption arise primarily from the similar CBDs and that the CDs provide only a comparatively small and not dissimilar contribution, this difference in adsorption free energy is attributed solely to entropic effects. The resulting standard adsorption entropy difference is then $\Delta S^0_{ads,Cel7A} - \Delta S^0_{ads,Cel7B} =$ 22 J / mol K. Hoshino *et al*. find a similar adsorption entropy difference of 49 J / mol K for *I. lacteus* endo- and exo-cellulases on a cellulose surface with 60% crystallinity.[52]

It is difficult to compare our sorption rates directly to available literature, as comparable work has not employed inhibition to separate adsorption and activity kinetics. For example, Hu *et al.* characterize irreversible enzyme adsorption to PVAm and gold surfaces, but noted that similar measurements on cellulose surfaces are difficult, as desorption cannot be decoupled from cellulase activity.[19] The frequency-shift data of this group also show evidence of irreversible adsorption, though the authors suggest that it could also be attributed to modification of the cellulose film.[19] A surface plasmon resonance (SPR) study conducted by Ma *et al.*[53] shows a similar quantitative picture of Cel7A adsorption in Figure 3.5. Upon washoff after 5 min of contact with the surface, approximately 40% of the enzyme desorbs, with the remaining 60% left irreversibly bound to the surface. This SPR study appears to show faster enzyme adsorption and irreversible binding rates than does our study. It is possible that this results from the difference

in morphology between our spin-cast cellulose films and the Whatman CF11 powdered cellulose substrate of Ma *et al*.[53]

3.7. Conclusions

Quartz crystal microgravimetry on a model cellulose film offers a continuous, non-invasive, inhibition-free assay of cellulase activity on a well-defined cellulose substrate of known surface area. Using small enzyme samples, this assay ascertains surface kinetic parameters that otherwise are impossible to obtain from traditional bulk assays on poorly-defined cellulose surfaces. We quantified adsorption and desorption kinetics of single cellobiohydrolase I (Cel7A) and single endoglucanase I (Cel7B) under glucose inhibition on a model cellulose surface. Both Cel7A and Cel7B irreversibly bind to the cellulose surface on time scales as short as 3 min after exposure to the surface. Up to 90% of adsorbed enzyme is irreversibly bound after 1 h exposure to the cellulose surface. Adsorption, desorption, and irreversible-binding kinetics were characterized using an extended Langmuir sorption kinetic model. Single-enzyme rate constants successfully predict the transient loading/washoff of binary mixtures of enzymes over a range of concentration ratios with no adjustable parameters. Cel7A exhibits a higher affinity (i.e., a larger Langmuir equilibrium constant) for the surface than does Cel7B, by both adsorbing more quickly and desorbing more slowly. However, the first-order rate constant governing irreversible adsorption is identical for the two enzymes. Apparently, irreversible binding is governed mainly by the interaction between the cellulose binding domain and the surface, rather than by partial denaturation of the entire two-domain enzyme. To explain the higher kinetic rates and affinity of Cel7A relative to Cel7B, we hypothesize that interaction of the CBD with the cellulose surface gives similar enthalpies and entropies for each enzyme. Entropic differences of the entire molecule account for the apparent higher affinity of Cel7A for the cellulose surface. Because Cel7A and Cel7B exhibit different sorption kinetics and affinities, effective enzymatic deconstruction mixtures must be based on surface concentrations rather than on bulk concentrations. Further, because both enzymes adsorb irreversibly even for relatively small exposure times, recovery and reuse of these enzymes is unlikely in a deconstruction process.

3.8. List of Symbols

ΔF : QCM frequency shift
ΔD : QCM energy-dissipation change
Δm : Film mass change per unit area, mg / m^2
Cel7B : *T. longibrachiatum* endoglucanase I
Cel7A : *T. longibrachiatum* cellobiohydrolase I
[E] : bulk enzyme concentration, ppm
$[Cel7B]_{bulk}$: Bulk Cel7B concentration, ppm
$[Cel7A]_{bulk}$: Bulk Cel7A concentration, ppm
Γ_E : Surface concentration of reversibly adsorbed enzyme, mg / m^2
$\Gamma_{E,0}$: Surface concentration of reversibly adsorbed enzyme at the beginning of washoff, mg / m^2
$\Gamma_{E,\infty}$: Surface concentration of reversibly adsorbed enzyme at t = ∞, mg / m^2
Γ_{Cel7B} : Surface concentration of reversibly adsorbed Cel7B, mg / m^2
Γ_{Cel7A} : Surface concentration of reversibly adsorbed Cel7A, mg / m^2
Γ_I : Surface concentration of irreversibly bound enzyme, mg / m^2

$\Gamma_{I,0}$: Surface concentration of irreversibly bound enzyme at the beginning of washoff, mg / m^2
$\Gamma_{I,\infty}$: Surface concentration of irreversibly bound enzyme at t = ∞, mg / m^2
$\Gamma_{Cel7A,I}$: Surface concentration of irreversibly bound Cel7A, mg / m^2
$\Gamma_{Cel7B,I}$: Surface concentration of irreversibly bound Cel7B, mg / m^2
Γ_{max} : Maximum enzyme adsorption, mg / m^2
Γ_T : Total surface concentration for all enzyme, mg / m^2
$\Gamma_{T,0}$: Total surface concentration for all enzyme at the beginning of washoff, mg / m^2
$\Gamma_{T,\infty}$: Total surface concentration for all enzyme at t = ∞, mg / m^2
Γ_O : Surface concentration of open enzyme adsorption sites, mg / m^2
k_A : Adsorption rate constant, ppm^{-1} h^{-1}
$k_{A,Cel7A}$: Adsorption rate constant for Cel7A, ppm^{-1} h^{-1}
$k_{A,Cel7B}$: Adsorption rate constant for Cel7B, ppm^{-1} h^{-1}
k_D : Desorption rate constant, h^{-1}
$k_{D,Cel7A}$: Desorption rate constant for Cel7A, h^{-1}
$k_{D,Cel7B}$: Desorption rate constant for Cel7B, h^{-1}
k_I : Irreversible binding rate constant, h^{-1}
$k_{I,Cel7A}$: Irreversible binding rate constant for Cel7A, h^{-1}
$k_{I,Cel7B}$: Irreversible binding rate constant for Cel7B, h^{-1}
K_L : Langmuir-type equilibrium constant, ppm^{-1}
$K_{L,Cel7A}$: Langmuir-type equilibrium constant for Cel7B, ppm^{-1}
$K_{L,Cel7B}$: Langmuir-type equilibrium constant for Cel7B, ppm^{-1}
t_0 : Time point at which washoff begins

3.9. References

(1) Himmel, M.; Ding, S. Y.; Johnson, D. K.; Adney, W. S.; Nimlos, M. R.; Brady, J. W.; Foust, T.D. Biomass Recalcitrance: Engineering Plants and Enzymes for Biofuels Production. *Science* **2007**, *315,* 804-807.

(2) Beguin, P.; Aubert, J. P. The Biological Degradation of Cellulose. *Fems Microbio Rev* **1994,** *13,* 25-58.

(3) Wyman, C. E. Ethanol from Lignocellulosic Biomass: Technology, Economics, and Opportunities. *Bioresource Technol*. **1994,** *50,* 3-16.

(4) Houghton, J.; Weatherwax, S.; Ferrell, J. Breaking the Biological Barriers to Cellulosic Ethanol: A Joint Research Agenda. *US DOE,* DOE/SC-0095, 2005.

(5) Macmillan, J. D. Bioethanol Production: Status and Prospects. *Renewable Energy* **1997,** *2-3,* 295-302.

(6) Pauly, M.; Keegstra, K. Cell-wall Carbohydrates and Their Modification as a Resource for Biofuels. *Plant Journal* **2008,** *54,* 559-568.

(7) Kumar, R.; Singh, S.; Singh, O. V. Bioconversion of Lignocellulosic Biomass: Biochemical and Molecular Perspectives. *J Ind Microbiol Biotechnol* **2008,** *35,* 377-391.

(8) Bai F. W.; Anderson W. A.; Moo-Young M. Ethanol Fermentation Technologies from Sugar to Starch Feedstocks. *Biotech Adv* **2008,** *26(1),* 89-105.

(9) Kontturi, E.; Tammelin, T.; Österberg, M. Cellulose—Model Films and the Fundamental Approach. *Chem Soc Rev* **2006,** *35,* 1287-1313.

(10) Lee, S.B; Shin, H.S.; Ryu, D. D. Y.; Mandels, M. Adsorption of Cellulase on Cellulose: Effect of Physicochemical Properties of Cellulose on Adsorption and Rate of Hydrolysis. *Biotechnol Bioeng* **1982**, *24,* 2137-2153.

(11) Abdmziem, K.; Passas, R.; Belgacem, M. N. Inverse Gas Chromatography as a Tool to Characterize the Specific Surface Area of Cellulose Fibers. *Cell Chem Technol* **2006,** *40,* 199-204.

(12) Maurer, S. A.; Bedbrook, C. N.; Radke, C. J. Cellulase Adsorption and Reactivity on a Cellulose Surface from Flow Ellipsometry. *I&ECR* **2012**. Submitted. (Dissertation Chapter 2)

(13) Gunnars S.; Wågberg L.; Stuart M. A. C. Model Films of Cellulose: I. Method Development and Initial Results. *Cellulose* **2002,** *9,* 239-249.

(14) Falt, S.; Wågberg, L.; Vesterlind, E. L.; Larsson, P. T. Model Films of Cellulose II - Improved Preparation Method and Characterization of the Cellulose Film. *Cellulose* **2004,** *11,* 151-162.

(15) Eriksson J.; Malmsten, M.; Tiberg, F.; Callisen, T. H.; Damhus, T.; Johansen, K. S. Enzymatic Degradation of Model Cellulose Films. *J Colloid Interface Sci* **2005,** *284,* 99-106.

(16) Turon X.; Rojas, O. J.; Deinhammer, R. S. Enzymatic Kinetics of Cellulose Hydrolysis: A QCM-D Study. *Langmuir* **2008,** *24,* 3880-3887.

(17) Josefsson P.; Henriksson G.; Wågberg L. The Physical Action of Cellulases Revealed by a Quartz Crystal Microbalance Study Using Ultrathin Cellulose Films and Pure Cellulases. *Biomacromolecules* **2008,** *9,* 249-254.

(18) Ahola, S.; Turon, X.; Österberg, M.; Laine, J.; Rojas, O J. Enzymatic Hydrolysis of Native Cellulose Nanofibrils and Other Cellulose Model Films: Effect of Surface Structure. *Langmuir* **2008,** 24, 11592 – 11599.

(19) Hu, G.; Heitmann, J. A.; Rojas, O. J. In Situ Monitoring of Cellulase Activity by Microgravimetry with a Quartz Crystal Microbalance. *J Phys Chem B*. **2009,** *113,* 14761-14768.

(20) Hu, G.; Heitmann, J. A.; Rojas, O. J. Quantification of Cellulase Activity Using the Quartz Crystal Microbalance Technique. *Anal Chem* 2009, 81, 1872–1880.

(21) Suchy, M.; Linder, M. B.; Tammelin, T.; Campbell, J. M.; Vuorinen, T.; Kontturi, E. Quantitative Assessment of the Enzymatic Degradation of Amorphous Cellulose by Using a Quartz Crystal Microbalance with Dissipation Monitoring. *Langmuir* **2011,** *27,* 8819-8828.

(22) Andersen, M.; Johansson, L. S.; Tanem, B. S.; Stenius, P.; Properties and Characterization of Hydrophobized Microfibrillated Cellulose. *Cellulose* **2006,** *13,* 665-677.

(23) Mohan, T.; Kargl, R.; Doliska, A.; Vesel, A.; Kostler, S.; Ribitsch, V.; Stana-Kleinschek, K. Wettability and Surface Composition of Partly and Fully Regenerated Cellulose Thin Films from Trimethylsilyl Cellulose. *J Colloid Interface Sci* **2011,** *358,* 604-610.

(24) Habibi Y.; Foulon, L.; Aguie-Beghin, V.; Molinari, M.; Douillard, R. Langmuir-Blodgett Films of Cellulose Nanocrystals: Preparation and Characterization. *J Colloid Interface Sci* **2007,** *316,* 388-397.

(25) Cheng, G.; Liu, Z.; Murton, J. K.; Jablin, M.; Dubey, M.; Majewski, K.; Halbert, C.; Browning, J.; Ankner, J.; Akgun, B.; Wang, C.; Esker, A. R.; Sale, K. L.; Simmons, B. A.; Kent, M.S. Neutron Reflectometry and QCM-D Study of the Interaction of Cellulases With Films of Amorphous Cellulose. *Biomacromolecules* **2011,** *12,* 2216-24.

(26) O'Sullivan, A. C. Cellulose*:* The Structure Slowly Unravels. *Cellulose* **1997,** *4,* 173-207.

(27) Gross, A.; Chu, J-W. On the Molecular Origins of Biomass Recalcitrance: The Interaction Network and Solvation Structures of Cellulose Microfibrils. *J Phys Chem B* **2010,** *114,* 13333.

(28) Cho, H. M.; Gross, A.; Chu, J-W. Dissecting Force Interactions in Cellulose Deconstruction Reveals the Required Solvent Versatility for Overcoming Biomass Recalcitrance. *JACS* **2011,** 133, 14033-14041.

(29) Zhang, Y. H. P.; Himmel, M. E.; Mielenz, J. Outlook for Cellulase Improvement: Screening and Selection Strategies. *Biotech Advances* **2005,** *24,* 452-481.

(30) Zhang, Y. H. P.; Lynd; L. R. A Functionally Based Model for Hydrolysis of Cellulose by Fungal Cellulase. *Biotech Bioeng* **2006,** *94(5),* 889-898.

(31) Fox, J. M.; Levine, S. E.; Blanch, H. W.; Clark, D. S. Initial- and Processive-Cut Products Reveal Cellobiohydrolase Rate Limitations and the Role of Companion Enzymes. *Biochemistry*. **2012**, *51(1)*, 442-452.

(32) Xu, F.; Ding, H. A New Kinetic Model for Heterogeneous (Or Spatially Confined) Enzymatic Catalysis: Contributions from the Fractal and Jamming (Overcrowding) Effects. *Applied Catalysis A-General* **2007,** *317,* 70-81.

(33) Linder, M.; Mattinen, M. L.; Kontteli, M.; Lindeberg, G.; Stahlberg, J.; Drakenberg, T.; Reinikainen, T.; Pettersson, G.; Annila, A. Identification of Functionally Important Amino-Acids in the Cellulose-Binding Domain of *Trichoderma-reesei* Cellobiohydrolase I. *Protein Sci* **1995,** *4,* 1056-1064.

(34) Tavagnacco, L.; Mason, P. E.; Schnupf, U.; Pitici, F.; Zhong, L. H.; Himmel, M.E.; Crowley, M.; Cesaro, A.; Brady, J.W. Sugar-Binding Sites on the Surface of the Carbohydrate-Binding Module of Cel7A from *T. reesei*. *Carbohydrate Research* **2011,** *346,* 839-846.

(35) Linder, M.; Teeri, T. T. The Cellulose-Binding Domain of the Major Cellobiohydrolase of Trichoderma Reesei Exhibits True Reversibility and a High Exchange Rate on Crystalline Cellulose. *Proceedings of the National Academy of Sciences* **1996**, *93,* 12251-12255.

(36) Jung, H.; Wilson, D.B.; Walker, L.P. Binding and Reversibility of *Thermobifida fusca* Cel5A, Cel6B, and Cel48A and Their Respective Catalytic Domains to Bacterial Microcrystalline Cellulose. *Biotech Bioeng* **2003,** *84,* 151-159.

(37) Cascão Pereira, L. G.; Hickel, A.; Radke, C. J.; Blanch, H. W. A Kinetic Model for Enzyme Interfacial Activity and Stability: pa-Hydroxynitrile Lyase at the Diisopropyl Ether/Water Interface. *Biotech Bioeng* **2002,** *78,* 595-605.

(38) Levine, S. E.; Fox, J. M.; Blanch, H. W.; Clark, D. S. A Mechanistic Model of the Enzymatic Hydrolysis of Cellulose. *Biotech Bioeng* **2010,** *107,* 37-51

(39) Bharadwaj, R.; Wong, A.; Knierim, B.; Singh, S.; Holmes, B. M.; Auer, M.; Simmons, B. A.; Adams, P. D.; Singh A. K. High-throughput Enzymatic Hydrolysis of Lignocellulosic Biomass Via In-situ Regeneration. *Bioresource Tech* **2011,** *102,* 1329-1337.

(40) Holtzapple, M.; Cognata, M.; Shu, Y.; Hendrickson, C. Inhibition of Trichoderma-Reesei Cellulase by Sugars and Solvents. *Biotech Bioeng* **1990,** *36,* 275-287.

(41) Rodahl, M.; Höök, F.; Krozer, A.; Brzezinski, P.; Kasemo, B. Quartz-Crystal Microbalance Setup for Frequency and Q-Factor Measurements in Gaseous and Liquid Environments. *Rev Sci Inst* **1995,** *66,* 3924-3930.

(42) Kwon, H. J.; Bradfield, C. K.; Dodge, B. T.; Agoki, G. S. Study of Simultaneous Fluid and Mass Adsorption Model in the QCM-D Sensor for Characterization of Biomolecular Interactions. Proceedings of the COMSOL Conference, **2009,** Boston.

(43) Srisodsuk M.; Lehtiö, J.; Linder, M.; Margolles-Clark, E.; Reinikainen, T.; Teeri, T. T. *Trichoderma reesei* Cellobiohydrolase I with an Endoglucanase Cellulose-Binding Domain: Action on Bacterial Microcrystalline Cellulose. *J Biotech* **1997,** *57,* 49 – 57.

(44) Bray, M. R.; Johnson, P. E.; Gilkes, N. R.; McIntosh, L. P.; Kilburn, D. G.; Warren, R. A. J. Probing the Role of Tryptophan Residues in a Cellulose-Binding Domain by Chemical Modification. *Protein Science* **1996,** *5,* 2311-2318.

(45) Soderquist, M. E.; Walton, A. G. Structural Changes in Proteins Adsorbed on Polymer Surfaces. *J Colloid Interface Sci* **1979,** *75,* 386-397.

(46) Castells, V.; Yang, S. X.; Van Tassel, P. R. Surface-induced Conformational Changes in Lattice Model Proteins by Monte Carlo Simulation. *Phys Rev E* **2002,** *65,* #031912.

(47) Larsson, A. M.; Bergfors, T.; Dultz, E.; Irwin, D. C.; Roos, A.; Driguez, H.; Wilson, D. B.; Jones, T. A. Crystal Structure of Thermobifida busca Endoglucanase Cel6A in Complex with Substrate and Inhibitor: The Role of Tyrosine Y73 in Substrate Ring Distortion. *Biochem* **2005,** *44,* 12915-12922.

(48) Taylor, C. B.; Talib, M. F.; McCabe, C.; Bu, L. T.; Adney, W. S.; Himmel, M. E.; Crowley, M. F.; Becham, G. T. Computational Investigation of Glycosylation Effects on a Family 1 Carbohydrate-Binding Module. *J Bio Chem* **2012**, *287,* 3147-3155.

(49) Teeri, T. T.; Reinikainen, T.; Ruohonen, L; Alwyn Jones, T.; Knowles, J. K. C. Domain Function in *Trichoderma reesei* Cellobiohydrolases. *J Biotech* **1992,** *24,* 169-176.

(50) Henrissat, B. Cellulases and Their Interaction with Cellulose. *Cellulose* **1994,** *1,* 169-196.

(51) Lin, Y.; Silvestre-Ryan, J.; Himmel, M.; Crowley, M.; Beckham, G. T.; Chu, J-W. Protein Allostery at the Solid-Liquid Interface: Endoglucanase Attachment to Cellulose Affects Glucan Clenching in the Binding Cleft. *JACS* **2011,** *133,* 16617-16624.

(52) Hoshino, E.; Kanda, T.; Sasaki, Y.; Nisizawa, K. Adsorption Mode of Exo- and Endo-Cellulases from *Irpex lacteus* (*Polyporus tulipiferae*) on Cellulose with Difference Crystallinities. *J Biochem* **1992,** *111,* 600-605.

(53) Ma, A.; Hu, Q.; Qu, Y.; Bai, Z.; Liu, W.; Zhuang, G. The Enzymatic Hydrolysis Rate of Cellulose Decreases with Irreversible Adsorption of Cellobiohydrolase I. *Enz Microb Tech* **2008**, *42(7)*, 543-547.

Appendix 3.A: Washoff Parameter

To obtain Equation 3.5, we write Equations 3.2 and 3.3 during washoff ($[E]_{bulk} = 0$) and integrate Equation 3.2 starting from $t = t_0$,

$$\Gamma_E(t) = \Gamma_{E,0} e^{-(k_D + k_I)(t - t_0)} \quad . \tag{3.A1}$$

This result is substituted into Equation 3.3 and followed by integration to give

$$\Gamma_I(t) = \Gamma_{I,0} + \Gamma_{E,0} \frac{k_I}{k_D + k_I} \left[1 - e^{-(k_D + k_I)(t - t_0)}\right] \quad . \tag{3.A2}$$

Total adsorption, Γ_T, is the sum of Γ_E and Γ_I:

$$\Gamma_T(t) = \Gamma_{I,0} + \Gamma_{E,0} \frac{k_I}{k_D + k_I} \left[1 - e^{-(k_D + k_I)(t - t_0)}\right] + \Gamma_{E,0} e^{-(k_D + k_I)(t - t_0)} \quad . \tag{3.A3}$$

Evaluation of Equation 3.A3 at $t = \infty$ specifies the final total adsorption after washout,

$$\Gamma_{T,\infty} = \Gamma_{I,0} + \Gamma_{E,0} \frac{k_I}{k_D + k_I} \quad , \qquad (3.A4)$$

and allows Equation 3.A3 to be re-expressed as Equation 3.6 of the text.

Appendix 3.B: Determination of Single Rate Constants k_D and k_I

To set bounds on the individual rate constants k_D and k_I, Equation 3.A4 is rearranged algebraically to obtain

$$\frac{\Gamma_{T,\infty} - \Gamma_{T,0}}{\Gamma_{T,0}} = \frac{\Gamma_{E,0}}{\Gamma_{T,0}} \frac{k_D}{k_D + k_I} \quad . \qquad (3.B1)$$

The left side of Equation 3.B1 represents the ratio of total surface cellulase that desorbs during the washoff phase. From Figures 3.6 and 3.7, we observe that this value lies in the range of 0.1 - 0.8, depending on the particular cellulase studied and on the time that bulk enzyme is in contact with the surface before washoff. The first ratio on the the right side of Equation 3.B1, that of reversibly adsorbed cellulase to total surface cellulase at the start of washoff, $\Gamma_{E,0} / \Gamma_{T,0}$, cannot exceed unity. Thus, the ratio $k_D / (k_D + k_I)$ must lie in the range of 0.1 – 1 for both Cel7A and Cel7B. Restricting the value of this ratio simplifies our parametric search for the rate constants k_D and k_I.

To determine individual values for k_D and k_I, we input into the kinetic model (separately for Cel7A and Cel7B) the previously calculated values for k_A, Γ_{max}, and $k_D + k_I$. We then choose values of k_D based on the known ratio $k_D / (k_D + k_I)$. Resulting predicted loading/washoff histories were compared to those measured for various washoff times and enzyme concentrations. By iterating over the small range of possible k_D values and comparing the least-squares fit of the model to data, we obtained individual best-fit values for k_D and k_I for each cellulase, as listed in Table 3.1.

Chapter 4

Surface Kinetics for Cooperative Fungal Cellulase Deconstruction of Cellulose from Quartz Crystal Microgravimetry

4.1. Abstract

The kinetic behavior of aqueous cellulase on insoluble cellulose is best quantified through surface-based assays on a well-defined cellulose substrate of known area. We use a quartz crystal microbalance (QCM) to measure the activity of binary mixtures of *T. longibrachiatum* cellobiohydrolase I (Cel7A) and endoglucanase I (Cel7B) on spin-coated cellulose films. By extending a previous surface kinetic model for cellulase activity, we obtain rate constants for competitive adsorption of Cel7A and Cel7B, their irreversible binding, their complexation with the cellulose surface, and their cooperative cellulytic activity. The activity of the two cellulases is linked through the formation of cellulose chain ends by Cel7B that provide complexation sites from which Cel7A effects cellulose chain scission. While the rate-limiting step in Cel7A activity is complexation, Cel7B activity is limited by adsorption to the cellulose surface. A 2:1 bulk mass ratio of aqueous Cel7A:Cel7B, corresponding to a 4:1 surface mass ratio, effects the greatest rate of cellulose degradation across a range of cellulase concentrations at 25 ºC. We find that surface chain-end concentration is a major predictor of Cel7A activity. Degradation rate is maximized by producing the maximum quantity of chain ends while maintaining a minimum of Cel7B irreversibly bound to the surface. Disruption of the hydrogen-bonding structure of cellulose enhances the activity of Cel7A on the cellulose surface.

4.2. Background

Enzymatic deconstruction of cellulose is the fundamental rate-limiting step in the production of renewable biofuels from lignocellulosic sources.[1 2 3] Despite continuing biofuels research, the kinetic mechanisms and parameters governing this surface interaction remain poorly understood. Cellulose is the most abundant biopolymer and a fundamental component of plant cell walls.[4] Cellulose is comprised of long 1,4-β-D-linked chains of glucose arranged together in a hydrogen-bonding network that provides plant cell walls with structural rigidity but also makes cellulose insoluble and recalcitrant to degradation.[5] In all industrial-scale biofuel production, cellulolytic enzymes known as cellulases are used to deconstruct cellulose into glucose oligomers that are subsequently fermented and processed to form fuel additives.[1]

Complete deconstruction of solid cellulose into soluble glycans requires cooperative action on the cellulose surface of two classes of enzyme: endoglucanases and cellobiohydrolases.[5] Endoglucanases complex with the surface and break 1,4-β-D-glycosidic linkages to create cellulose chain ends that are lifted from the hydrogen-bonding matrix. Cellobiohydrolases then complex with exposed chain ends and degrade the cellulose into oligomers of 2 – 6 glucose units.[6] Both surface-active enzymes have two domains, a cellulose binding domain (CBD) and a catalytic domain (CD), joined by a flexible glycosylated linker.

Cellulose binding in fungal cellulases is typically mediated by the interaction of three tyrosine residues on the CBD with the cellulose surface.[7] Although the CBDs of many fungal cellulases are similar,[8] the CDs for endoglucanases and cellobiohydrolases are different, reflecting their different functions. The endoglucanase CD has a binding cleft that interacts with single sites on the cellulose surface to create chain ends, whereas the cellobiohydrolase CD is a barrel in which cellulose chains are degraded.[6] Breaking a glycosidic linkage to create a glucose oligomer requires significant distortion of the cellulose chain and the interaction of at least four cellobiohydrolase amino acid residues with the chain.[9] Once a cellobiohydrolase CD complexes with a chain end, it works processively on that chain, making many chain scissions before decomplexation. The mechanisms and kinetics of cellulase processivity are not yet well-defined. Typical estimates of cellobiohydrolase processive length are 10 – 100 cellobiose units.[10 11]

Despite ongoing study of enzymatic cellulose degradation, the mechanism and kinetic parameters governing these surface reactions remain poorly understood. Most assays are based in the bulk,[12] and, therefore, cannot elucidate surface interactions, particularly as the enzyme-accessible surface of cellulose is not well-characterized.[13] Extended kinetic models include surface phenomena such as chain length,[14] changes in cellulose morphology,[15] and surface enzyme diffusion.[16] Surface-based assays are critical to establish a more complete understanding.

Recently, thin films of cellulose adhered to metal supports have become available.[17] Properties of these films and corresponding enzyme activity have been explored using ellipsometry,[18 19] quartz crystal micrography,[20 21 22 23 24 25 26] Brewster angle microscopy,[27] neutron interferometry,[28] and AFM.[29 30] Most work has been directed toward the characterization of the cellulose films rather than deconstruction kinetics. We measure enzyme adsorption and activity on deposited cellulose films via quartz crystal microbalance (QCM), an acoustic technique that detects changes in the mass adsorbed to a gold-coated sensor via changes in the resonance of a quartz crystal.[31] Current literature offers basic characterization of cellulose films and cellulase activity via QCM,[21 22 23 24] but little quantitative modeling of cellulase activity using this surface-based technique is available.

We use QCM to elaborate a surface kinetic model of cellulase activity on deposited cellulose films. Intrinsic rate constants governing cellulase activity are obtained from single-enzyme systems, and subsequently incorporated into a two-enzyme kinetic model describing cooperative activity. We compare predicted two-enzyme activity to experiment, building on our previous efforts using ellipsometry[18] and QCM.[20] In this work, we extend an existing single-enzyme activity model[18] and two-enzyme competitive adsorption model[20] to describe the cooperative activity of *T. longibrachiatum* cellobiohydrolase I (Cel7A) and endoglucanase I (Cel7B).

4.3. Kinetic Model

Figure 4.1 illustrates the proposed surface kinetic model describing the cooperative activity of Cel7A and Cel7B on the cellulose surface. Separate surface adsorption and complexation of individual endoglucanases and cellobiohydrolases are included, along with corresponding competitive adsorption and cooperative activity to create and degrade exposed cellulose chain ends. Paramount is the irreversible adsorption of the two enzymes on the cellulose surface.

A four-step Langmuir-Michaelis-Menten kinetic model[18] is adopted for the activity of individual endoglucanases and cellobiohydrolases on the cellulose surface: (1) a cellulase adsorbs to the cellulose surface from bulk solution through a mass-transfer boundary layer and binds to the surface through its CBD; (2) the cellulase forms an enzyme-substrate complex with the surface; (3) a reaction is catalyzed within the enzyme-substrate complex, leaving the cellulase bound to the surface; and (4) the enzyme returns to its original adsorbed, uncomplexed state.

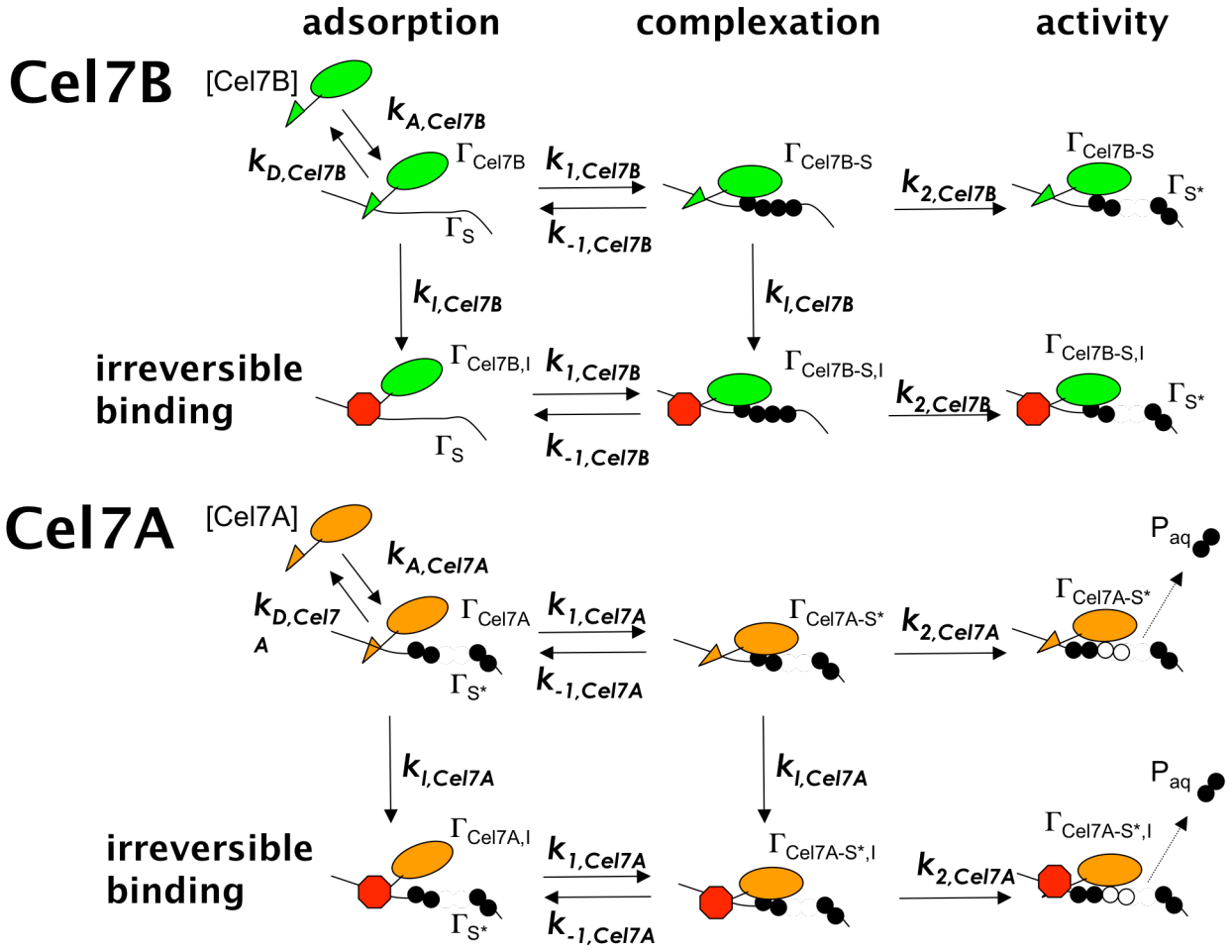

Figure 4.1. Surface kinetic model for adsorption and activity of endoglucanase I (Cel7B) and cellobiohydrolase I (Cel7A). Enzymes are shown as a catalytic domain (CD, oval) joined to a celluose binding domain (CBD, triangle). The irreversibly bound CBD is shown as a hexagon. Cellulose chains shown as thin lines, with individual glucose units denoted as filled circles. Small open circles represent glucose units degraded by Cel7A and liberated into bulk solution. Surface concentrations are denoted by Γ. Rate constants are indicated.

The activities of Cel7A and Cel7B are coupled by the creation and utilization of cellulose chain ends. Cel7B complexes nonspecifically with the cellulose surface and creates chain ends. Cel7A then complexes with the resulting chain ends, cleaving 1,4-β-glycosidic bonds and releasing glucose oligomers into solution. We assume that Cel7B does not effect cellulose chain scissions and release oligomers from the cellulose surface, i.e., the sole function of its activity is to create chain ends. Similarly, we assume that Cel7A complexes only with cellulose chain ends and that its primary function is to cleave glucose oligomers from the cellulose surface. Isolated CBDs from bacterial cellulases have been shown to disrupt the hydrogen-bonding network of cellulose.[32] However, in a separate study, Cel7A interaction with the cellulose surface was not associated with an increased concentration of chain ends.[11] We, therefore, discount this effect as minor compared to the rate of Cel7B chain-end formation during cooperative cellulase activity.

Thus, in Figure 4.1, cellulases adsorb to and desorb from bulk solution at the cellulose surface. Once adsorbed, enzymes complex and decomplex with cellulose, and undergo activity while remaining complexed. Adsorbed Cel7B complexes with the cellulose surface, of surface concentration Γ_S, and creates chain ends, of surface concentration Γ_{S^*}. Adsorbed Cel7A complexes with the chain ends and creates glucose oligomers that are released into bulk solution. Chain-end surface concentration does not affect Cel7A adsorption, as Cel7A can adsorb to any open surface site. However, Cel7A complexes only with chain ends.

Previously, QCM was used to determine the adsorption and desorption rate constants for Cel7A and Cel7B on the cellulose surface under glucose inhibition (k_A and k_D in Figure 4.1).[20] Glucose does not bind competitively for surface sites with either Cel7A or Cel7B and does not change the rates of adsorption of either enzyme.[18 20] Thus, the rate constants obtained under glucose inhibition remain valid for inhibition-free cellulase activity. Cel7A adsorbs to the cellulose surface with 14 times higher affinity than does Cel7B, likely due to the differing geometries of the molecules.[20] Irreversible binding of Cel7A and Cel7B to the cellulose surface is significant, with up to 80% of each enzyme binding irreversibly after 1 h of contact with the surface. An extended Langmuir kinetic model well characterizes this irreversible adsorption, with adsorbed enzyme transitioning to an irreversibly bound state according to first-order kinetics.[20 33] The kinetic constant governing irreversible adsorption (k_I in Figure 4.1) was identical between Cel7A and Cel7B.[20] Irreversible binding is, thus, mediated primarily by the CBD rather than by the entire cellulase molecule. In the expanded kinetic model for cooperative cellulase activity shown in Figure 4.1, both adsorbed uncomplexed and adsorbed complexed enzyme gradually bind irreversibly to the cellulose surface. Complexed and uncomplexed enzyme on the cellulose surface bind irreversibly according to the same first-order rate constant, k_I, since adsorption irreversibility is dominated by the similar CBDs of each enzyme.

Numerical embodiment of the kinetic model illustrated in Figure 4.1 is described in Appendix 4.A. Our method is to establish the intrinsic kinetic parameters in the proposed kinetic model from experiment and then validate the proposed depolymerization model by comparison to deconstruction kinetics obtained from QCM in a two-enzyme mixture.

4.4. Materials and Methods

4.4.1. Cellulases

Isolated *T. longibrachiatum* cellulases were obtained from Megazyme (Bray, Ireland). These fungal cellulases are typical for kinetic studies of cellulytic activity.[34 35] Cellobiohydrolase I (Cel7A; Megazyme E-CBHI, MW 65,000) was obtained at a concentration of 10,000 ppm in a

suspension of 3.2-M ammonium sulfate/2 wt% ammonium azide. *Endo*-cellulase contaminant was minimal; the enzyme mixture shows 0.003 U/mg *endo*-cellulase activity in comparison to 0.1 U/mg Cel7A activity. Endoglucanase I (Cel7B; Megazyme E-CELTR, MW 57,250) was obtained at a concentration of 9,400 ppm in a solution of 3.2-M ammonium sulfate/2% ammonium azide, again with minimal glucosidase contaminants. Enzymes were used as supplied after dilution to concentrations of 1 – 100 ppm in an aqueous solution of sodium dihydrogen phosphate buffer (9.5-mM NaH_2PO_4, pH 5.5; Sigma-Aldrich #S9638).

4.4.2. Cellulose Films

Thin cellulose films were deposited on cleaned gold-coated QCM sensors by a modification of the method of Gunnars *et al.*.[19] Sensors were coated in cationic poly-diallyl-dimethyl-ammonium chloride (PDADMAC). Cellulose was dissolved in 4-methyl-morpholine-N-oxide (4MMO) at 103 °C and the resulting solution spin-coated onto the prepared sensors. The deposited films were soaked in water to remove nascent 4MMO. Materials and methods were identical to those in previous work.[20] Degradation kinetics of cellulose films prepared according to this method is identical to that of Avicel, an industry standard for quantifying cellulase activity.[18]

4.4.3. Enzyme Activity via QCM

A cellulose-coated sensor was placed into the flow cell of a quartz crystal microbalance (Q-Sense E4, Västra Frölunda, Sweden). The flow cell was subsequently filled with a 9.5-mM NaH_2PO_4 aqueous buffer solution (pH 5.5). The coated cellulose film was allowed to swell in the buffer solution until a constant frequency shift was reached, typically 1 – 2 h after exposure to the solution. After swelling, a solution of cellulase at the desired concentration in buffer was flowed over the cellulose-coated wafer at a flowrate of 100 μL/min, typically for 1 – 12 h, during which time the frequency-shift and energy-dissipation response of the cellulose film were measured continuously. Following enzyme adsorption and activity, nascent buffer solution was flowed over the wafer to remove reversibly adsorbed surface enzyme and degradation products. Mass-transfer effects were not limiting for the flowcell geometry, bulk enzyme concentrations, and flowrates used in this work.[20] All experiments were conducted at 25 ºC.

4.4.4. QCM Frequency and Dissipation Histories

Figure 4.2 shows typical frequency-shift (ΔF) and energy-dissipation (ΔD) histories for the activity of a 5-ppm solution of Cel7A on a cellulose film for 2 h. Responses on the third overtone ($\Delta F_3/3$, ΔD_3) are shown, as those obtained using the fundamental frequency (ΔF_1, ΔD_1) are typically noisy. When the film is first exposed to Cel7A solution at t = 0.25 h, ΔF decreases, indicating adsorption of enzyme to the surface. The subsequent linear increase in ΔF, beginning around t = 0.5 h, corresponds to pseudo-steady degradation of the cellulose film by adsorbed, complexed Cel7A and release of products into aqueous solution.[18] At washoff, a rapid increase in ΔF reflects desorption of reversibly bound Cel7A. As Cel7A adsorbs to and then degrades the cellulose surface, dissipation, ΔD, increases from its initial value, indicating a decrease in film rigidity caused by enzyme adsorption to the surface. Due to the low energy dissipation observed, the Sauerbrey equation[31] was applied to relate the frequency-shift response linearly to the change in mass of the film,

$$\Delta m = -c\Delta F \quad , \qquad (4.1)$$

where Δm represents change in film mass and c = 0.18 mg s / m^2 is the Sauerbrey constant, a function of material parameters of quartz. The Sauerbrey equation was applied using the QTools 3.01 software included with the Q-Sense instrument to convert primary frequency data to film mass and thickness.

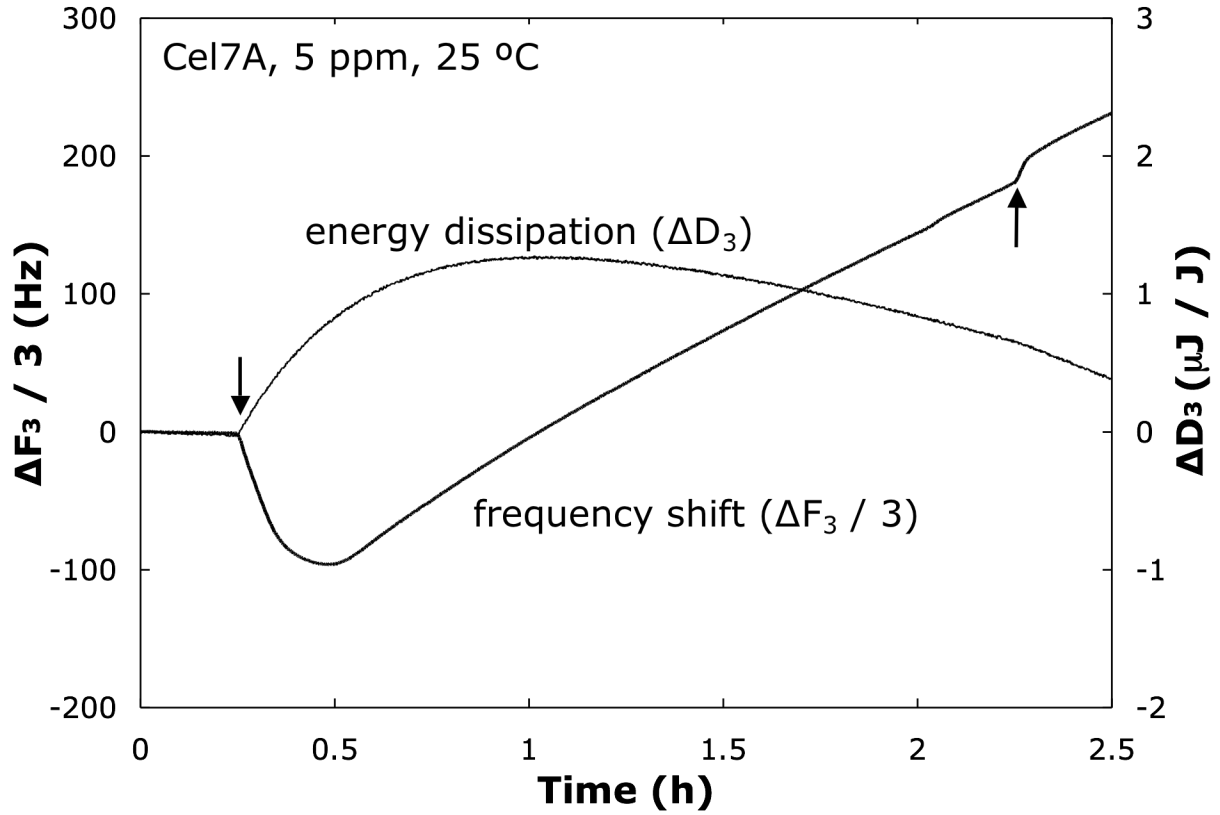

Figure 4.2. Typical frequency shift (ΔF, thick line) and dissipation (ΔD, thin line) histories for Cel7A activity on a model cellulose film. First vertical arrow indicates loading of enzyme in flowcell. Second vertical arrow indicates washoff. Data were measured on the third overtone of a Q-Sense QCM operating at 5 MHz. 5-ppm *T. longibrachiatum* Cel7A in aqueous buffer at 25 ºC.

Figure 4.3 displays a sample frequency-shift and energy-dissipation response history for the activity of a 100-ppm solution of Cel7B on a cellulose film over a 3 h period. When Cel7B is exposed to the cellulose film, ΔF decreases as enzyme adsorbs to the surface. However, since Cel7B exhibits little or no cellulytic activity, ΔF does not subsequently increase, as it does when Cel7A degrades the cellulose film. Upon washoff, a brief increase in ΔF is observed as reversibly bound Cel7B desorbs, followed by a continued linear decrease. A corresponding increase in ΔD over the period of enzyme adsorption indicates that the film becomes less rigid over the period of Cel7B exposure. Energy-dissipation response is much higher relative to

frequency-shift response for Cel7B compared to Cel7A. Josefsson *et al.* also observed a decrease in film rigidity for endoglucanases acting on model cellulose films and attributed it to swelling of the film resulting from disruption of the film surface allowing additional water to penetrate into the film.[24] The larger ΔD precludes use of the Sauerbrey equation. In this case, the Voigt model for viscoelastic film resonance[36] was used to quantify film mass and viscosity change. The Voigt model is also included in the QTools 3.01 software. Typically, ΔF and ΔD data from the third, fifth, and/or seventh overtones were used in the Voigt model to generate film mass and viscosity.

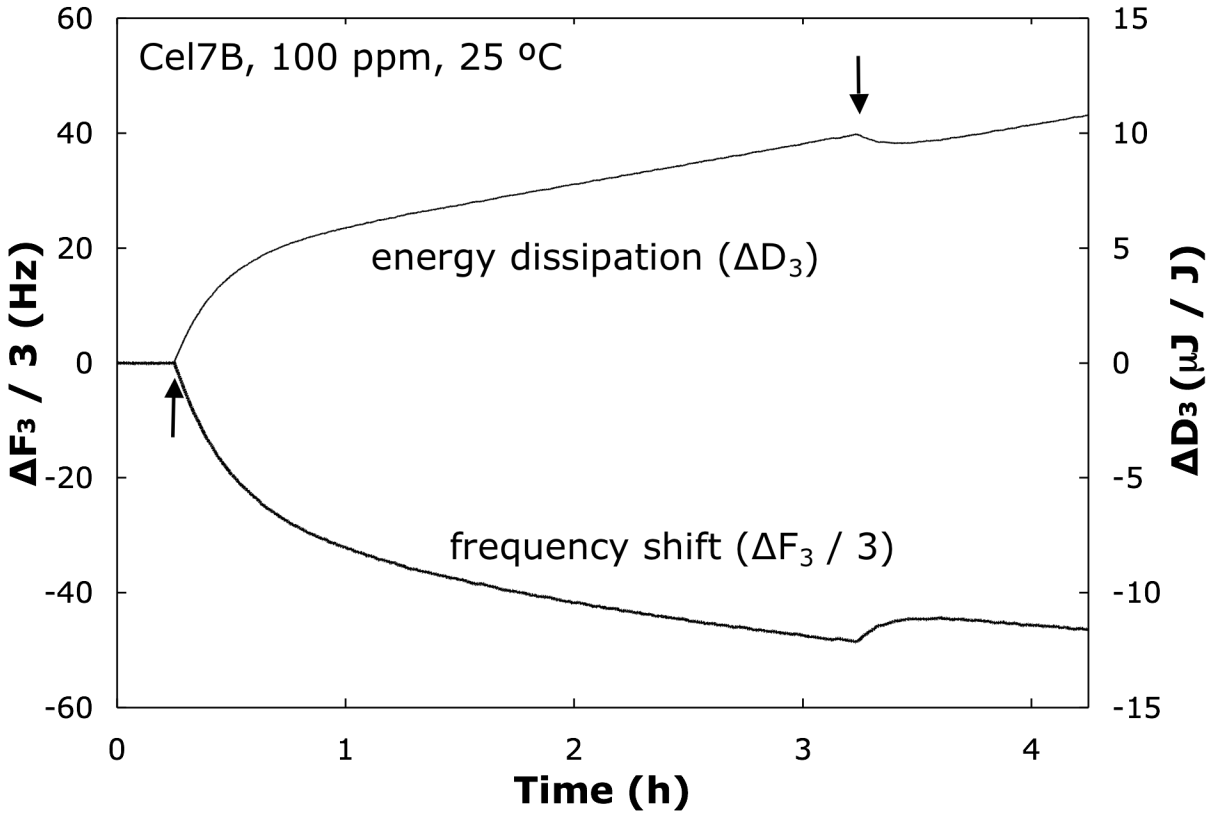

Figure 4.3. Typical frequency shift (ΔF, thick line) and dissipation (ΔD, thin line) histories for Cel7B activity on a model cellulose film. First vertical arrow indicates loading of enzyme in flowcell. Second vertical arrow indicates washoff. Data were measured on the third overtone of a Q-Sense QCM operating at 5 MHz. 100-ppm *T. longibrachiatum* Cel7B in aqueous buffer at 25 ºC.

4.5. Experimental Results

4.5.1. Cel7A Activity on the Cellulose Surface

Figure 4.4 shows a typical mass history for activity of Cel7A on a cellulose film, generated by using Equation 4.1 to convert the ΔF-response data from Figure 4.2 to mass change, Δm. Initial adsorption is clearly seen (t = 0.25 – 0.5 h), followed by complexation of Cel7A with the cellulose surface and subsequent degradation of the cellulose film. The linear decrease in film mass, and, therefore, the cellulose degradation rate, is constant after about 30 min. After 2 h of Cel7A contact with the surface, the enzyme is eluted by washing with buffer. A constant, though smaller, rate of decrease in film mass is subsequently observed, indicating that cellulose degradation continues, even with reversibly adsorbed enzyme washed from the surface.

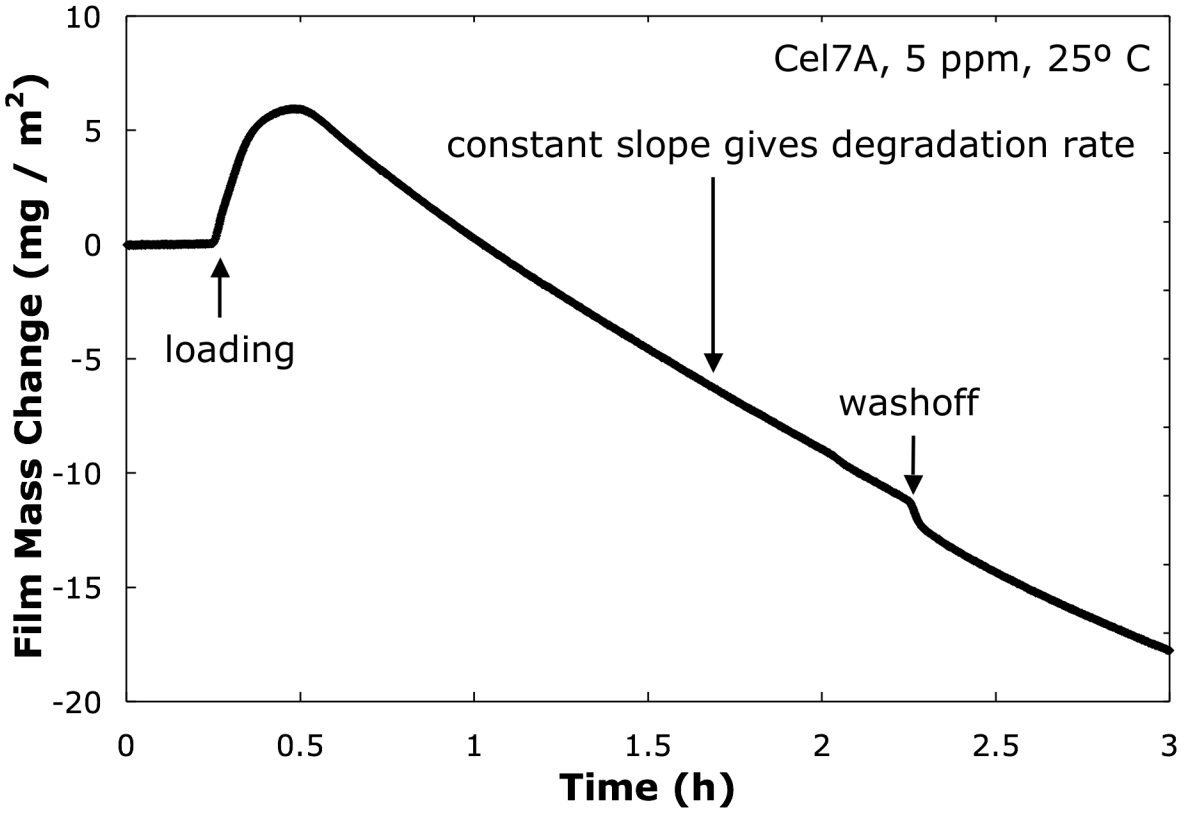

Figure 4.4. Mass history for adsorption and activity of Cel7A on a cellulose film for 2 h. Adsorption, constant degradation rate, and washoff are seen. 5-ppm *T. longibrachiatum* Cel7A in aqueous buffer at 25 ºC.

In Figure 4.5, Cel7A was loaded onto the cellulose surface for 12 h to probe for possible long-term loss of enzyme activity, a factor suggested in kinetic slowdown of cellulases on the cellulose surface.[37] Cel7A film-degradation rate remained constant on our model cellulose films over time scales as long as 12 h, even though Cel7A binds irreversibly to cellulose films over time scales shorter than 1 h.[20] This result is surprising, since irreversibility is typically associated with partial denaturation.[33] Apparently, irreversible binding is governed by the cellulose binding domain and not the catalytic domain. Cel7A does not denature completely on the cellulose surface over a time scale of 12 h. Rather, it remains bound and active on the cellulose surface, even during elution with buffer.

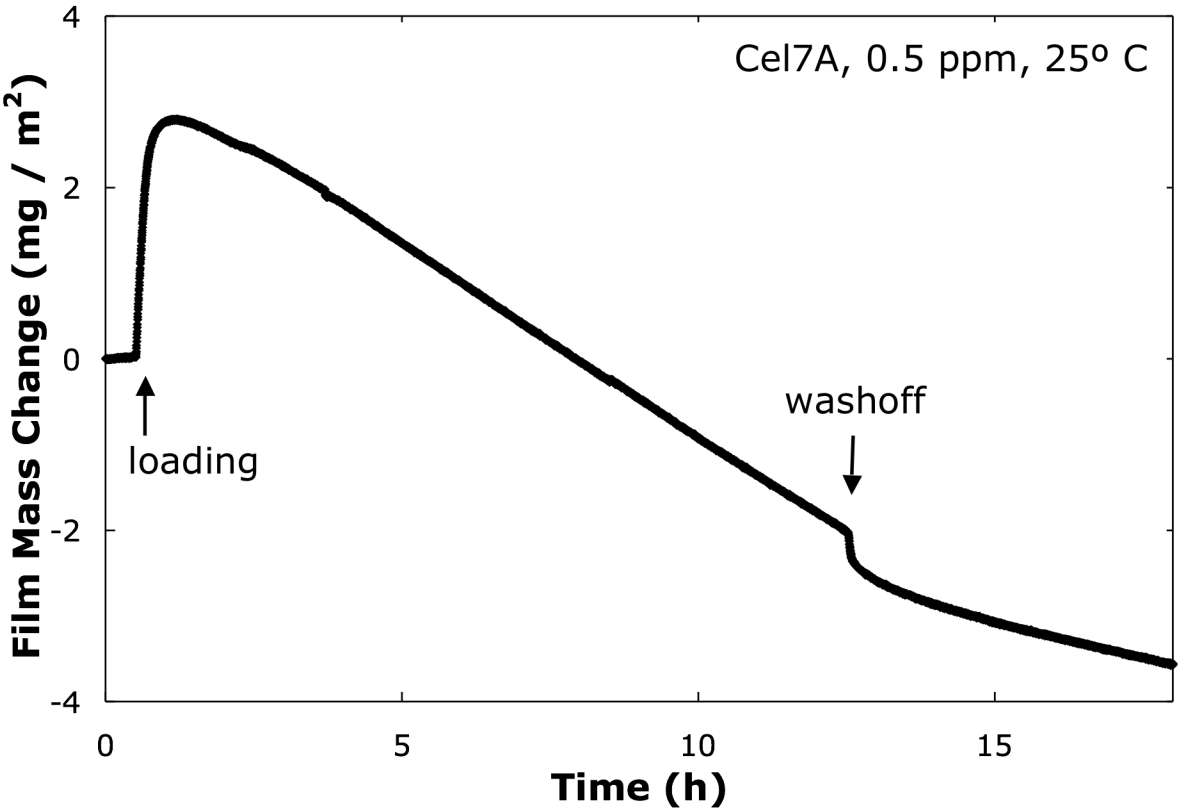

Figure 4.5. Mass history for adsorption and activity of Cel7A on a cellulose film for 12 h. Adsorption, constant degradation rate, and washoff are seen. Degradation rate remains constant from t = 4 – 12 h. 0.5-ppm *T. longibrachiatum* Cel7A in aqueous buffer at 25 ºC.

Figure 4.6 reports constant cellulose degradation rates (open diamonds) taken from the measured adsorption histories, such as those in Figures 4.4 and 4.5, as a function of bulk Cel7A concentration. The cellulose degradation rate is initially linear in Cel7A concentration and then plateaus,[18] corresponding to the maximum adsorption plateau.[20] Thus, cellulose degradation rate by Cel7A is limited by the maximum amount of enzyme adsorbed to the cellulose surface rather

than solely by substrate concentration typical in the Michaelis-Menten kinetic mechanism. This result is consistent with our previous findings of minimal cellulase penetration into the deposited cellulose film.[18] The smooth line in Figure 4.6 corresponds to the theoretical pseudo-steady-state degradation rate as a function of Cel7A concentration, as described by Equation 4.B1 in Appendix 4.B using the kinetic constants listed in Table 4.1.

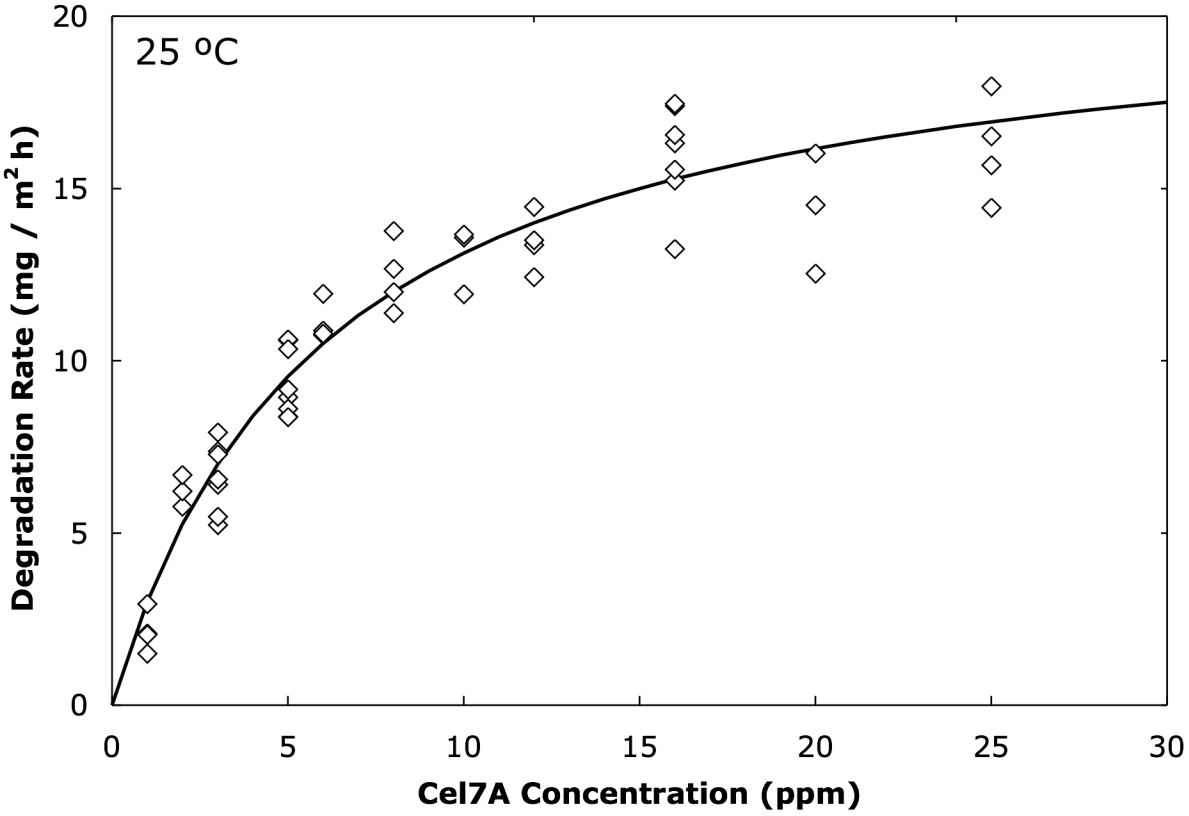

Figure 4.6. Pseudo-steady-state cellulose film degradation rate as a function of bulk Cel7A concentration. Degradation rate initially increases linearly in bulk enzyme concentration, then reaches a plateau. Results from kinetic model are plotted as a smooth line. *T. longibrachiatum* Cel7A in aqueous buffer at 25 ºC.

The kinetic model in Figure 4.1 posits that Cel7A complexes only with chain ends on the cellulose surface and that Cel7B activity increases the surface concentration of these chain ends. Since cellulose degradation is observed in Figure 4.6 in the absence of Cel7B, there must be a native concentration of chain ends on the deposited cellulose surface. The native chain-end concentration is quantified in Appendix 4.B, along with the other model kinetic constants.

4.5.2. Cel7B Activity on the Cellulose Surface

The Voigt model permitted conversion of ΔF- and ΔD-response data in Figure 4.3 into film mass histories for Cel7B activity, as illustrated in Figure 4.7. When the cellulose film is exposed to Cel7B, film mass monotonically increases. Figure 4.3 shows a corresponding decrease in film rigidity (increase in ΔD) over this time period. Upon Cel7B exposure, mass increase is initially rapid, but eventually slows to a linear rise. Following washoff at t = 3 h, and an immediate decrease in film mass, there remains a continuing increase in film mass and decrease in rigidity.

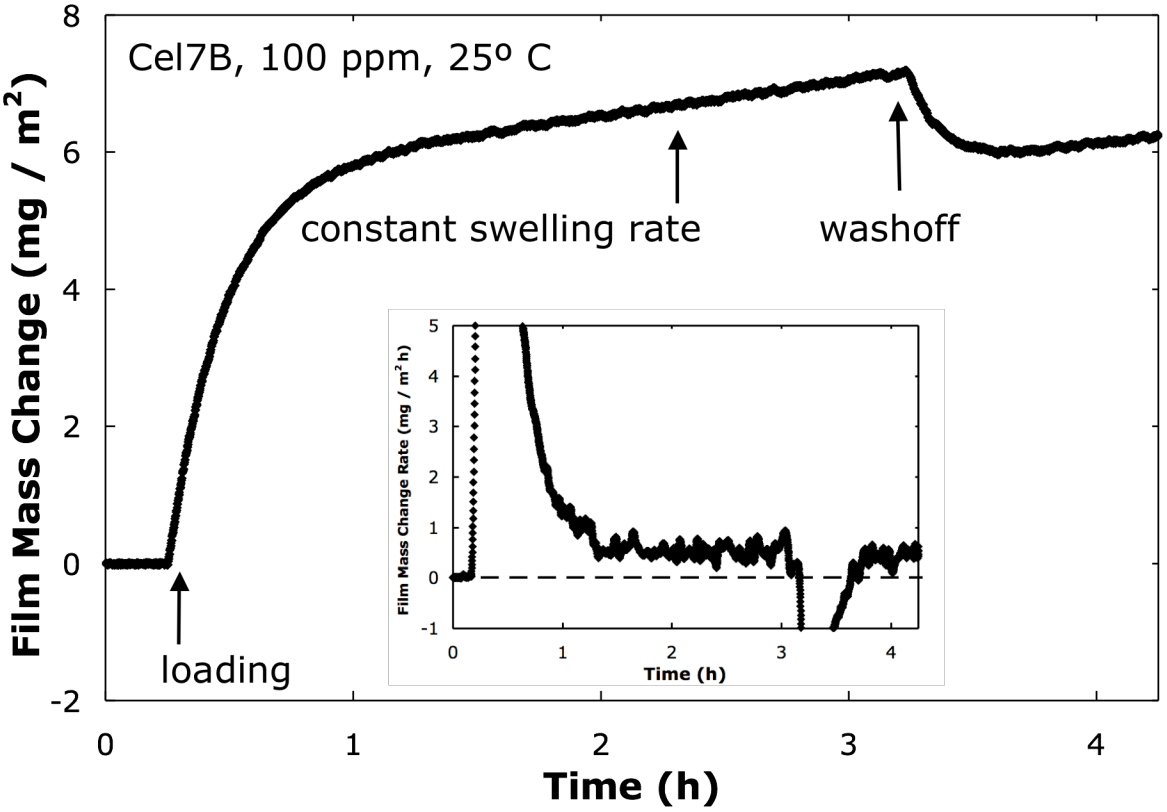

Figure 4.7. Mass history for adsorption and activity of Cel7B on a cellulose film for 3 h. Adsorption, film swelling, and washoff are seen. Inset shows first derivative of mass change data, revealing that swelling rate approaches a constant, positive value before washoff, and a smaller, constant positive value after washoff. 100-ppm *T. longibrachiatum* Cel7B in aqueous solution at 25 ºC.

The inset of Figure 4.7 shows the derivative of the mass-history data, confirming that the rate of mass increase reaches a constant value prior to washoff, and a smaller constant value subsequent to washoff. Since the total increase in film mass exceeds the steric maximum of 6.8 mg / m^2 for endoglucanase adsorption on a cellulose film[20] and because mass increase continues

after Cel7B elution, the constant increase in film mass cannot be attributed to increased surface-enzyme mass alone. Rather, as Cel7B creates chain ends and disrupts the hydrogen-bonding structure of the cellulose surface, water penetrates and swells the film.[24] We quantify the observed swelling rate as a measure of Cel7B activity toward chain-end production. Thus, the faster is the film-swelling rate, the faster is the rate of chain-end production. In our model, we assume that film swelling is linearly related to chain-end formation (see Appendix 4.A).

Cel7B pseudo-steady-state swelling rates (filled triangles) are plotted against bulk Cel7B concentration in Figure 4.8. Film-swelling rates follow the same Langmuir-type curve yielding a maximum-enzyme-activity plateau, similar to Cel7A and to a lyophilized cellulase mixture.[18] For both Cel7A and Cel7B, enzyme-activity limitations correspond to measured enzyme-adsorption limitations, reflecting maximum adsorption coverage at high bulk concentrations.[20] The smooth line in Figure 4.8 similarly corresponds to the theoretical pseudo-steady-state degradation rate as a function of Cel7B concentration, as described in Equation 4.B2 of Appendix 4.B using the kinetic constants given in Table 4.1.

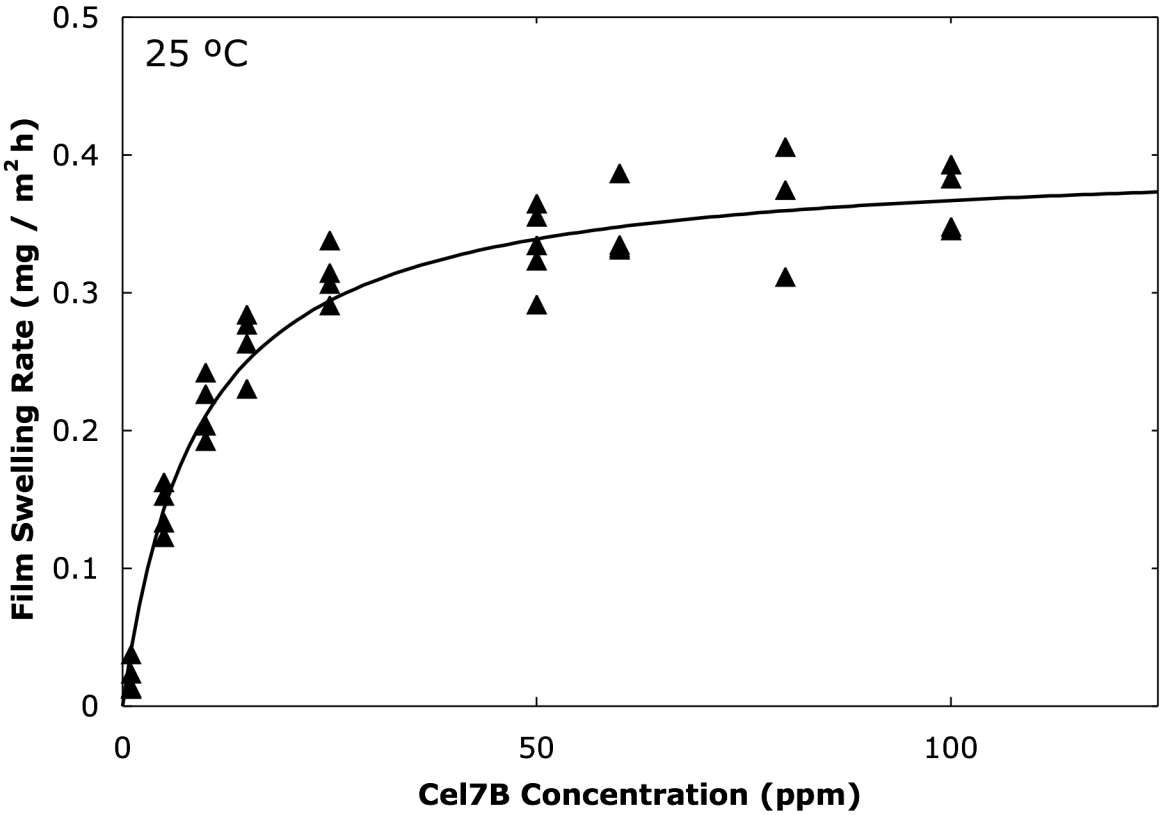

Figure 4.8. Pseudo-steady-state cellulose-film-swelling rate as a function of bulk Cel7B concentration. Swelling rate initially increases linearly in bulk enzyme concentration, then reaches a plateau. The plateau is reached at a higher bulk concentration than that for Cel7A. Results from kinetic model are plotted as a smooth line. *T. longibrachiatum* Cel7B in aqueous buffer at 25 ºC.

Recent neutron-reflectivity measurements on completely amorphous cellulose films indicate rapid film penetration and homogeneous deconstruction by some endoglucanases.[28] Our previous results,[18 20] and those in Figures 4.6 and 4.8 suggest minimal homogeneous film penetration into our partially crystalline deposited cellulose layers. We take the kinetic rates reported in Figures 4.6 and 4.8 as occurring near the film/aqueous solution interface.

4.5.3. Activity of Binary Enzyme Mixtures on the Cellulose Surface

In addition to quantifying the kinetics of single Cel7A and Cel7B enzymes acting on the deposited cellulose surface, we explored the cooperative activity of binary mixtures. Corresponding competitive adsorption kinetics is considered elsewhere.[20] Due to high energy dissipation values, it was again necessary to adopt the Voigt model to convert raw ΔF and ΔD data to mass histories.

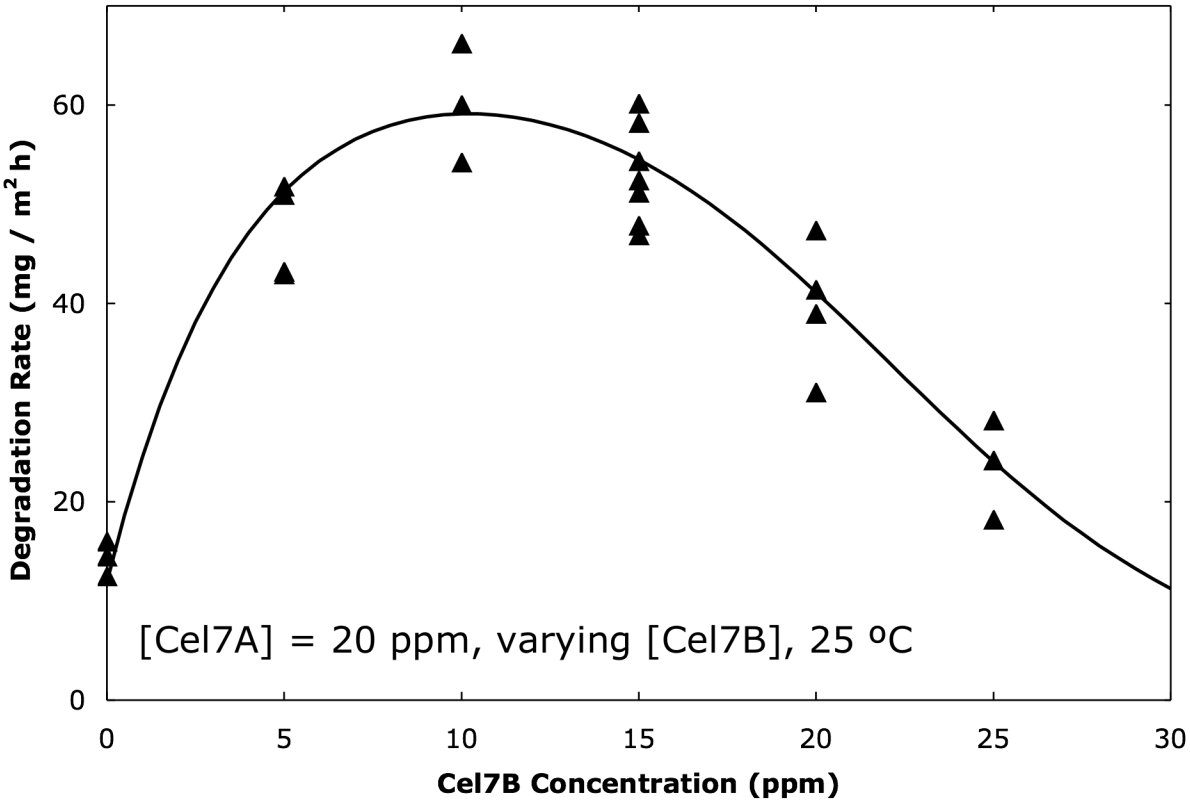

Figure 4.9. Pseudo-steady-state cellulose film swelling rate for Cel7A-Cel7B binary mixture as a function of Cel7B concentration. Cel7A concentration is 20 ppm for all experiments. Degradation rate reaches a maximum at 20-ppm Cel7A and 10-ppm Cel7B. Results from kinetic model are plotted as a solid line. *T. longibrachiatum* Cel7A and Cel7B in aqueous buffer at 25 ºC.

Pseudo-steady-state cellulose degradation rates (i.e., those when the degradation rate is constant, as observed for Cel7A activity in Figures 4.4 and 4.5) are plotted in Figure 4.9 for 20-ppm Cel7A over a range of Cel7B concentrations (filled triangles). As Cel7B concentration increases, cellulytic activity initially increases up to a maximum at 10-ppm Cel7B, and then decreases for larger Cel7B concentrations. Figure 4.10 graphs the corresponding pseudo-steady-state cellulose degradation rates for 20-ppm Cel7B over a range of Cel7A concentrations (filled triangles). Again, degradation rate initially increases as Cel7A concentration increases, but after reaching a maximum at 20-ppm Cel7A, decreases for larger Cel7A concentrations.

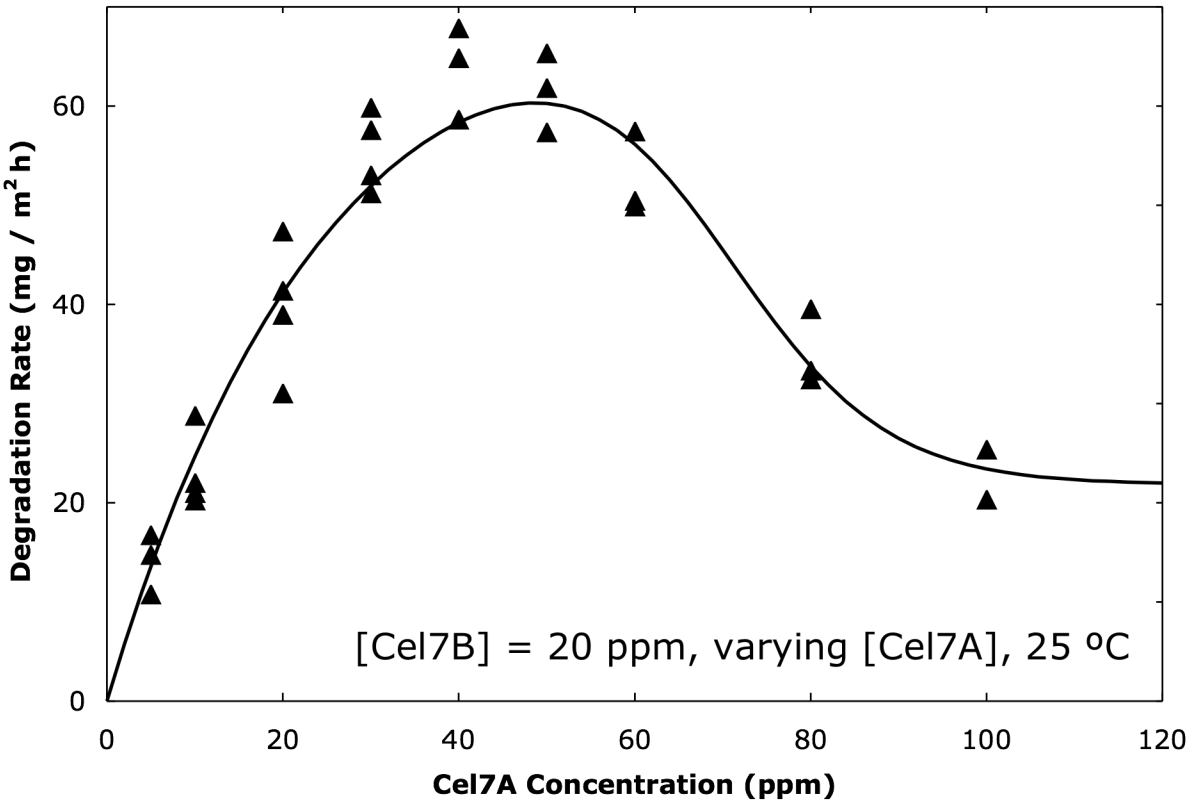

Figure 4.10. Pseudo-steady-state cellulose film swelling rate for Cel7A-Cel7B binary mixture as a function of Cel7A concentration. Cel7B concentration is 20 ppm for all experiments. Degradation rate reaches a maximum at 40-ppm Cel7A and 20-ppm Cel7B. Results from kinetic model are plotted as a solid line. *T. longibrachiatum* Cel7A and Cel7B in aqueous buffer at 25 ºC.

For both sets of enzyme-mixture experiments above, a maximum degradation rate value was observed for a 2:1 bulk mass ratio of Cel7A:Cel7B. Theoretical degradation rates obtained from the proposed kinetic model are shown as smooth lines in Figure 4.9 and Figure 4.10. These predictions are discussed further in Section 5.2.

4.6 Kinetic Model Results

4.6.1 Derivation of Rate Constants from Kinetic Model

By comparing mass-history data, such as those in Figures 4.4 – 4.10, to the surface-based kinetic model described in Appendix 4.A, all kinetic constants were established for cooperative Cel7A and Cel7B activity illustrated in Figure 4.1. Detailed calculations are described in Appendix 4.B; all parameters are listed in Table 4.1. Pseudo-steady-state kinetic constants for Cel7A and Cel7B were ascertained directly from the single-enzyme experimental data in Figures 4.6 and 4.8. The transient kinetic numerical model (see Appendix 4.A) was then solved via a Runge-Kutta algorithm to obtain decomplexation constants for Cel7A and Cel7B, as well as the film-swelling constant, α_{sw}, to relate observed Cel7B swelling activity (Figures 4.7 and 4.8) to the rate of chain-end formation. The kinetic model was not sensitive to chosen decomplexation constants over several orders of magnitude. Thus, the film-swelling constant α_{sw} is the only adjustable model parameter. All other parameters arise from analysis of data obtained from single-enzyme systems.

Table 4.1. Kinetic parameters for *T. longibrachiatum* Cel7A and Cel7B activity. Parameters k_A, k_D, K_L, k_I, and Γ_{max} were determined in previous work.[20] All other kinetic parameters from this manuscript. All kinetic parameters are defined on a mass basis for incorporation into the kinetic model described in Appendix 4.A. Calculations are detailed in Appendix 4.B.

	Cel7A	Cel7B
k_A	0.28 ppm^{-1} h^{-1}	0.07 ppm^{-1} h^{-1}
k_D	6.6 h^{-1}	24.0 h^{-1}
K_L	0.042 ppm^{-1}	0.0029 ppm^{-1}
k_I	1.7 h^{-1}	1.6 h^{-1}
Γ_{max}	6.8 mg / m^2	6.8 mg / m^2
$k_1 \Gamma_S$	6.44 h^{-1}	77 h^{-1}
k_{-1}	2.8 h^{-1}	23.3 h^{-1}
K_C	2.3	3.3
$\varepsilon_{S^*,N}$	0.0088	
k_2	140 h^{-1}	23.3 h^{-1}
α_{sw}	0.36 mg water / mg chain ends	

4.6.2. Prediction of Transient Enzyme Activity

To verify further our proposed kinetic model and associated kinetic parameters, we compared theory to experiment for several transient cases of cooperative cellulase activity. Figure 4.11 illustrates via kinetic model many of the tradeoffs inherent in the cooperative activity of Cel7A and Cel7B. Figure 4.11a plots a film-mass history for a binary mixture of 5 ppm Cel7A and 5 ppm Cel7B (black data) and kinetic model (gray line). Excellent agreement between data and model is seen. Figure 4.11b graphs corresponding results from the kinetic

model for total enzyme adsorption (both complexed and uncomplexed, thicker line) and the irreversibly bound enzyme adsorption (thinner line) during film degradation. At the 1:1 bulk mass ratio used in this experiment, the surface enzyme concentration of Cel7A is approximately 2.5 times that of Cel7B. Both surface enzyme concentrations remain approximately constant after about 1 h exposure to the cellulose surface, highlighting the importance of cellulose mixture design informed by surface parameters. Figure 4.11c plots the predicted surface concentration of complexed enzyme (thicker line) and the corresponding irreversibly bound amount (thinner line). Complexation kinetics are slower for Cel7A than Cel7B, as seen also in Table 4.1, where the complexation and decomplexation rate constants $k_1\Gamma_S$ and k_{-1} are each an order of magnitude smaller for Cel7A than for Cel7B. This result is reflected in Figure 4.11c, where the surface concentration of complexed Cel7B over the period from 0 – 0.5 h is slightly larger than the corresponding surface concentration of Cel7A, despite a higher total surface concentration of Cel7A. Figure 4.11d plots the surface chain-end fraction ε_{S*}, which increases over time as complexed Cel7B creates chain ends on the cellulose surface.

Importantly, although the chain-end fraction increases at a constant rate in Figure 4.11d, the surface concentration of complexed Cel7A, seen in Figure 4.11c, does not increase at a similar rate. From t = 1 – 3 h, $\Gamma_{Cel7A\text{-}S*}$ increases by only about 15%, despite the surface concentration of chain ends nearly doubling. Given the strong cooperativity between Cel7A and Cel7B in Figures 4.9 and 4.10, a corresponding large increase in complexed Cel7A surface concentration, and, therefore, a large increase in cellulose degradation rate might be expected. In fact, the minimal increase in complexed Cel7A surface concentration, despite a large increase in chain-end concentration, results from the slow kinetics of complexation and decomplexation for Cel7A. Although chain-end concentration increases continually, the slow complexation and decomplexation rates limit the proportion of enzyme that can take advantage of higher of concentration of chain ends at later reaction times. The implications of the slow complexation kinetics of Cel7A are discussed further in the Section 6.

Calculated chain-end fractions, ε_{S*}, in our kinetic model increase indefinitely at a constant but small rate, as shown in Figure 4.11d. Due to the small observed complexation and decomplexation rate constants in the kinetic model, only small chain-end surface concentrations arise. Thus, no physical upper bound for ε_{S*} is necessary in the kinetic formulation. Strictly, a varying ε_{S*} is not consistent with a pseudo-steady state. In both experiment and kinetic modeling, degradation rates were taken to represent pseudo-steady-state when they varied by less than 5% over 1 h.

Predicted pseudo-steady-state degradation rates comprise the smooth lines shown in Figures 4.9 and 4.10. Again, good agreement with experimental data is found, a noteworthy result since all kinetic constants but one (α_{sw}) were obtained from single-enzyme experiments. In Figure 4.9, at sufficiently high Cel7B bulk concentration, surface concentration of Cel7A tends to zero, and the deconstruction rate falls to zero. In Figure 4.10, a finite degradation rate at high Cel7A bulk concentration arises from the native surface concentration of chain ends. This degradation rate necessarily asymptotes to 18.5 mg / m^2 h, the upper limit of pseudo-steady-state film degradation rate for single Cel7A shown in Figure 4.6.

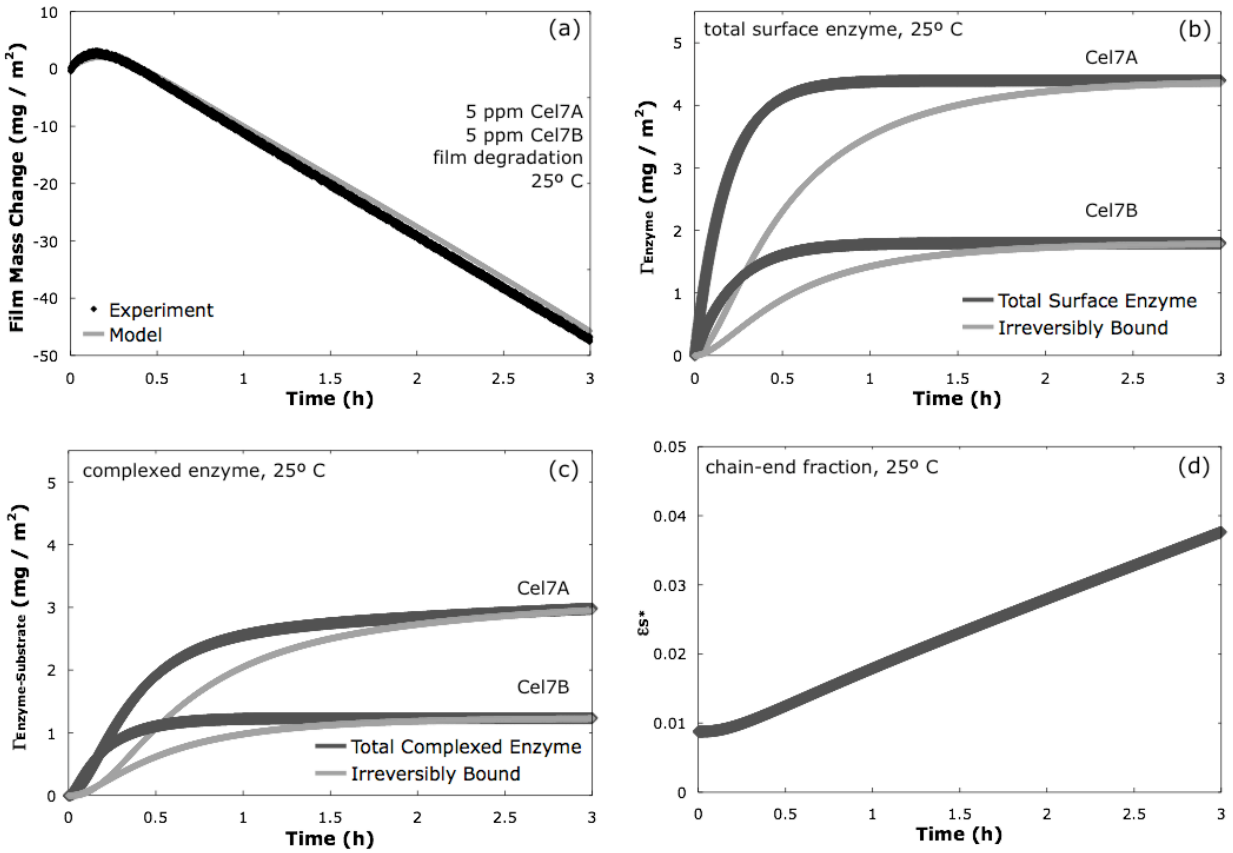

Figure 4.11. Comparison of experiment and kinetic model for activity of a binary mixture of 5 ppm Cel7A and 5 ppm Cel7B on a deposited cellulose surface. Cellulases from *T. longibrachiatum* in aqueous buffer at 25 ºC. (a) shows excellent agreement between experimental degradation history (black data) and model (gray line). (b) graphs corresponding predicted total adsorbed enzyme surface concentration (both complexed and uncomplexed, thicker gray line) as well as the irreversibly bound enzyme surface concentration (thinner gray line). (c) graphs predicted corresponding adsorbed complexed enzyme surface concentration (thicker gray line) and irreversibly bound complexed enzyme surface ceoncentration. (d) illustrates predicted cellulose chain-end fraction.

Figure 4.12 compares experimental and kinetic-model results for the following order-of-addition process: 5-ppm Cel7B solution is flowed over the surface for 0.5 h to create chain ends, the surface is washed with buffer for 0.5 h, then 5 ppm Cel7A solution is injected for 1 h to effect chain scission, after which the surface is again washed with buffer. This process corresponds to creating chain ends with Cel7B before deconstructing the surface by Cel7A. At t = 0, Cel7B adsorbs to the surface, complexes with it, and creates chain ends, thereby swelling the cellulose film. From t = 0.5 – 1 h, about 30% of the adsorbed Cel7B washes off. The remaining 70% irreversibly adsorbed Cel7B continues to create chain ends and swell the film. At t = 1 h, Cel7A adsorbs to and degrades the film surface. The observed pseudo-steady-state degradation rate, 15 mg / m^2 h, is indeed higher than that for single Cel7A (8 – 10 mg / m^2 h, from Figure 4.6). However, it is not as high as the 25 mg / m^2 h degradation

rate reported in Figure 4.11a. This is because the high surface concentration of irreversibly bound Cel7B blocks Cel7A adsorption. Cel7A adsorbs to a smaller surface concentration than that dictated by competitive adsorption. The result is a lower surface concentration of Cel7A-chain-end complexes and a lower activity.

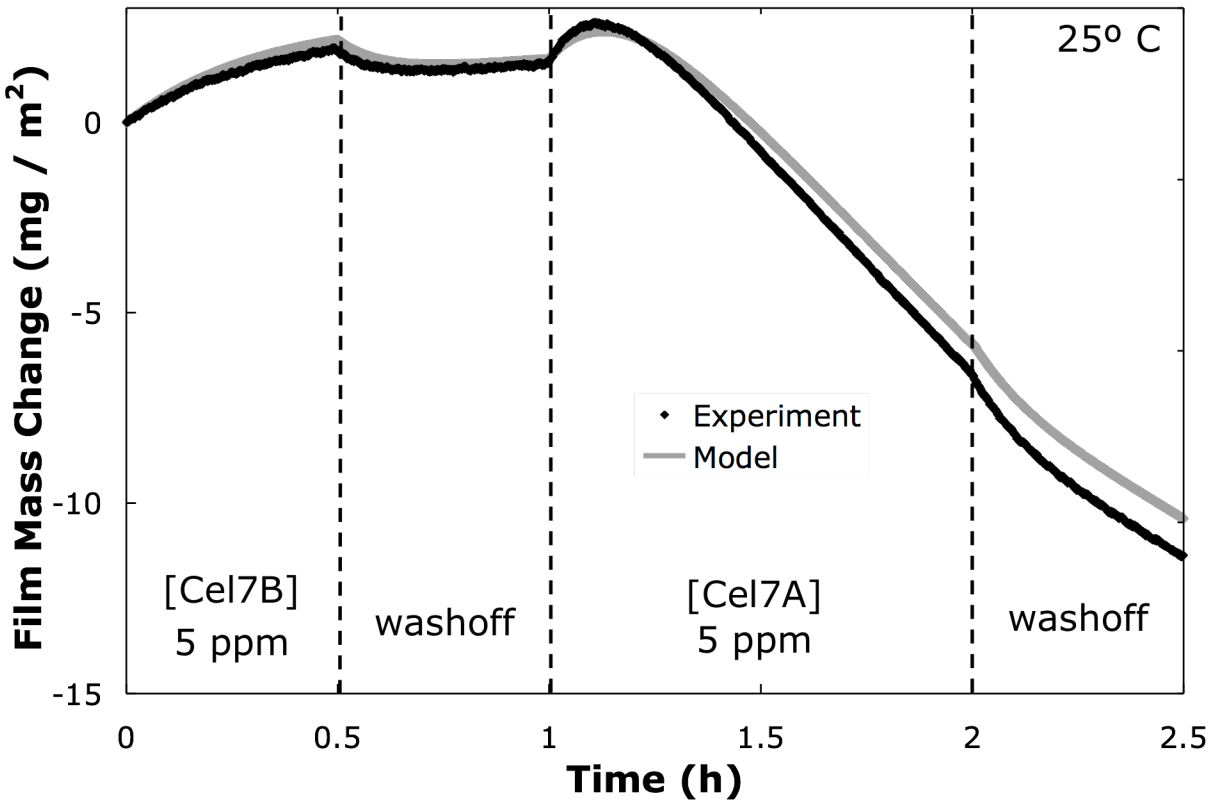

Figure 4.12. Mass history for successive Cel7B and Cel7A adsorption and activity on deposited cellulose film. At t = 0 h, the film is exposed to 5 ppm Cel7B. At t = 0.5 h, the film is exposed to buffer, washing off some Cel7B. The film is subsequently exposed to 5 ppm Cel7A at t = 1 h, with a second washoff at t = 2 h. Not all Cel7A washes off. Therefore, degradation continues at about 15 mg / m^2 h after washoff. Experiment (black) and kinetic model (gray) are indicated. *T. longibrachiatum* Cel7A and Cel7B in aqueous buffer at 25 ºC.

Figure 4.13 shows a similar experimental result with the order of addition of Cel7A and Cel7B reversed. 5-ppm Cel7A solution was flowed over the surface for 0.5 h, washed with buffer for 0.5 h, then 5-ppm Cel7B solution was flowed over the surface for 1 h before washing again with buffer. Film degradation occurs almost immediately upon addition of Cel7A at t = 0. Some Cel7A remains adsorbed and continues to degrade the film during the washoff period from t = 0.5 – 1 h. When Cel7B is added at t = 1 h, the degradation rate increases from approximately 6 mg / m^2 h to 10 mg / m^2 h. Consistent with the slow Cel7A complexation kinetics observed in

Figure 4.11, the degradation-rate increase is comparatively minor, and is delayed after the addition of Cel7B. After elution with buffer at t = 2 h, continued activity of irreversibly adsorbed enzyme is again observed. Once again, good agreement between experiment and model is apparent, with minor divergence in the cooperative degradation rate from t = 1 – 2 h.

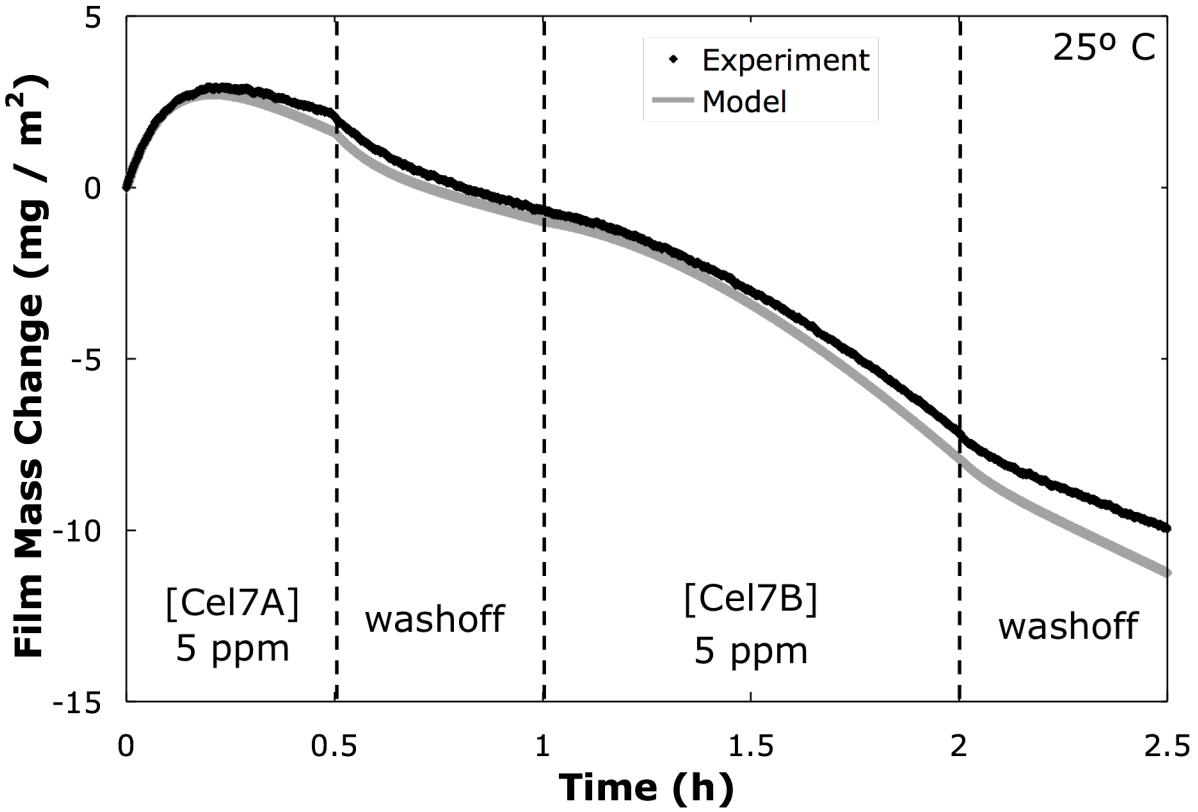

Figure 4.13. Mass history for successive Cel7A and Cel7B activity on deposited cellulose film. At t = 0 h, the film is exposed to 5 ppm Cel7A. At t = 0.5 h, the film is exposed to buffer, washing off some Cel7A. The film is subsequently exposed to 5 ppm Cel7B at t = 1 h, increasing the degradation rate, with another washoff at t = 2 h. Some Cel7A and Cel7B remains bound. Therefore, degradation continues after washoff. Experimental (black) and kinetic model (gray) are indicated. *T. longibrachiatum* Cel7A and Cel7B in aqueous buffer at 25 ºC.

4.7. Discussion

The pseudo-steady-state deconstruction rates shown in Figures 4.9 and 4.10 suggest that there are optimal bulk-solution mixtures of Cel7A and Cel7B that produce maximum cellulose degradation rates. To explore these mixtures, pseudo-steady-state deconstruction rates were predicted from the kinetic model for a variety of binary mixtures of Cel7A and Cel7B. Results are shown in Figure 4.14 for five Cel7B concentrations (point-labeled lines) for varying Cel7A

bulk concentration. All enzyme mixtures reach a maximum degradation rate of 60 mg / m^2 h at a bulk solution mass ratio of about 2:1 Cel7A:Cel7B. This suggests that at 25 ºC and over the concentration range analyzed, this bulk ratio sets a surface concentration ratio (about 4:1) that produces maximum cooperativity between Cel7A and Cel7B. Because enzyme adsorption is ultimately limited by steric effects, higher absolute bulk concentrations at this optimal ratio do not effect faster degradation. The degradation rate predicted for 20 ppm Cel7A:10 ppm Cel7B is similar to that predicted for 40 ppm Cel7A:20 ppm Cel7B. No more enzyme can adsorb to the surface at the higher concentration, thus the maximum degradation rate is similar.

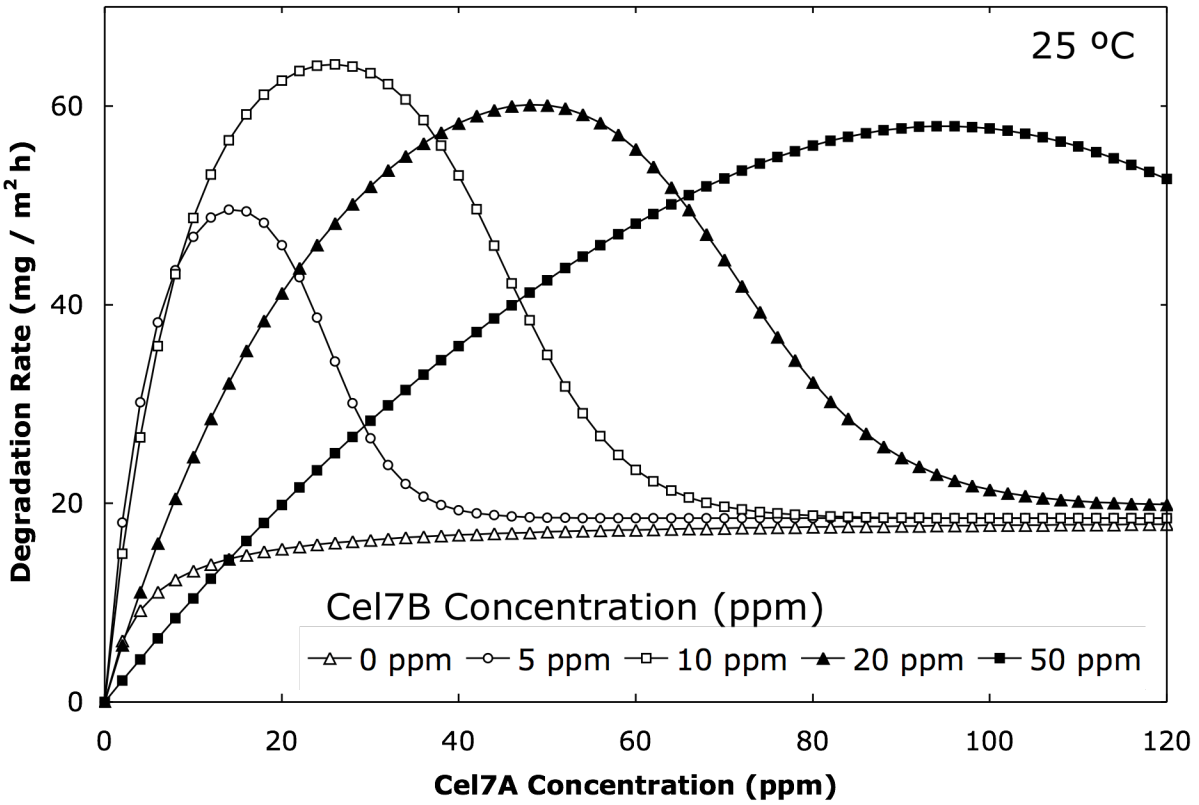

Figure 4.14. Calculated pseudo-steady-state degradation rates (point-labeled-lines) for *T. longibrachiatum* Cel7A-Cel7B mixtures on cellulose at 25 ºC. Bulk Cel7A concentration was varied at Cel7B bulk concentrations of 0, 5, 10, 20, and 50 ppm.

Above this optimal bulk-solution concentration ratio, Cel7A, which has a higher adsorptive affinity for the cellulose surface, outcompetes Cel7B for surface sites, thereby reducing surface concentration of Cel7B and the number of available surface chain ends. Accordingly, degradation activity falls, despite the higher surface concentration of Cel7A. An optimal concentration of Cel7B must be present on the surface near the beginning of degradation to create sufficient chain ends for Cel7A complexation. As Cel7A bulk concentration increases

without bound, regardless of Cel7B bulk concentration, the degradation rate tends toward 18.5 mg / m^2 h, the observed maximum degradation rate in the absence of Cel7B (Figure 4.6). This asymptote represents the case where Cel7A completely outcompetes Cel7B for surface sites, negating chain-end formation. This optimal 2:1 bulk concentration ratio is confirmed in the experimental data of both Figures 4.9 and 4.10. Rational choice of bulk enzyme-concentration ratio is particularly important given the data in Figure 4.11, which show that more than 75% of enzyme is bound irreversibly after 1 h.

It is likely surface enzyme does not truly transition to a 100% irreversibly bound state, as is formulated in the kinetic model. Rather, film degradation might result in the liberation of large chunks of cellulose with enzymes attached, thereby freeing bound enzyme. However, given that activity rates remain essentially constant even after significant degradation of the cellulose surface (Figure 4.11a), such surface-breakdown effects are assumed to be minor.

As described in Section 5.2 and illustrated in Figures 4.11c and 4.11d, the surface concentration of chain-end-complexed Cel7A and the cellulose degradation rate remain nearly constant despite a significant increase in chain-end concentration later in degradation. This result is due to the slow complexation and decomplexation kinetics of Cel7A. In fact, complexation is the rate-limiting step in cellulytic activity of Cel7A, whereas enzyme adsorption to the surface is rate-limiting for Cel7B. Despite similar Michaelis-Menten complexation equilibrium constants (K_C), the complexation exchange kinetics for Cel7B are an order of magnitude faster. Faster complexation/decomplexation rates for Cel7B is consistent with the structural characteristics of Cel7A and Cel7B. It is more difficult for Cel7A to form a complex with a cellulose chain end in its binding barrel than it is for Cel7B to form a complex between its binding cleft and the cellulose surface.[6] However, once Cel7A forms an enzyme-substrate complex, the significant distortion of the cellulose chain within the binding site prevents decomplexation.[9] This finding is not possible without separate study of adsorption[20] and complexation kinetics.

The processive activity of Cel7A is also reflected in its high turnover number. By assuming a molecular weight of 65,000 for Cel7A and an average product degree-of-polymerization of 3 (MW = 504), the mass-based turnover number listed in Table 4.1, $k_{2,Cel7A}$ = 140 h^{-1}, is converted to the more useful molar basis, $k_{2,Cel7A,molar}$ = 4.8 s^{-1}. Thus, a single complexed adsorbed Cel7A molecule affects, on average, 4.8 scissions per second. Although typical literature values are somewhat smaller,[38 39] most do not consider adsorbed, irreversibly bound, and complexed enzyme states separately. Thus, in less rigorous models, a large portion of surface enzyme that is reversibly adsorbed or irreversibly bound may incorrectly be assigned as complexed. A higher assumed concentration of complexed enzyme and, therefore, a lower turnover number emerges.

To optimize the activity of the Cel7A/Cel7B binary enzyme mixture given the slow complexation and decomplexation kinetics of Cel7A, the goal is first to create as many chain ends as possible and then to produce a high surface concentration of Cel7A to complex with those chain ends and effect chain scission. Unfortunately, there is an inherent tradeoff in preconditioning with Cel7B to create chain ends (see Figure 4.12), as Cel7B adsorbs irreversibly and blocks surface sites for subsequent Cel7A adsorption. Since Cel7A has a higher affinity for the cellulose surface than does Cel7B, if the two enzymes are exposed to the surface simultaneously, Cel7A bulk concentration still must be reduced to allow sufficient adsorption of Cel7B. This tradeoff is highlighted in the different degradation rates reported for Figure 4.11a and Figure 4.12. Both cases utilize Cel7A and Cel7B to degrade the cellulose surface at a bulk

concentration of 5 ppm for each enzyme. In Figure 4.11a, they arrive at the surface at the same time, producing a pseudo-steady-state degradation rate of about 25 mg / m^2 h. In Figure 4.12, however, Cel7B is first exposed to the cellulose surface to create chain ends, then eluted, followed by exposure to Cel7A. A higher degradation rate might be expected in this second scenario, since there is now a higher surface concentration of chain ends for Cel7A complexation. However, the observed degradation rate, 15 mg / m^2 h, is lower than that for mixed solution, as irreversibly bound Cel7B blocks subsequent Cel7A adsorption.

Clearly, Cel7A activity can be increased by increasing $\varepsilon_{S^*,N}$, the native concentration of chain ends on the cellulose surface, without permitting Cel7B to bind irreversibly on the surface. Figure 4.15 displays the calculated degradation rate as a function of single-Cel7A concentration (point-labeled line) over a range of native chain-end surface concentrations. In the absence of competitive adsorption of Cel7B but in the presence of surface chain ends, Cel7A activity at 25 ºC is increases up to 105 mg / m^2 h for comparatively low bulk Cel7A concentration (less than 20 ppm). Increasing native surface concentration of chain ends greatly increases Cel7A activity. Thus, pretreatment methods[40] to lower the polymerization of cellulose feedstock, disrupt its hydrogen-bonding structure, and create chain ends facilitate deconstruction.

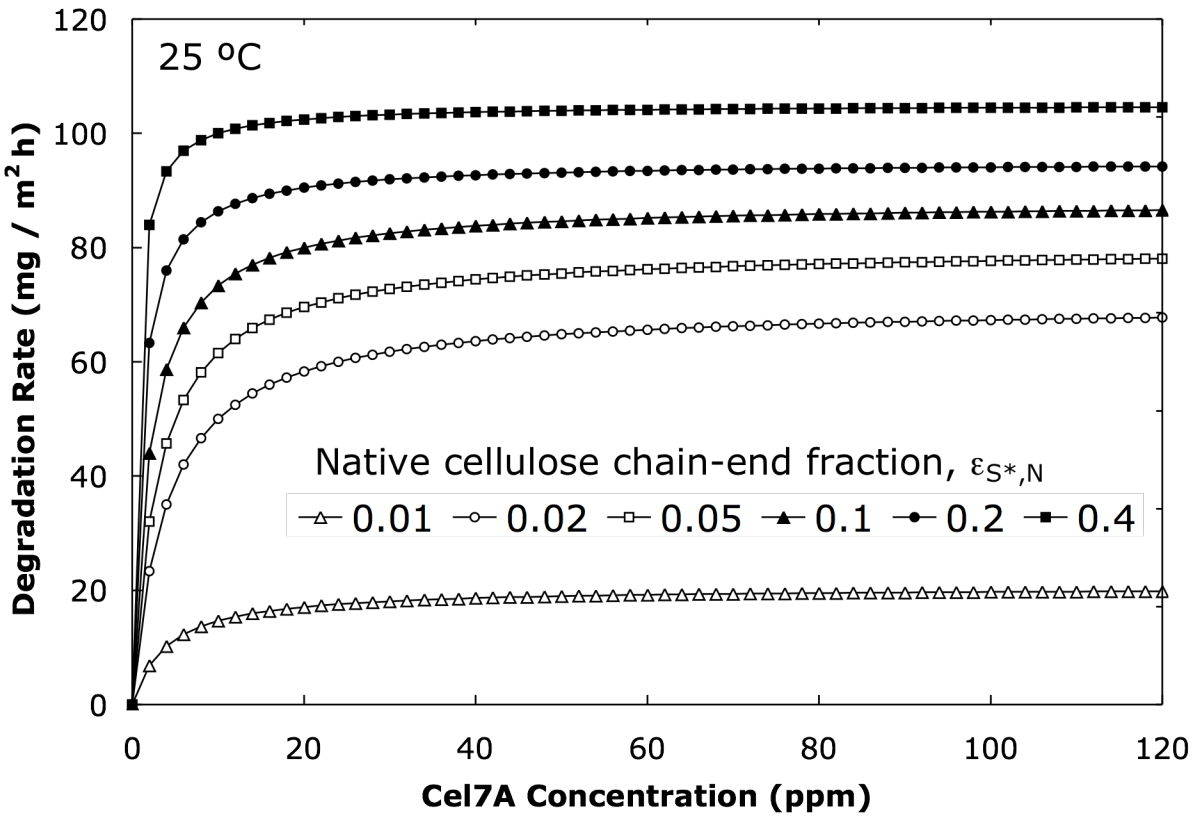

Figure 4.15. Calculated pseudo-steady-state degradation rates (point-labeled-lines) for *T. longibrachiatum* Cel7A on cellulose at 25 ºC. Different native cellulose chain-end fractions of $\varepsilon_{S^*,N}$ = 0.01, 0.02, 0.5, 0.1, 0.2, and 0.4 are indicated. Cel7B is not present. Native chain-end fraction for deposited cellulose films in this manuscript was 0.0088.

4.8. Conclusions

Quartz crystal micrography (QCM) is an invaluable tool to quantify surface kinetics of cellulose deconstruction. New kinetic degradation rates are provided for a binary mixture of *T. longibrachiatum* cellobiohydrolase I (Cel7A) and endoglucanase I (Cel7B) on a model cellulose surface at 25 ºC. Building on a previous single-enzyme model of cellulase activity elucidated by ellipsometry,[18] we devise a two-enzyme kinetic model including competitive adsorption, irreversible binding, complexation, and cooperative cellulytic activity. From single-Cel7A and single-Cel7B experiments at pseudo-steady state, we determined the intrinsic rate constants governing desconstruction. Only one adjustable mixture parameter (α_{sw}) relating Cel7B activity to chain-end formation was necessary in the proposed kinetic model. Model predictions using these rate constants show excellent agreement with experimental results for the activity of Cel7A/Cel7B cellulase mixtures on the deposited cellulose surface over a large range of bulk solution concentrations and for various orders of addition.

Using the kinetic model, we determined that the surface concentrations of Cel7A and Cel7B in binary mixture are established quickly upon exposure to the cellulose surface with up to 80% irreversibly bound after 1 h. Since typical industrial degradation occurs over timescales of 12 – 24 h, rational design of cellulose mixtures requires knowledge of surface concentrations. Although enzyme is irreversibly bound over short time scales, activity of Cel7A remains constant on cellulose for up to 12 h, suggesting that irreversible binding events do not involve complete enzyme denaturation at 25 ºC. Cel7A activity is affected strongly by the surface concentration of chain ends. However, deploying additional Cel7B to create chain ends before adding Cel7A results in decreased Cel7A adsorption and, thus, lower overall cellulytic activity than deploying the enzymes simultaneously. We found that a 2:1 bulk solution concentration ratio of Cel7A:Cel7B produced maximum degradation rates. However, increasing chain-end concentration without introducing irreversibly bound Cel7B to the system (e.g., via cellulose pretreatment) further increases degradation rates.

Present calculations pertain to the activity of two enzymes at 25 ºC on a defined cellulose surface of constant area, and in an excess bulk solution with no mass transfer limitations. Application of the kinetic model to other processing conditions requires extension of the mass conservation statements listed in Appendix 4.A.

4.9. List of Symbols

ΔF : QCM frequency shift
ΔD : QCM energy-dissipation change
Δm : Film mass per unit area, mg / m^2
Cel7B : *T. longibrachiatum* endoglucanase I
Cel7A : *T. longibrachiatum* cellobiohydrolase I
$[Cel7B]_{bulk}$: Bulk Cel7B concentration, ppm
$[Cel7A]_{bulk}$: Bulk Cel7A concentration, ppm
Γ_S : Surface concentration of cellulose, mg / m^2
Γ_{S^*} : Surface concentration of cellulose chain ends, mg / m^2
$\Gamma_{S^*,N}$: Native surface concentration of cellulose chain ends (before Cel7B activity), mg / m^2
ε_{S^*} : Fraction of surface cellulose available as chain ends
$\varepsilon_{S^*,N}$: Native fraction of surface available as cellulose chain ends (before Cel7B activity)

Γ_{Cel7B} : Surface concentration of reversibly adsorbed, uncomplexed Cel7B, mg / m^2
$\Gamma_{Cel7B\text{-}S}$: Surface concentration of reversibly adsorbed, complexed Cel7B, mg / m^2
$\Gamma_{Cel7B,I}$: Surface concentration of irreversibly bound, uncomplexed Cel7B, mg / m^2
$\Gamma_{Cel7B\text{-}S,I}$: Surface concentration of irreversibly bound, complexed Cel7B, mg / m^2
Γ_{Cel7A} : Surface concentration of reversibly adsorbed, uncomplexed Cel7A, mg / m^2
$\Gamma_{Cel7A\text{-}S^*}$: Surface concentration of reversibly adsorbed, complexed Cel7A, mg / m^2
$\Gamma_{Cel7A,I}$: Surface concentration of irreversibly bound, uncomplexed Cel7A, mg / m^2
$\Gamma_{Cel7A\text{-}S^*,I}$: Surface concentration of irreversibly bound, complexed Cel7A, mg / m^2
Γ_{max} : Maximum enzyme adsorption, mg / m^2
Γ_T : Total surface concentration for all enzyme, mg / m^2
Γ_O : Surface concentration of open enzyme adsorption sites, mg / m^2
P : Oligomeric product produced per unit area, mg / m^2
$k_{A,Cel7B}$: Adsorption rate constant for Cel7B, ppm^{-1} h^{-1}
$k_{D,Cel7B}$: Desorption rate constant for Cel7B, h^{-1}
$K_{L,Cel7B}$: Langmuir equilibrium constant for Cel7B, ppm^{-1}
$k_{I,Cel7B}$: Irreversible binding rate constant for Cel7B, h^{-1}
$k_{1,Cel7B}$: Complexation rate constant for Cel7B, m^2 / mg h
$k_{-1,Cel7B}$: Decomplexation rate constant for Cel7B, h^{-1}
$K_{C,Cel7B}$: Michaelis-Menten equilibrium constant for Cel7B, m^2 / mg
$k_{2,Cel7B}$: Activity rate constant for Cel7B, h^{-1}
$r_{ads,Cel7B}$: Rate of Cel7B adsorption to the cellulose surface, mg / m^2 h
$r_{des,Cel7B}$: Rate of Cel7B desorption from the cellulose surface, mg / m^2 h
$r_{comp,Cel7B}$: Rate of Cel7B complexation with the cellulose surface, mg / m^2 h
$r_{decomp,Cel7B}$: Rate of Cel7B decomplexation from to the cellulose surface, mg / m^2 h
$r_{irr,Cel7B}$: Rate of Cel7B irreversible binding to the cellulose surface, mg / m^2 h
$r_{act,Cel7B}$: Rate of chain-end creation by complexed Cel7B, mg / m^2 h
$k_{A,Cel7A}$: Adsorption rate constant for Cel7A, ppm^{-1} h^{-1}
$k_{D,Cel7A}$: Desorption rate constant for Cel7A, h^{-1}
$K_{L,Cel7A}$: Langmuir equilibrium constant for Cel7A, ppm^{-1}
$k_{I,Cel7A}$: Irreversible binding rate constant for Cel7A, h^{-1}
$k_{1,Cel7A}$: Complexation rate constant for Cel7A, m^2 / mg h
$k_{-1,Cel7A}$: Decomplexation rate constant for Cel7A, h^{-1}
$K_{C,Cel7A}$: Michaelis-Menten equilibrium constant for Cel7A, m^2 / mg
$k_{2,Cel7A}$: Activity rate constant for Cel7A, h^{-1}
r_{sw} : Film-swelling rate, mg / m^2 h
α_{sw} : Film-swelling constant, mg swelling / mg chain ends
$r_{ads,Cel7A}$: Rate of Cel7A adsorption to the cellulose surface, mg / m^2 h
$r_{des,Cel7A}$: Rate of Cel7A desorption from the cellulose surface, mg / m^2 h
$r_{comp,Cel7A}$: Rate of Cel7A complexation with the cellulose surface, mg / m^2 h
$r_{decomp,Cel7A}$: Rate of Cel7A decomplexation from to the cellulose surface, mg / m^2 h
$r_{irr,Cel7A}$: Rate of Cel7A irreversible binding to the cellulose surface, mg / m^2 h
$r_{act,Cel7A}$: Rate of chain-end creation by complexed Cel7A, mg / m^2 h

4.10. References

(1) Himmel, M.; Ding, S. Y.; Johnson, D. K.; Adney, W. S.; Nimlos, M. R.; Brady, J. W.; Foust, T.D. Biomass Recalcitrance: Engineering Plants and Enzymes for Biofuels Production. *Science* **2007**, *315,* 804-807.

(2) Houghton, J.; Weatherwax, S.; Ferrell, J. Breaking the Biological Barriers to Cellulosic Ethanol: A Joint Research Agenda. *US DOE,* DOE/SC-0095, 2005.

(3) Wyman, C. E. Ethanol from Lignocellulosic Biomass: Technology, Economics, and Opportunities. *Bioresource Technol*. **1994,** *50,* 3-16.

(4) O'Sullivan, A. C. Cellulose*:* The Structure Slowly Unravels. *Cellulose* **1997,** *4,* 173-207.

(5) Zhang, Y. H. P.; Himmel, M. E.; Mielenz, J. Outlook for Cellulase Improvement: Screening and Selection Strategies. *Biotech Advances* **2005,** *24,* 452-481.

(6) Gupta, R.; Lee, Y. Y. Mechanism of Cellulase Reaction on Pure Cellulosic Substrates. *Biotech Bioeng* **2008**, *102,* 1570-1581.

(7) Linder, M.; Mattinen, M. L.; Kontteli, M.; Lindeberg, G.; Stahlberg, J.; Drakenberg, T.; Reinikainen, T.; Pettersson, G.; Annila, A. Identification of Functionally Important Amino-Acids in the Cellulose-Binding Domain of *Trichoderma-reesei* Cellobiohydrolase I. *Protein Sci* **1995,** *4,* 1056-1064.

(8) Srisodsuk M.; Lehtiö, J.; Linder, M.; Margolles-Clark, E.; Reinikainen, T.; Teeri, T. T. *Trichoderma reesei* Cellobiohydrolase I with an Endoglucanase Cellulose-Binding Domain: Action on Bacterial Microcrystalline Cellulose. *J Biotech* **1997,** *57,* 49 – 57.

(9) André, G.; Kanchanawong, P.; Palma, R.; Cho, H.; Deng, X.; Irwin, D.; Himmel, M. E.; Wilson, D. B.; Brady, J. W. Computational and Experimental Studies of the Catalytic Mechanism of Thermobifida Fusca Cellulase Cel6A (E2). *Protein Eng* **2003,** *16*, 125-134.

(10) Fox, J. M.; Levine, S. E.; Blanch, H. W.; Clark, D. S. Initial- and Processive-Cut Products Reveal Cellobiohydrolase Rate Limitations and the Role of Companion Enzymes. *Biochemistry*. **2012**, *51(1)*, 442-452.

(11) Kipper, K.; Väljamäe, P.; Johansson, G. Processive Action of Cellobiohydrolase Cel7A from Trichoderma Reesei Is Revealed as Burst Kinetics on Fluorescent Polymeric Model Substrates. *Biochem J*. **2005,** *385,* 527-535.

(12) Bansal, P.; Hall, M.; Realff, M. J.; Lee, J. H.; Bommarius, A. S. Modeling Cellulase Kinetics on Lignocellulosic Substrates. *Biotech Advances* **2009,** *6,* 833-848.

(13) Abdmziem, K.; Passas, R.; Belgacem, M. N. Inverse Gas Chromatography as a Tool to Characterize the Specific Surface Area of Cellulose Fibers. *Cell Chem Technol* **2006,** *40,* 199-204.

(14) Levine, S. E.; Fox, J. M.; Blanch, H. W.; Clark, D. S. A Mechanistic Model of the Enzymatic Hydrolysis of Cellulose. *Biotech Bioeng* **2010,** *107,* 37-51

(15) Hall, M.; Bansal, P.; Lee, J. H.; Realff, M. J.; Bommarius, A. S. Cellulose Crystallinity – a Key Predictor of the Enzymatic Hydrolysis Rate. *Febs Journal* **2010,** *277,* 1571-1582.

(16) Xu, F.; Ding, H. S. A New Kinetic Model for Heterogeneous (or Spatially Confined) Enzymatic Catalysis: Contributions from the Fractal and Jamming (Overcrowding) Effects. *App Cat A General* **2007,** *317,* 70-81.

(17) Kontturi, E.; Tammelin, T.; Österberg, M. Cellulose—Model Films and the Fundamental Approach. *Chem Soc Rev* **2006,** *35,* 1287-1313.

(18) Maurer, S. A.; Bedbrook, C. N.; Radke, C. J. Cellulase Adsorption and Reactivity on a Cellulose Surface from Flow Ellipsometry. *I&ECR* **2012**. Submitted. (Dissertation Chapter 2)

(19) Gunnars S.; Wågberg L.; Stuart M. A. C. Model Films of Cellulose: I. Method Development and Initial Results. *Cellulose* **2002,** *9,* 239-249.

(20) Maurer, S. A.; Bedbrook, C. N.; Radke, C. J. Competitive Sorption Kinetics of Inhibited Endo- and Exo-glucanases on a Model Cellulose Substrate. *Langmuir* **2012**. Submitted. (Dissertation Chapter 3)

(21) Turon X.; Rojas, O. J.; Deinhammer, R. S. Enzymatic Kinetics of Cellulose Hydrolysis: A QCM-D Study. *Langmuir* **2008,** *24,* 3880-3887.

(22) Hu, G.; Heitmann, J. A.; Rojas, O. J. In Situ Monitoring of Cellulase Activity by Microgravimetry with a Quartz Crystal Microbalance. *J Phys Chem B*. **2009,** *113,* 14761-14768.

(23) Hu, G.; Heitmann, J. A.; Rojas, O. J. Quantification of Cellulase Activity Using the Quartz Crsytal Microbalance Technique. *Anal Chem* 2009, 81, 1872–1880.

(24) Josefsson P.; Henriksson G.; Wågberg L. The Physical Action of Cellulases Revealed by a Quartz Crystal Microbalance Study Using Ultrathin Cellulose Films and Pure Cellulases. *Biomacromolecules* **2008,** *9,* 249-254.

(25) Ahola, S.; Turon, X.; Österberg, M.; Laine, J.; Rojas, O J. Enzymatic Hydrolysis of Native Cellulose Nanofibrils and Other Cellulose Model Films: Effect of Surface Structure. *Langmuir* **2008,** 24, 11592 – 11599.

(26) Suchy, M.; Linder, M. B.; Tammelin, T.; Campbell, J. M.; Vuorinen, T.; Kontturi, E. Quantitative Assessment of the Enzymatic Degradation of Amorphous Cellulose by Using a Quartz Crystal Microbalance with Dissipation Monitoring. *Langmuir* **2011,** *27,* 8819-8828.

(27) Habibi Y.; Foulon, L.; Aguie-Beghin, V.; Molinari, M.; Douillard, R. Langmuir-Blodgett Films of Cellulose Nanocrystals: Preparation and Characterization. *J Colloid Interface Sci* **2007,** *316,* 388-397.

(28) Cheng, G.; Datta, S.; Liu, Z.; Wang, C.; Murton, J.; Brown, P. A.; Jablin, M. S.; Dubey, M.; Majewski, J.; Halbert, C. E.; Browning, J. F.; Esker, A. R.; Watson, B. J.; Zhang, H.; Hutcheson, S. W.; Huber, D. L.; Sale, K. L.; Simmons, B. A.; Kent, M. S. Interactions of Endoglucanases with Amorphous Cellulose Films Resolved by Neutron Reflectometry and Quartz Crystal Microbalance with Dissipation Monitoring. *Langmuir* **2012.** In press.

(29) Andersen, M.; Johansson, L. S.; Tanem, B. S.; Stenius, P.; Properties and Characterization of Hydrophobized Microfibrillated Cellulose. *Cellulose* **2006,** *13,* 665-677.

(30) Mohan, T.; Kargl, R.; Doliska, A.; Vesel, A.; Kostler, S.; Ribitsch, V.; Stana-Kleinschek, K. Wettability and Surface Composition of Partly and Fully Regenerated Cellulose Thin Films from Trimethylsilyl Cellulose. *J Colloid Interface Sci* **2011,** *358,* 604-610.

(31) Rodahl, M.; Höök, F.; Krozer, A.; Brzezinski, P.; Kasemo, B. Quartz-Crystal Microbalance Setup for Frequency and Q-Factor Measurements in Gaseous and Liquid Environments. *Rev Sci Inst* **1995,** *66,* 3924-3930.

(32) Din, N.; Gilkes, N. R.; Tekant, B.; Miller Jr., R. C.; Warren, R. A. J.; Kilburn, D. G. Non-Hydrolytic Disruption of Cellulose Fibres by the Binding Domain of a Bacterial Cellulase.

(33) Cascão Pereira, L. G.; Hickel, A.; Radke, C. J.; Blanch, H. W. A Kinetic Model for Enzyme Interfacial Activity and Stability: pa-Hydroxynitrile Lyase at the Diisopropyl Ether/Water Interface. *Biotech Bioeng* **2002,** *78,* 595-605.

(34) Schuster, A.; Schmoll, M. Biology and Biotechnology of *Trichoderma*. *App Microbio and Biotech* **2010,** *87,* 787-799.

(35) Bharadwaj, R.; Wong, A.; Knierim, B.; Singh, S.; Holmes, B. M.; Auer, M.; Simmons, B. A.; Adams, P. D.; Singh A. K. High-throughput Enzymatic Hydrolysis of Lignocellulosic Biomass Via In-situ Regeneration. *Bioresource Tech* **2011,** *102,* 1329-1337.

(36) Larsson, C.; Rodahl, M.; Höök, F. Characterization of DNA Immobilization and Subsequent Hybridization on a 2D Arrangement of Streptavidin ona Biotin-Modified Lipid Bilayer Supported on SiO2. *Analytical Chem* **2003,** *75,* 5080-5087.

(37) Eriksson, T.; Karlsson, J.; Tjerneld, F. A Model Explaining Declining Rate in Hydrolysis of Lignocellulose Substrates with Cellobiohydrolase I (Cel7A) and Endoglucanase I (Cel7B) of *Trichoderma reesei*. *Appl Biochem Biotech* **2002,** *101,* 41-60.

(38) Praestgaard, E.; Elmerdahl, J.; Murphy, L.; Nymand, S.; McFarland, K. C.; Borch, K.; Westh, P. A Kinetic Model for the Burst Phase of Processive Cellulases. *FEBS Journal* **2011,** *278,* 1547-1560.

(39) Kurasin, M.; Väljamäe, P. Processivity of Cellobiohydrolases is Limited by the Substrate. *J Biol Chem* **2011,** *286,* 169-177.

(40) Yang, B.; Wyman, C. Pretreatment: The Key to Unlocking Low-Cost Cellulosic Ethanol. *Biofuels, Bioprod Bioref* **2008,** *2,* 26-40.

Appendix 4.A: Kinetic Model

Figure 4.1 illustrates the kinetic model for cooperative cellulase activity on the cellulose surface. In this appendix, rate equations for the proposed kinetic model are elucidated along with mass conservation laws appropriate to the QCM flow cell.

4.A.1. Cellulase Adsorption

Enzyme adsorption and desorption kinetics on the cellulose surface follow the Langmuir kinetic model, for the rates of adsorption and desorption

$$r_{ads,Cel7A} = k_{A,Cel7A}[Cel7A]_{bulk}\Gamma_O \quad , \tag{4.A1}$$

and

$$r_{des,Cel7A} = k_{D,Cel7A}\Gamma_{Cel7A} \quad , \tag{4.A2}$$

where $k_{A,Cel7A}$ and $k_{D,Cel7A}$ are the adsorption and desorption rate constants for Cel7A; $[Cel7A]_{bulk}$ is the bulk enzyme concentration; Γ_{Cel7A} is the surface concentration of reversibly adsorbed, uncomplexed Cel7A, and Γ_O is the surface concentration of open sites available for cellulase binding. We relate Γ_O to the surface concentration of adsorbed enzyme via a surface-site balance,

$$\Gamma_O = \Gamma_{\max} - \Gamma_T \quad , \tag{4.A3}$$

where $\Gamma_{\max}$ = 6.8 mg / m^2 is the observed maximum enzyme adsorption for both Cel7A and Cel7B,[20] and Γ_T is the total surface concentration of all adsorbed enzymes.

Adsorbed enzymes bind irreversibly to the surface according to first-order surface kinetics,[20 33]

$$r_{irr,Cel7A} = k_{I,Cel7A}\Gamma_{Cel7A} \quad , \tag{4.A4}$$

where $k_{I,Cel7A}$ is the first-order irreversible binding rate constant. The resulting surface concentration of irreversibly bound, uncomplexed Cel7A is denoted as $\Gamma_{Cel7A,I}$. In general, the surface concentration of any enzyme in the irreversibly bound state is denoted with an additional subscript I. Enzyme in the irreversibly bound state cannot transition back to the reversibly adsorbed state.

Equations 4.A1 – 4.A4 are also written for Cel7B. Adsorption, desorption, and irreversible binding of Cel7B follow an identical scheme, with the subscript Cel7A replaced by Cel7B.

4.A.2. Cellulase Complexation

Once adsorbed, enzymes form an enzyme-substrate complex with appropriate surface sites. In our model, Cel7A complexes only with chain ends (surface concentration denoted by Γ_{S*}), while Cel7B complexes nonspecifically with the insoluble cellulose substrate (surface concentration denoted Γ_S). The fraction ε_{S*} relates surface concentration of chain ends to total surface concentration of cellulose,

$$\varepsilon_{S^*} = \frac{\Gamma_{S^*}}{\Gamma_S} \quad . \tag{4.A5}$$

where Γ_S is assumed to be in excess and constant throughout all enzyme activity. The surface chain end-concentration, Γ_{S^*}, changes through Cel7B activity. Complexation and decomplexation rates for Cel7A and Cel7B on the cellulose surface both follow Michaelis-Menten kinetics,

$$r_{comp,Cel7A} = k_{1,Cel7A}\Gamma_{Cel7A}\varepsilon_{S^*}\Gamma_S \quad , \tag{4.A6}$$

$$r_{decomp,Cel7A} = k_{-1,Cel7A}\Gamma_{Cel7A-S^*} \quad , \tag{4.A7}$$

$$r_{comp,Cel7B} = k_{1,Cel7B}\Gamma_{Cel7B}\Gamma_S \quad , \tag{4.A8}$$

and

$$r_{decomp,Cel7B} = k_{-1,Cel7B}\Gamma_{Cel7B-S} \quad , \tag{4.A9}$$

where k_1 and k_{-1} are, respectively, the Michaelis-Menten complexation and decomplexation constants; and $\Gamma_{Cel7A\text{-}S^*}$ and $\Gamma_{Cel7B\text{-}S}$ are, respectively, the surface concentrations of cellulose-complexed Cel7A and Cel7B. Complexed cellulase cannot desorb from the surface into bulk solution. Rather, each complexed cellulase must decomplex from its substrate before desorption can occur from the uncomplexed state according to Equation 4.A2.

Surface concentrations of both cellulose and chain ends are assumed to be large in comparison to surface enzyme concentration, allowing the Michaelis-Menten model to be applied. This assumption is consistent with Figure 4.5, where no significant decline in Cel7A activity is observed over 12 h, implying Γ_{S^*} remains essentially constant over 12 h, with no significant chain-end consumption (see also Figure 4.11d showing the small change in Γ_{S^*} over time).

Because irreversible binding is mediated primarily by the cellulose-binding domain[19] and because complexation is, by definition, mediated entirely by the catalytic domain, we assume that these processes are independent. Thus, complexed enzymes transition to an irreversibly bound state at the same rate as noncomplexed enzymes, and irreversibly bound enzymes have the same complexation and activity constants as reversibly adsorbed enzymes. Equation 4.A4 is written for complexed Cel7A as,

$$r_{irr,Cel7A-S^*} = k_{I,Cel7A}\Gamma_{Cel7A-S^*} \quad , \tag{4.A10}$$

with the irreversible-binding constant $k_{I,Cel7A}$ identical to that for the noncomplexed state. Similarly, Equation 4.A6 is written for irreversibly bound Cel7A with identical complexation constant $k_{1,Cel7A}$,

$$r_{comp,Cel7A,I} = k_{1,Cel7A}\Gamma_{Cel7A,I}\varepsilon_{S^*}\Gamma_S \quad . \tag{4.A11}$$

From the principles elucidated in Equations 4.A1 – 4.A11, corresponding rate expressions can be written that govern the remaining adsorption, complexation, and irreversible binding processes

illustrated in Figure 4.1. These include: decomplexation of irreversibly bound Cel7A; complexation and decomplexation of irreversibly bound Cel7B; and irreversible binding of complexed Cel7B.

4.A.3. Cellulase Activity

Following Michaelis-Menten kinetics, activity of both Cel7A and Cel7B is first-order in the concentration of enzyme-substrate complex according to the rate constant k_2:

$$r_{act,Cel7A} = k_{2,Cel7A}\Gamma_{Cel7A-S^*} \tag{4.A12}$$

and

$$r_{act,Cel7B} = k_{2,Cel7B}\Gamma_{Cel7B-S} \quad . \tag{4.A13}$$

Both enzymes are assumed to remain complexed with the cellulose surface after activity, transitioning separately back to the uncomplexed adsorbed state according to Equations 4.A7 and 4.A9. As with k_1 and k_{-1} above, the rate constant k_2 is identical for the reversibly adsorbed and irreversibly bound states of each enzyme.

The activity of Cel7A is assumed solely to degrade the cellulose surface into glucose oligomers that are then released into aqueous solution. The activity of Cel7B is assumed to create cellulose chain ends, thereby inducing film swelling by water (Section 4.3). The mass of the cellulose film itself changes according to degradation by Cel7A and to swelling as a result Cel7B activity. The rate of swelling by water is related linearly to the rate of Cel7B activity via the constant α_{sw},

$$r_{ws} = \alpha_{sw} r_{act,Cel7B} \quad . \tag{4.A14}$$

4.A.4. Mass Balances

Equations 4.A1 – 4.A14 constitute the surface-kinetic-rate expressions used for incorporation into mass balances appropriate for a QCM flow-cell application. When the bulk solution is well mixed and in excess, and when the cellulase substrate surface area is constant, Equations 4.A15 – 4.A22 give the rate of change of the surface concentrations of both Cel7A and Cel7B in the complexed, uncomplexed, reversibly adsorbed, and irreversibly bound states:

$$\frac{d\Gamma_{Cel7B}}{dt} = k_{A,Cel7B}[Cel7B]_{bulk}(\Gamma_{\max} - \Gamma_T) - k_{D,Cel7B}\Gamma_{Cel7B} - k_{1,Cel7B}\Gamma_{Cel7B}\Gamma_S + k_{-1,Cel7B}\Gamma_{Cel7B-S} - k_{I,Cel7B}\Gamma_{Cel7B} \tag{4.A15}$$

$$\frac{d\Gamma_{Cel7B-S}}{dt} = k_{1,Cel7B}\Gamma_{Cel7B}\Gamma_S - k_{-1,Cel7B}\Gamma_{Cel7B-S} - k_{I,Cel7B}\Gamma_{Cel7B-S} \tag{4.A16}$$

$$\frac{d\Gamma_{Cel7B,I}}{dt} = -k_{1,Cel7B}\Gamma_{Cel7B,I}\Gamma_S + k_{-1,Cel7B}\Gamma_{Cel7B-S,I} + k_{I,Cel7B}\Gamma_{Cel7B} \tag{4.A17}$$

$$\frac{d\Gamma_{Cel7B-S,I}}{dt} = k_{1,Cel7B}\Gamma_{Cel7B,I}\Gamma_S - k_{-1,Cel7B}\Gamma_{Cel7B-S,I} + k_{I,Cel7B}\Gamma_{Cel7B-S} \tag{4.A18}$$

$$\frac{d\Gamma_{Cel7A}}{dt} = k_{A,Cel7A}[Cel7A]_{bulk}(\Gamma_{\max} - \Gamma_T) - k_{D,Cel7A}\Gamma_{Cel7A} - k_{1,Cel7A}\Gamma_{Cel7A}\varepsilon_{S^*}\Gamma_S + k_{-1,Cel7A}\Gamma_{Cel7A-S^*} - k_{I,Cel7A}\Gamma_{Cel7A} \tag{4.A19}$$

$$\frac{d\Gamma_{Cel7A-S^*}}{dt} = k_{1,Cel7A}\Gamma_{Cel7A}\varepsilon_{S^*}\Gamma_S - k_{-1,Cel7A}\Gamma_{Cel7A-S^*} - k_{I,Cel7A}\Gamma_{Cel7A-S^*} \tag{4.A20}$$

$$\frac{d\Gamma_{Cel7A,I}}{dt} = -k_{1,Cel7A}\Gamma_{Cel7A,I}\varepsilon_{S^*}\Gamma_S + k_{-1,Cel7A}\Gamma_{Cel7A-S^*,I} + k_{I,Cel7A}\Gamma_{Cel7A} \tag{4.A21}$$

$$\frac{d\Gamma_{Cel7A-S^*,I}}{dt} = k_{1,Cel7A}\Gamma_{Cel7A,I}\varepsilon_{S^*}\Gamma_S - k_{-1,Cel7A}\Gamma_{Cel7A-S^*,I} + k_{I,Cel7A}\Gamma_{Cel7A-S^*} \tag{4.A22}$$

The total surface concentration of all adsorbed enzyme is defined as the sum of all enzyme states above,

$$\Gamma_T = \Gamma_{Cel7B} + \Gamma_{Cel7B,I} + \Gamma_{Cel7B-S} + \Gamma_{Cel7B-S,I} + \Gamma_{Cel7A} + \Gamma_{Cel7A,I} + \Gamma_{Cel7A-S^*} + \Gamma_{Cel7A-S^*,I}. \tag{4.A23}$$

Activity of complexed Cel7A deconstructs the cellulose surface into oligomeric product,

$$\frac{dP}{dt} = k_{2,Cel7A}(\Gamma_{Cel7A-S^*} + \Gamma_{Cel7A-S^*,I}) \quad , \tag{4.A24}$$

while the activity of complexed Cel7B creates cellulose chain ends,

$$\Gamma_S \frac{d\varepsilon_{S^*}}{dt} = k_{2,Cel7B}(\Gamma_{Cel7B-S} + \Gamma_{Cel7B-S,I}) \quad , \tag{4.A25}$$

where $\varepsilon_{S^*} << 1$. Provided that $k_{2,Cel7B}$ is small, ε_{S^*} changes slowly, thereby permitting a pseudo-steady-state degradation rate. Chain-end creation is associated with film swelling governed by the proportionality constant α_{sw} ,

$$r_{sw} = \alpha_{sw}k_{2,Cel7B}(\Gamma_{Cel7B-S} + \Gamma_{Cel7B-S,I}) \quad . \tag{4.A26}$$

Finally, the total film mass change, which is the quantity measured by the QCM, is described as the sum of enzyme adsorption and film swelling rate minus the deconstruction rate of the film,

$$\frac{dm_{film}}{dt} = \frac{d\Gamma_T}{dt} + r_{sw} - \frac{dP}{dt} \quad . \tag{4.A27}$$

Appendix 4.B: Derivation of Rate Constants for Kinetic Model

4.B.1. Kinetic Constants for Cel7A Activity from Pseudo-Steady-State Data

Cellulytic activity of cellobiohydrolase I (Cel7A) in the absence of endoglucanase I (Cel7B) and in the pseudo-steady state is given by

$$\left[\frac{dP}{dt}\right]_{PSS} = \frac{k_{2,Cel7A}k_{1,Cel7A}\Gamma_{S^*}\Gamma_{\max}K_{L,Cel7A}[Cel7A]_{bulk}}{k_{-1,Cel7A} + K_{L,Cel7A}[Cel7A]_{bulk}(k_{-1,Cel7A} + k_{1,Cel7A}\Gamma_{S^*})} \quad , \qquad (4.B1)$$

where $[dP/dt]_{PSS}$ is the measured pseudo-steady-state areal degradation rate (mg cellulose degraded / m^2 / h) in Figure 4.6; $K_{L,Cel7A} = k_{A,Cel7A} / k_{D,Cel7A}$ is the Langmuir equilibrium adsorption constant; and all other quantities are as defined in Appendix 4.A. Derivation of this equation for a single-enzyme system is found elsewhere.[18] The chain-end concentration Γ_{S^*} is assumed to be constant during the period of constant degradation rate. In agreement with Figure 4.6, degradation rate is linear in $[Cel7A]_{bulk}$ at low bulk Cel7A concentration, but reaches an asymptote at higher Cel7A concentration, since $[Cel7A]_{bulk}$ appears in both numerator and denominator on the right side of Equation 4.B1.

From previous work: $K_{L,Cel7A}$ = 0.042 ppm^{-1} and $\Gamma_{\max}$ = 6.8 mg / m^2.[20] Upon examining Equation 4.B1 in the limits of bulk high and low enzyme concentration, we obtain the parameters $k_{2,Cel7A}$ (the turnover number for Cel7A) and $K_{C,Cel7A} = k_{1,Cel7A}\Gamma_{S^*} / k_{-1,Cel7A}$ (the Cel7A complexation equilibrium constant).[18] We establish these parameters from the data in Figure 4.6 in the limits of low and high enzyme concentration[18] to obtain $K_{C,Cel7A}$ = 2.3 and $k_{2,Cel7A}$ = 140 h^{-1}. The solid line in Figure 4.6 is then predicted from these parameters.

The irreversible binding rate constant $k_{I,Cel7A}$ does not appear in Equation 4.B1. Because irreversible binding is primarily a CBD-mediated phenomenon and complexation/activity is a CD-mediated process, we assume that both reversibly adsorbed and irreversibly bound Cel7A have equal probability of complexing with cellulose and effecting a chain scission. We also assume that adsorbed uncomplexed and adsorbed complexed enzyme have equal probabilities of irreversibly binding. Since reversibly and irreversibly adsorbed enzymes have identical activity, Equation 4.B1 holds when degradation rate is constant, although some enzyme may still transition from the reversibly adsorbed to the irreversibly bound state.

4.B.2. Kinetic Constants for Cel7B Activity from Pseudo-Steady-State Data

Similarly, we characterize Cel7B activity on the cellulose surface using the pseudo-steady-state swelling rate r_{sw}, plotted in Figure 4.8, to quantify Cel7B activity as a function of bulk concentration. As noted in Equation 4.A14, we assume that the film-swelling rate depicted in Figures 4.7 and 4.8 is linearly proportional to the rate of chain-end formation by Cel7B according to a swelling constant α_{sw}. Thus, similar to Equation 4.B1, we describe the pseudo-steady-state single-enzyme activity of Cel7B by

` $$[r_{sw}]_{PSS} = \frac{\alpha_{sw}k_{2,Cel7B}k_{1,Cel7B}\Gamma_S\Gamma_{\max}K_{L,Cel7B}[Cel7B]_{bulk}}{k_{-1,Cel7B} + K_{L,Cel7B}[Cel7B]_{bulk}(k_{-1,Cel7B} + k_{1,Cel7B}\Gamma_S)} \quad . \qquad (4.B2)$$

In Equation 4.B2, all kinetic parameters for Cel7A are replaced by those for Cel7B, and the chain-end surface concentration Γ_{S^*} is replaced by the cellulose surface concentration Γ_S, since Cel7B complexes nonspecifically with the entire cellulose surface rather than solely with chain ends. Application of Equation 4.B2 to the data in Figure 4.8 in the limits of low and high Cel7B concentration, using our previous results of $K_{L,Cel7B}$ = 0.0029 ppm^{-1} and Γ_{max} = 6.8 mg / m^2,[20] gives $\alpha_{sw}k_{2,Cel7B}$ = 0.42 h^{-1} and $K_{C,Cel7B} = k_{1,Cel7B}\Gamma_S / k_{-1,Cel7B}$ = 3.3.

4.B.3. Kinetic Constants for Cooperative Activity from Kinetic Model

The remaining kinetic constants illustrated in Figure 4.1 were obtained from the transient kinetic model. We evaluated Equations 4.A15 – 4.A27 using a Runge-Kutta algorithm to quantify transient enzyme adsorption, swelling, chain-end formation, and film degradation.

To apply Equations 4.A15 – 4.A27, it was first necessary to ascertain the rate constants governing transient complexation and decomplexation, k_1 and k_{-1}, for both Cel7A and Cel7B. The pseudo-steady-state analysis, described above, specifies only the equilibrium constants $\varepsilon_{S^*}K_{C,Cel7A} = k_{1,Cel7A}\varepsilon_{S^*}\Gamma_S / k_{-1,Cel7A}$ and $K_{C,Cel7B} = k_{1,Cel7B}\Gamma_S / k_{-1,Cel7B}$. Complexation rate constants are best established by defining the ratio k_2 / k_{-1}, representing the number of enzyme activity events that occur for each decomplexation event.[40] Cel7A degrades cellulose chains processively within the active site, inducing a major conformational change in the cellulose chain within its barrel-shaped catalytic domain and keeping the chain complexed while effecting multiple chain scissions.[8 9] Accordingly, processive length values in the literature for Cel7A range from 10 – 100 scission events per decomplexation event.[10 11] Upon examining single-component activity histories of Cel7A (such as Figures 4.4 and 4.5), we find that our kinetic model is not sensitive to choices in this range. We chose $k_{2,Cel7A} / k_{-1,Cel7A}$ = 50, i.e., Cel7A makes on average 50 chain scissions per decomplexation event. Endoglucanases have a cleft-like active-site structure encompassing fewer interactions with the cellulose surface. Cel7B does not act processively,[40] suggesting a smaller activity/decomplexation ratio. From single-component histories (such as in Figure 4.7), we found that our kinetic model is not sensitive to $k_{2,Cel7B} / k_{-1,Cel7B}$ ratios between 0.5 (half of all complexation events are nonproductive) and 10. We chose $k_{2,Cel7B} / k_{-1,Cel7B}$ = 1, or Cel7B on average creates one chain scission per complexation with the chain surface.

To complete the description of cooperative Cel7A-Cel7B deconstruction kinetics, we must also determine the swelling constant α_{sw}. This constant relates linearly measured pseudo-steady-state film-swelling rates induced by Cel7B to the rate of chain-end formation, which, in turn, characterizes the reactive synergy between Cel7A and Cel7B. To determine the swelling constant α_{sw}, we used the transient kinetic model to predict PSS degradation rates for the Cel7A-Cel7B mixture concentrations shown in Figures 4.9 and 4.10. Due to the difficulty of modeling competitive adsorption kinetics and swelling in conjunction with Cel7A activity, no closed-form expression is available for these degradation rates, necessitating the use of the fully transient kinetic model. As described in the Section 5.3, the kinetic model result was taken to have reached pseudo-steady-state when degradation rate varied by less than 5% over a period of 1 h. Different values of the swelling constant were chosen until agreement was found for all enzyme mixtures. A swelling ratio of α_{sw} = 0.36 mg water / mg chain ends was determined, characterizing the film swelling observed in Figure 4.7 and by Josefsson *et al.*[24] in terms of the rate of chain-end formation. In calculating this swelling constant, we also arrived at a native-cellulose-chain-end fraction on deposited cellulose films, $\varepsilon_{S^*,N}$ = 0.0088. This native fraction

governs the rate of cellulose deconstruction for single Cel7A on the surface in the absence of Cel7B, such as that shown in Figure 4.6. This fraction is likely specific to the particular film coating method.

Chapter 5

Conclusion

Production of biofuels from lignocellulosic feedstocks is a complex industrial problem. Modeling of microbial cellulytic and fermentation activity at an industrial level involves hundreds of kinetic parameters.[1] Despite considerable effort, the kinetics governing the fundamental rate-limiting step of this process—the enzymatic deconstruction of cellulose—remains poorly understood. Most assays of cellulase activity are performed in the bulk, and, therefore, fail to decouple or evaluate the surface phenomena involved in enzymatic depolymerization. This thesis demonstrates the usefulness of flow ellipsometry and flow quartz crystal microgravimetry (QCM) on model cellulose films to conduct continuous, non-invasive, inhibition-free assays of cellulase adsorption and activity on well-defined cellulose substrates of known area.

The utility of such assays was established in Chapter 2. Flow ellipsometry was used to evaluate the adsorption and activity of a lyophilized cellulase mixture from *T. reesei* on a thin, spin-coated cellulose film. Both cellulase adsorption and cellulytic activity were shown to increase as a function of bulk enzyme concentration up to a maximum plateau (Figure 2.4). Increasing bulk enzyme concentration beyond this point does not increase the concentration of enzymes on the cellulose surface, and, therefore, does not increase the cellulose degradation rate. This finding underscores the importance of considering surface concentration in evaluating enzyme activity and, therefore, the importance of using surface assays to measure cellulase kinetics.

Critically, measured degradation rates were shown to be identical between the flow-ellipsometry assay and the standard sulfuric-acid assay on the laboratory standard cellulose Avicel. The surface-based ellipsometry assay is superior to the bulk assay, as it allows continuous, non-invasive measurement of both enzyme adsorption and activity. In the sulfuric-acid assay, the reaction mixture must be sampled after discrete time intervals, the reaction must be stopped completely to determine solution concentration of released glycans, and no information about surface adsorption is available. Given the commensurate results of the two assays, a surface assay is clearly preferred to a functionalized glycan product assay for elucidating cellulase surface kinetics.

Using the data collected from this surface assay, a kinetic model was developed to describe the activity of cellulase on the cellulose surface (Figure 2.1). Cellulase adsorption and cellulose-binding-domain (CBD) association with the cellulose surface were modeled according to reversible Langmuir kinetics. Complexation and activity of surface cellulase were interpreted via a Michaelis-Menten framework. Kinetic constants for each process were obtained. The only adjustable parameter necessary to implement the transient model was cellulase processive length (enzyme activity events per decomplexation event), and the kinetic model was found to be insensitive to choice of this parameter over several orders of magnitude. These ascertained kinetic constants predicted well transient cellulase activity on the cellulose surface and are concordant with existing data for surface enzyme activity. However, the single-enzyme model is

a coarse depiction of enzyme activity on the cellulose surface, as it considers all enzyme activity to be cellulytic, not accounting for the separate activity of endoglucanases, which mainly create cellulose-chain ends, and cellobiohydrolases, which mainly complex with these chain ends and work processively to degrade cellulose.

Chapters 3 and 4 detail the development of a more sophisticated two-enzyme model to account for the cooperative activity of endoglucanases and cellobiohydrolases on the cellulose surface. The fungal cellulases cellobiohydrolase I (CBHI, Cel7A) and endoglucanase I (EGI, Cel7B) were used in this study. Chapter 3 describes the adsorption of these cellulases to the cellulose surface. After long-time exposure to the cellulose surface, both cellulases adsorb up to the same sterically-limited adsorption maximum, Γ_{max} = 6.8 mg / m^2. Yet Cel7A has 14 times higher affinity for the cellulose surface (i.e., higher effective Langmuir equilibrium constant) than does Cel7B. Both enzymes bind irreversibly to the cellulose surface on time scales as short as 30 – 60 min, leaving a fraction of adsorbed cellulase that cannot be removed by eluting with buffer (Figures 3.6, 3.7). Irreversible binding was quantified via a modified Langmuir model, where reversibly adsorbed cellulase transitions to an irreversibly bound state according to first-order kinetics. Despite the differing affinities of Cel7A and Cel7B for the cellulose surface, the first-order kinetic constant governing irreversible binding was identical for the two enzymes. Irreversible binding was, thus, hypothesized to be a phenomenon mediated only by the CBD, which is similar in structure between these two fungal cellulases. The differing affinities of Cel7A and Cel7B for the cellulose surface were then quantified in terms of differences in the enthalpy and entropy of adsorption between the cellulase and the cellulose surface. The proposed entropy difference was found to be similar to literature measurements of cellulase binding with the cellulose surface.

In Chapter 4, the modified Langmuir adsorption model was incorporated into a more complex model for the cooperative activity of Cel7A and Cel7B on the cellulose surface (Figure 4.1). Both Cel7A and Cel7B activity on the cellulose surface plateau at high bulk enzyme concentrations of these isolated enzymes (Figures 4.6, 4.8). Using the Langmuir-Michaelis-Menten kinetic framework established in Chapter 2 and the sorption constants determined in Chapter 3, kinetic constants for Cel7A and Cel7B complexation were determined. By measuring the degradation rates of enzyme mixtures, the kinetic constants governing the cooperative activity of these two enzymes were established. Kinetic constants (Table 4.1) agree with the known structure and function of Cel7A and Cel7B. While the binding cleft of Cel7B complexes and decomplexes rapidly with the cellulose surface, the binding barrel of Cel7A complexes slowly but tightly, and works processively to degrade cellulose with a high turnover number. While complexation is the rate-limiting step in Cel7A activity, adsorption is the rate-limiting step for Cel7B activity.

The proposed two-enzyme Langmuir-Michaelis-Menten kinetic model with irreversible binding predicts well the cooperative activity of Cel7A and Cel7B on the cellulose surface in a variety of test cases—for example, flowing one enzyme over the surface, eluting, and then flowing the other. An optimal ratio of 2:1 Cel7A:Cel7B bulk concentration was found to effect the highest cellulose degradation rates. Below this optimal concentration ratio, Cel7A outcompetes Cel7B for surface sites, resulting in a low concentration of chain ends and limiting the maximum activity of Cel7A. Above this ratio, high concentrations of bulk Cel7B outcompete Cel7A for surface sites, and, therefore, less cellulytic activity on the surface is observed.

This optimal ratio and kinetic model is valid only for this specific Cel7A/Cel7B enzyme mixture. Other endoglucanases and cellobiohydrolases would have independent kinetic parameters. Most cellulytic fungi synthesize suites of several endoglucases and exoglucanases.[2] Thus, a simultaneous kinetic model of many enzymes in solution is necessary. Further work to determine kinetic parameters for different cellulases and to incorporate these parameters into an extended, multiple-enzyme kinetic model would inform the design of better cellulases and cellulase mixtures.

While this two-enzyme model thus predicts well and provides significant information about the activity of cellulases on the cellulose surface and design of optimal enzyme mixtures, many parameters remain to be analyzed. First, as described in Chapter 4, to simplify the kinetic model, the activity of Cel7B was assumed to be solely chain-end creation, and the activity of Cel7A was assumed to be solely cellulose chain degradation. In reality, there is crossover between these enzymatic activities. Cel7B does liberate chain-ends from the surface at a lesser rate,[3] while the CBD interaction of Cel7A with the cellulose surface does create chain-ends.[4] These secondary activity rates are likely minor compared to the primary activities of the enzyme, and may not proceed through the same four-step adsorption-complexation-activity-decomplexation model suggested in this thesis. However, quantifying these rates remains a first step for improving the kinetic model from available data.

All work in this thesis was conducted at 25 ºC. Typical industrial biofuel production occurs at a temperature of 37 ºC – 48 ºC.[5] Due to the complex, multi-step nature of the cellulase-cellulose interaction, increasing temperature likely changes not only activity constants, but also adsorption and complexation. Increased temperature might also hasten denaturation of surface enzymes. Surface enzyme denaturation and subsequent loss of enzyme activity was found in this thesis to be minor at 25 ºC over time-scales up to 12 h (Figure 4.6). However, at increased temperatures, the surface and thermal denaturation rates might be larger. Denaturation is hypothesized as a cause of kinetic slowdown in industrial biofuel production.[6] For any given cellulose mixture, there is likely an optimal activity temperature, at which deconstruction rate is maximized, but denaturation rates are at a minimum.

Another possible factor in kinetic slowdown of cellulase activity is a change in the surface properties of cellulose, leaving a layer of intractable cellulose.[7] It is known that the crystallinity of cellulose changes within microfibrils, with more crystalline cellulose residing near the center.[8] The surface interaction of cellulases with crystalline versus amorphous cellulose is not well-understood. Some sources suggest that highly crystalline cellulose is more resistant to enzymatic degradation due to its stronger hydrogen-bonding network.[9] Other sources suggest that crystalline cellulose provides an ordered substrate that allows improved CBD recognition of cellulose microstructures and facilitates processive activity.[10] Surface-based assays such as ellipsometry and QCM allow enzyme adsorption and activity to be quantified individually, and therefore allow these two factors to be understood separately. An increase in adsorption rate might be expected on highly crystalline cellulose, as an increased concentration of ordered cellulose microfeatures would allow better interaction of the CBD amino-acid residues necessary for enzyme adsorption. However, this larger adsorption rate on crystalline cellulose might come with a smaller enzyme activity rate.

While the cellulose films examined in this thesis have uniform crystallinity of approximately 42% (Chapter 2), it is possible to synthesize model cellulose films with higher and lower crystallinities. Cellulose from microorganisms such as *Tunicin* and *Valonia* can be deposited on metal substrates,[11] allowing QCM assessment of enzyme activity on substrates with

crystallinity in the range of 80 – 90%. Deposited cellulose films can also be treated with ionic liquids or annealed to produce fully amorphous crystalline films.[12] Thus, both highly crystalline and highly amorphous films are available to explore the effect of crystallinity on enzyme activity. Amorphous films are also penetrable to enzymes,[12] necessitating bulk diffusion and concentration modeling.

Finally, kinetic slowdown may be caused by aqueous glycans acting as inhibitors of cellulose activity. Both glucose oligomers produced from cellulose degradation and other polysaccharides released during xylan/lignin deconstruction are known inhibitors of cellulose activity.[13 14] Inhibition was employed in this thesis to examine cellulase binding constants in the absence of complexation and activity—high concentrations of glucose were used to completely inhibit cellulase complexation. This concentration of aqueous glucose was not found to interfere with cellulase adsorption (Figure 2.6). However, the kinetic effect of such inhibitors on cellulose binding and activity rates remain poorly understood.

Flow QCM and flow ellipsometry assays demonstrated in this thesis are particularly useful because they allow inhibition-free assays of cellulose activity—all glycan products released into aqueous solution are immediately washed away from the film, removing the effects of inhibition that typically confound cellulose degradation data. To explore the effect of inhibition on binding, complexation, and activity constants, different concentrations of inhibitor could be added to the enzyme mixture before it is flowed across the cellulose film. This allows precise control of inhibition, and, therefore, detailed analysis of inhibition constants.

However, in order for such inhibition data to be valid, it is first necessary to establish that inhibitors do not interact with the cellulose film. In preliminary work, when cellobiose was employed as an inhibitor of cellulase activity at a 10:1 cellobiose:enzyme concentration, the disaccharide destabilized the cellulose film, greatly swelling the film and producing noisy adsorption results. It may be necessary to synthesize cellulose films with higher crystallinity or otherwise improved stability before inhibition studies can be attempted.

Surface-based assays are, therefore, uniquely suited to explore many hypothesized causes of kinetic slowdown, a major limitation in industrial production of feedstocks from lignocellulosic sources. In this thesis, the development of surface-based assays and interpretation of surface degradation and adsorption data through a two-enzyme kinetic model was shown. Continued research should expand this model to include the action of other enzymes, secondary enzyme activities, inhibition, denaturation, temperature effects, and changes in surface properties. This thesis has only scratched the surface of these assays.

5.1. References

(1) Kumar, R.; Singh, S.; Singh, O. V. Bioconversion of Lignocellulosic Biomass: Biochemical and Molecular Perspectives. *J Industrial Microbio and Biotech* **2008,** *35,* 377-391.

(2) Schuster, A.; Schmoll, M. Biology and Biotechnology of *Trichoderma*. *App Microbio and Biotech* **2010,** *87,* 787-799.

(3) Karlsson, J.; Siika-Aho, M.; Tenkanen, M.; Tjerneld, F. Enzymatic Properties of the Low Molecular Mass Endoglucanases Cel12A (EG III) and Cel45A (EG V) of *Trichoderma reesei*.

(4) Din, N.; Gilkes, N. R.; Tekant, B.; Miller Jr., R. C.; Warren, R. A. J.; Kilburn, D. G. Non-Hydrolytic Disruption of Cellulose Fibres by the Binding Domain of a Bacterial Cellulase.

(5) Cardona, C. A.; Sanchez, O. J. Fuel Ethanol production: Process Design Trends and Integration Opportunities. *Bioresource Tech* **2007,** *98,* 2415-2457.

(6) Eriksson, T.; Karlsson, J.; Tjerneld, F. A Model Explaining Declining Rate in Hydrolysis of Lignocellulose Substrates with Cellobiohydrolase I (Cel7A) and Endoglucanase I (Cel7B) of *Trichoderma reesei*. *Appl Biochem Biotech* **2002,** *101,* 41-60.

(7) Turon X.; Rojas, O. J.; Deinhammer, R. S. Enzymatic Kinetics of Cellulose Hydrolysis: A QCM-D Study. *Langmuir* **2008,** *24,* 3880-3887.

(8) Himmel, M.; Ding, S. Y.; Johnson, D. K.; Adney, W. S.; Nimlos, M. R.; Brady, J. W.; Foust, T.D. Biomass Recalcitrance: Engineering Plants and Enzymes for Biofuels Production. *Science* **2007**, *315,* 804-807.

(9) Chundawat, S. P. S.; Bellesia, G.; Uppugundla, N.; Sousa, L. D.; Gao, D. H.; Cheh, A. M.; Agarwal, U. P.; Bianchetti, C. M.; Phillips, G. N.; Langan, P.; Balan, V.; Gnanarakan, S.; Dale, B. E. Restructuring the Crystalline Cellulose Hydrogen Bond Network Enhances Its Depolymerization Rate. *J Am Chem Soc* **2011,** *133,* 11163-11174.

(10) Teeri, T. T.; Koivula, A.; Linder, M.; Wohlfahrt, G.; Divne, C.; Jones, T. A. *Trichoderma reesei* Cellobiohydrolases: Why So Efficient on Crystalline Cellulose? *Biochemical Society Transaction* **1998,** *26,* 173-178.

(11) Habibi, Y.; Foulon, L.; Véronique, A. B.; Molinari, M.; Douillard, R. Langmuir-Blodgett Films of Cellulose Nanocrystals: Preparation and Characterization. *J Colloid Interface Sci* **2007,** *316,* 388-397.

(12) Cheng, G.; Datta, S.; Liu, Z.; Wang, C.; Murton, J.; Brown, P. A.; Jablin, M. S.; Dubey, M.; Majewski, J.; Halbert, C. E.; Browning, J. F.; Esker, A. R.; Watson, B. J.; Zhang, H.; Hutcheson, S. W.; Huber, D. L.; Sale, K. L.; Simmons, B. A.; Kent, M. S. Interactions of Endoglucanases with Amorphous Cellulose Films Resolved by Neutron Reflectometry and Quartz Crystal Microbalance with Dissipation Monitoring. *Langmuir* **2012.** In press.

(13) Holtzapple, M.; Cognata, M.; Shu, Y.; Hendrickson, C. Inhibition of *Trichoderma-reesei* Cellulase by Sugars and Solvents. *Biotech Bioeng* **1990,** *36,* 275-287.

(14) Qing, Q.; Yang, B.; Wyman, C. E. Xylooligomers Are Strong Inhibitors of Cellulose Hydrolysis by Enzymes. *Bioresource Tech* **2010,** *24,* 9624-9630.